THE
PHYSICAL REVIEW
A Journal of Experimental and Theoretical Physics Established by E. L. Nichols in 1893
VOL. 50, NO. 3 AUGUST 1, 1936 SECOND SERIES

The Enhancement of Certain L- and M-Series X-Ray Satellite Lines by the Auger Effect

F. R. HIRSH, JR., *Cornell University*
(Received May 20, 1936)

Integrated relative energies for the satellites of $L\beta_1$ are measured by a photographic method. A marked change in relative intensity exists at $Z=40$, which is to be explained by enhancement of the $L\beta_1$ satellites due to the Auger effect. The enhancement of M-series satellites by the Auger effect is discussed. The theory explains the almost identical frequency separations and nearly equal intensities observed for the satellite groups of the $M\alpha_1$ and $M\beta$ lines of Bi(83). Some experimental evidence of an intensity anomaly due to the Auger effect, for the satellites of $M\alpha_1$, is presented.

A. THE ENHANCEMENT OF L-SERIES SATELLITES BY THE AUGER EFFECT

Introduction

IN 1922, D. Coster[1] published certain microphotometric curves which indicated that the satellites of the x-ray diagram line $L\alpha_1$ decreased markedly in intensity, relative to their parent line, in going from Rh(45) to In(49). In the same atomic number range, he did not observe a corresponding change for the satellites of $L\beta_1$.

A later study[2] of the $L\alpha_1$ satellites confirmed this rapid decrease in relative intensity (for cathode ray excitation), from $Z=45$ to $Z=47$, and indicated that there was a maximum relative intensity at $Z=45$.

A further study[3] shows that the $L\alpha_1$ satellites also "fade out"[4] near $Z=52$.

Another investigation,[5] made in the Cornell x-ray laboratory, showed that a similar maximum relative intensity existed for the satellites of $L\beta_2$ near $Z=47$.

The probability of the transition $L_I \rightarrow L_{III}$ with the emission of radiation, although the transition is permitted by "selection rules," is very small. Coster[1] reported a search for radiation corresponding to this transition, but failed to find such a line; however, Coster and Kronig[6] report that such a radiation has been observed.

Coster and Kronig[6] point out that the total amount of energy in the L_I-series of lines is smaller, compared to the energy in the L_{II}- and L_{III}-series, than would be expected from the radiative transition probability.

On the basis of these facts, Coster and Kronig[6] proposed their theory of a new Auger effect. This theory explains the $L\alpha_1$ and $L\beta_2$ satellite line groups as follows: the transition $L_I \rightarrow L_{III}$ is a radiationless transition which causes the simultaneous ejection of an $M_{IV,\,V}$ electron. This is possible for atomic numbers less than $Z=50$; $(E_{L_I}-E_{L_{III}})_z < (E_{M_{IV,\,V}})_{z+1}$ for certain atomic numbers above $Z=50$. (E here stands for energy.)

[1] D. Coster, Phil. Mag. **43**, 1089 (1922).
[2] F. R. Hirsh, Jr. and F. K. Richtmyer, Phys. Rev. **44**, 955 (1933).
[3] F. R. Hirsh, Jr., Phys. Rev. **48**, 722 (1935).
[4] By "fade out" is meant that the satellite's relative intensity becomes too small to be measured photographically, although, as will be shown later in the present article, a microphotometric record may give positive evidence of the existence of such satellites.
[5] A. ... Pearsall, Phys. Rev. **46**, 694 (1934).
[6] D. Coster and R. de L. Kronig, Physica **2**, 13 (1935).

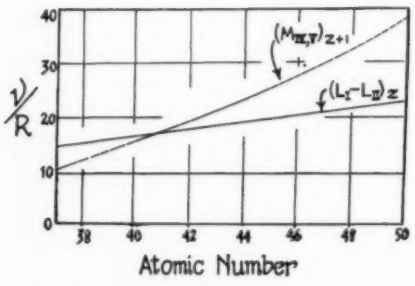

FIG. 1. The energy provided by the radiationless transition $L_I \rightarrow L_{II}$ and the energy required to eject an $M_{IV, V}$ electron, plotted against atomic number.

An atom is thus left doubly ionized, with L_{III} and $M_{IV, V}$ electrons missing, and therefore in the initial state, according to Druyvesteyn,[7] for the emission of the $L\alpha_1$ or $L\beta_2$ satellite groups. Single electron transitions, between these doubly ionized states, $L_{III}M_{IV, V} \rightarrow (M_{IV, V})^2$ or $L_{III}M_{IV, V} \rightarrow M_{IV, V}N_V$, cause the appearance of satellite lines. The single electron transitions $L_{III} \rightarrow M_V$ or $L_{III} \rightarrow N_V$ give rise to the parent $L\alpha_1$ or $L\beta_2$ lines.

If we admit that observed satellite intensity anomalies are partial evidence for the existence of the Auger effect, it follows that when it is known the Auger effect is possible and that it should enhance satellites over a given range of atomic numbers, we may similarly expect the existence of an intensity anomaly for these satellites.

Coster and Kronig[5] pointed out that for the satellites of $L\beta_1$ the Auger effect cannot exist if $Z > 40$, for the radiationless transition $L_I \rightarrow L_{II}$ can no longer cause ionization of the $M_{IV, V}$ shell (see Fig. 1). It was later reported[8] that at $Z = 40$ an intensity anomaly does exist for the satellites of $L\beta_1$. It is the purpose of the first part of the present paper to report more fully on this point.

Experimental

The $L\beta_1$ lines of the elements included between atomic numbers 30 and 48 (excited by 20 kv electrons) were photographed in a Siegbahn vacuum spectrograph using a gypsum (selenite) crystal. The radius of this instrument was 18.36 cm; a slit width of 0.1 mm was used. All lines of elements from $Z = 30$ to $Z = 40$ were photometered; the necessary constants were secured, and a density section through each line was plotted (see Fig. 2). These density plots are intensity plots for the x-ray lines. The range of wave-lengths studied in the present investigation (5.0 to 12.0A) is partly covered by the results of a previous study.[9] A linear region was found for density-exposure time curves of up to 5.4A in wave-length, overlapping the region of the present study. The region 6.0 to 12.0A has not been carefully studied[10] but, in view of the increasing extent with increasing wave-length of the region of linearity as found in the former investigation,[9] the density plots of Fig. 2 will be assumed to have their usual significance.

On these density plots, the short wave-length side of the parent line, i.e., the satellite background, was sketched in, and estimates of the integrated relative energy (total satellite energy divided by parent line energy) were made by planimetering areas (see Table I).

For the $L\beta_1$ lines of atomic numbers 41 through 48, no density sections were made. The microphotometric records are shown in Fig. 3. Satellites for these elements arise from double ionization by single electron impacts, and are extremely faint. For these elements, satellites which are present (see curve for Mo $L\beta_1$) would be completely masked by accidental irregularities (see Fig. 3). The satellite intensity, in all cases in Fig. 3, is estimated at less than one percent of the parent line intensity.

Fig. 4 shows a plot against atomic number, of the integrated relative energy of the satellites $L\beta_1'$ and $L\beta_1''$ of the x-ray diagram line $L\beta_1$. The estimates here show the existence of the satellite

TABLE I. *Values of the integrated relative energies of satellite and parent line.*

Element	Atomic Number	Integrated Relative Energy, (S/P)
Zn	30	0.100
Ga	31	0.100
Ge	32	0.107
As	33	0.099
Se	34	0.114
Br	35	0.122
Rb	37	0.200
Sr	38	0.327
Zr	40	0.143
$40 < Z < 49$, $(S/P) < 0.01$		

[7] M. J. Druyvesteyn, Dissertation, Groningen (1928).
[8] F. R. Hirsh, Jr., Phys. Rev. **48**, 776 (1935).
[9] F. R. Hirsh, Jr., J. O. S. A. **25**, 229 (1935).
[10] It will be studied shortly.

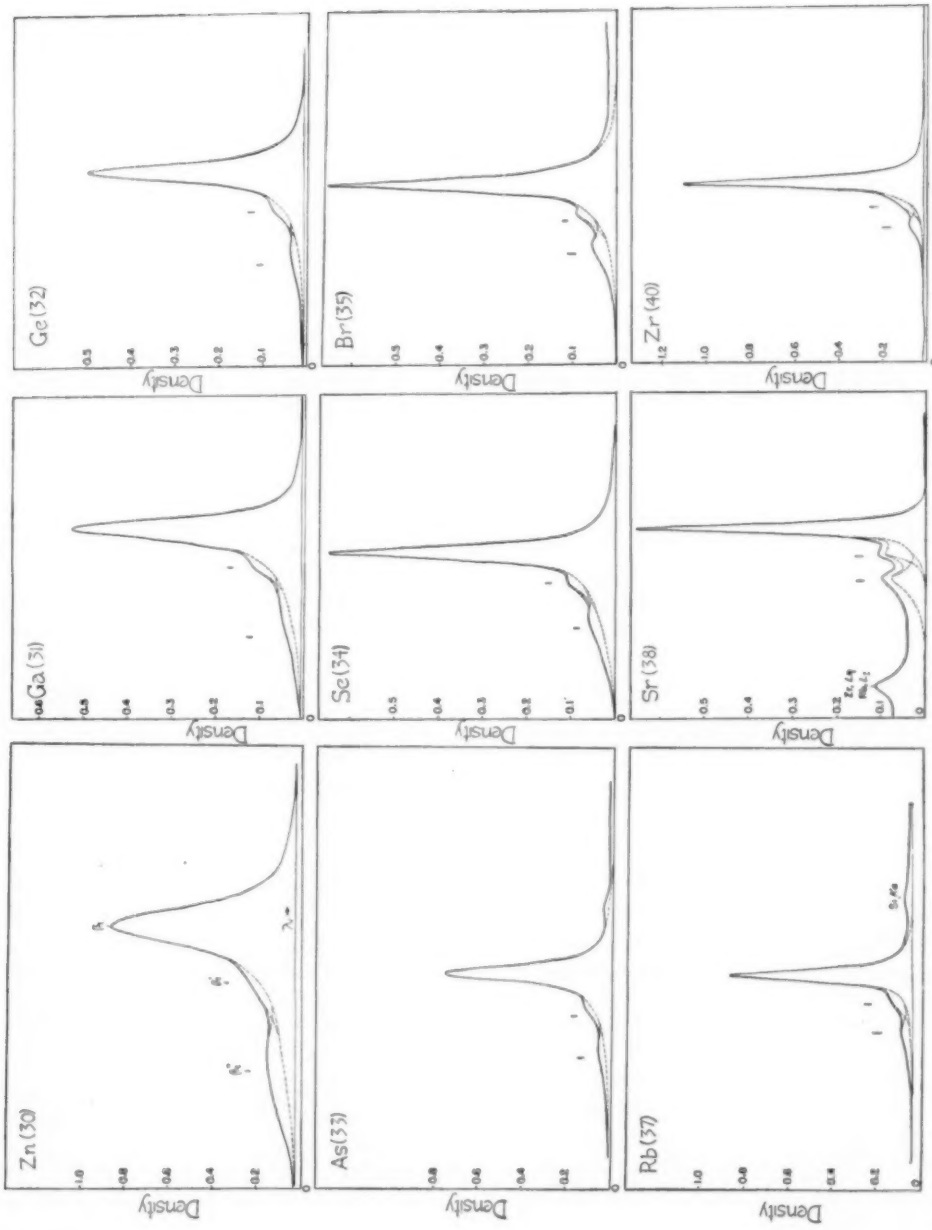

FIG. 2. Density, (intensity), plots of the $L\beta_1$ lines of the elements from Zn(30) through Zr(40) excited by 20 kv electrons. Vertical lines indicate positions at which satellites have been measured visually by Druyvesteyn, reference 7.

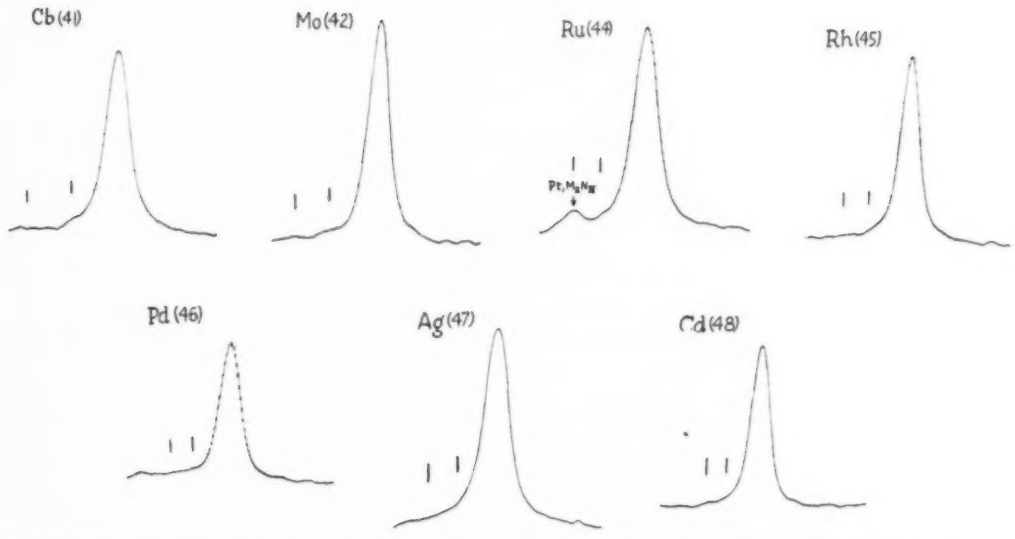

FIG. 3. Microphotometric records of the $L\beta_1$ lines of the elements from Cb(41) to Cd(48), excited by 20 kv electrons. Vertical lines indicate positions at which satellites have been measured visually by Druyvesteyn, reference 7.

intensity anomaly at $Z=40$. (This can also be seen in the density plots of Fig. 2.)

It must be emphasized here that these estimates involve a considerable error, chiefly due to the lack of resolving power of the single crystal spectrograph, and the consequent difficulty of drawing in a suitable satellite background. More careful studies in this field, with the use of the two crystal vacuum spectrometer, are clearly desirable.

B. Enhancement of M-Series Satellites by the Auger Effect

Introduction

In their paper[6] on the "new" Auger effect, Coster and Kronig remark in their summary, "it seems most reasonable to assume that in the M-region similar radiationless transitions occur with analogous results." Since the time when the present author studied M-series satellites,[11] no reasonable explanation of their origin has been advanced. As suggested by Coster and Kronig,[6] the theory of the Auger effect seems to hold promise of a solution of this problem.

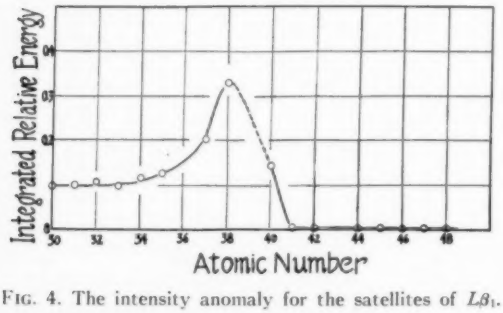

FIG. 4. The intensity anomaly for the satellites of $L\beta_1$.

Experimental considerations and results

The two strongest lines of the M-series, which are accompanied by satellites, are $M\alpha_1$, $(M_{\text{V}}N_{\text{VII}})$, and $M\beta$, $(M_{\text{IV}}N_{\text{VI}})$. A subsequent investigation of the plates previously obtained[11] shows that the greatest intensity of the satellites of $M\alpha_1$ and $M\beta$ is near $Z=83$. Another experimental fact appeared in the previous study: the semi-Moseley graphs for the $M\alpha_1$ and $M\beta$ satellite groups are remarkably similar (see p. 922, ref. 11). An explanation of the origin of these two satellite groups should involve two very similar initial doubly ionized states; since $M\alpha_1$ and $M\beta$ arise from two very similar transitions, the final doubly ionized states will also be similar. This would explain the similarity of the semi-Moseley diagrams for the $M\alpha_1$ and $M\beta$ satellite groups.

[11] F. R. Hirsh, Jr., Phys. Rev. **38**, 914 (1931).

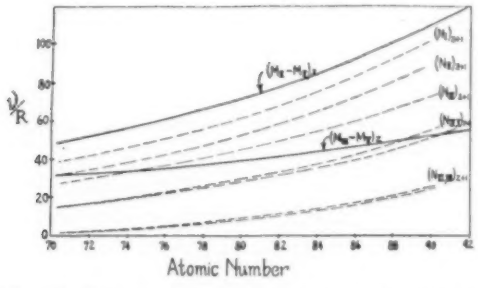

FIG. 5. The energy, in ν/R units, provided by the radiationless transitions $M_{II} \rightarrow M_V$ and $M_{III} \rightarrow M_V$, and the ionization energies, in ν/R units, of the N-shells, plotted against atomic number.

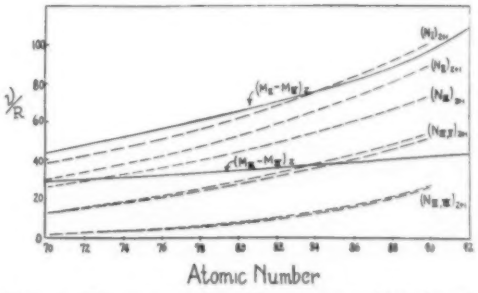

FIG. 6. The energy, in ν/R units, provided by the radiationless transitions $M_{II} \rightarrow M_{IV}$ and $M_{III} \rightarrow M_{IV}$, and the ionization energies in ν/R units, of the N-shells, plotted against atomic number.

Enhancement of the satellites of $M\alpha_1$ and $M\beta$ by the Auger effect must involve radiationless transitions leaving the M_V and M_{IV} shells respectively ionized, and, in addition, some N-shell (or shells).

In Fig. 5 are plotted the ionization energies of the N-shells (dashed lines) for $Z+1$ since an M shell will also be ionized,[12] and the energy, in ν/R units, provided by the radiationless transitions $M_{II} \rightarrow M_V$ and $M_{III} \rightarrow M_V$ (full curves).

If the energy provided by the radiationless transition is much greater than the ionization energy of any particular N-shell, the coupling between the electron involved in the radiationless transition and any electron in that N-shell is very weak; hence the Auger effect has small probability. Thus the radiationless transitions $M_I \rightarrow M_V$ and $M_{II} \rightarrow M_V$ (see Fig. 5) will not give rise to strong enhancement due to the Auger effect, in causing the ionization of M_V shell and some N-shell. Likewise the radiationless transition $M_{III} \rightarrow M_V$ can ionize the $N_{VI,\,VII}$ shells, but only with small probability.

However the curve for the energy difference M_{III}-M_V crosses the ionization energy curves for the $N_{IV,\,V}$ shells near $Z=89$. Because of strong coupling, the $N_{IV,\,V}$ shell will be left ionized as a result of the radiationless transition $M_{III} \rightarrow M_V$; the atom is left doubly ionized, M_V and $N_{IV,\,V}$ electrons missing, and therefore the atom is in an initial state for the emission of satellites. The radiationless transition $M_{IV} \rightarrow M_V$ is not considered, since, as may be seen from Fig. 5, the energy released is too small to cause the ionization of any N-shell.

Accounting for the enhancement of the $M\beta$ satellites, a similar plot, Fig. 6, shows the N-shell ionization energies and the curves for the energy differences M_{II}-M_{IV} and M_{III}-M_{IV}, corresponding to the radiationless transitions which leave the M_{IV} shell ionized.

For simplicity, let us disregard the energy difference curve M_{II}-M_{IV}. As it crosses the N_I shell at $Z=84$, it undoubtedly may be of some significance in causing satellite enhancement due to an M_{IV} and N_I double ionization for several atomic numbers below $Z=84$. However N_I is a single shell, while $N_{IV,\,V}$ is a double shell as in the case of the $L\alpha_1$ and $L\beta_2$ satellites, where $M_{IV,\,V}$, a double shell, is the second (outermost) ionized shell according to Coster and Kronig.[6] The coupling is enhanced as the probabilities of ionization of the two shells are here added, in the event of the ionization of this double shell as a result of a radiationless transition.

We see in Fig. 6 that the curve for the energy difference M_{III}-M_{IV} crosses and goes above the ionization energy curve for the $N_{IV,\,V}$ shell at about $Z=84$, and we therefore expect strong enhancement of the satellites of $M\beta$ for several atomic numbers below $Z=84$. The radiationless transition $M_{III} \rightarrow M_{IV}$ can cause the ionization of the $N_{IV,\,V}$ shell, and the atom may be left doubly ionized by the Auger effect because of the strong electron coupling. The energy released by the radiationless transition $M_{III} \rightarrow M_{IV}$ can also cause ionization of the $N_{VI,\,VII}$ shells throughout the entire atomic number range of Fig. 6, but this event is of small importance because of the weak

[12] The use of $Z+1$ is, of course, merely an approximation, but it is sufficiently good for the purpose at hand.

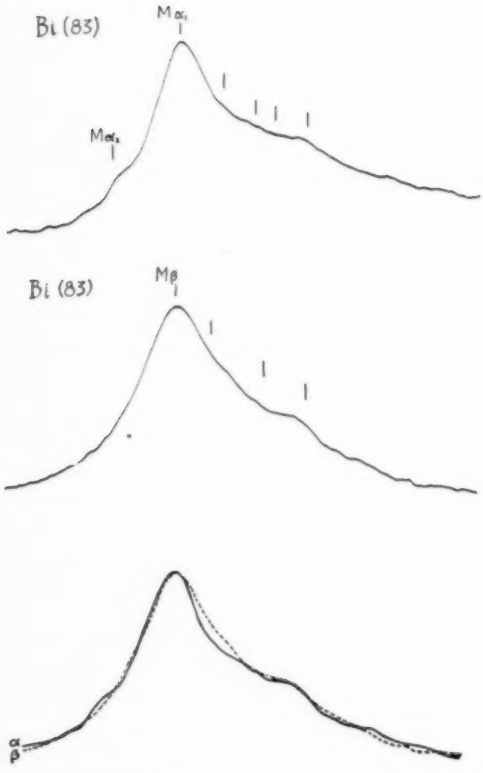

FIG. 7. Microphotometric records of the M-lines of Bi(83). Upper curve, $M\alpha_1$; middle curve, $M\beta$; lower curve, $M\alpha_1$ and $M\beta$ superimposed.

coupling between the electron involved in the radiationless transition and an $N_{VI,\ VII}$ electron. Likewise the radiationless transition $M_I \rightarrow M_{IV}$ is not considered because of weak coupling with the N-shells.

From the above discussion it is seen that we may have enhancement due to the Auger effect under very similar conditions for the satellites of the diagram lines $M\alpha_1$ and $M\beta$. Considering Fig. 5, we see that for the $M\alpha$ satellites the radiationless transition $M_{III} \rightarrow M_V$ will, with high probability for certain atomic numbers, cause ionization of the $N_{IV,\ V}$ shell, leaving the atom doubly ionized. Considering Fig. 6, we see that for the $M\beta$ satellites, ionization of the $N_{IV,\ V}$ shell may be caused, with high probability for certain atomic numbers, by the radiationless transition $M_{III} \rightarrow M_{IV}$. Thus we might expect that the satellites of $M\alpha_1$ and $M\beta$ would have approximately the same frequency separations from their respective parent lines, because of the great similarity of both the initial and the final doubly ionized states; for $M\alpha_1$ satellites, the transition is $M_V N_{IV,\ V} \rightarrow N_{VII} N_{IV,\ V}$, while for the $M\beta$ satellites the transition is $M_{IV} N_{IV,\ V} \rightarrow N_{VI} N_{IV,\ V}$. To confirm this, one can inspect the superimposed semi-Moseley graphs, as shown in Fig. 5, p. 922, ref. 11. The curves for $M\alpha^{ii}$ and $M\beta^{ii}$, the strongest satellites in their respective groups, are practically coincident, while $M\alpha^{i}$ and $M\beta^{i}$ and likewise $M\alpha^{iv}$ and $M\beta^{iii}$ have roughly the same frequency separations.

While making the wave-length measurements previously mentioned[11] a plate was made of the Bi(83) x-ray spectrum which shows both the $M\alpha_1$ and $M\beta$ lines. The $M\alpha_1$ line ($\lambda = 5.11$A) has a density of 0.59 on this particular plate, while the $M\beta$ line ($\lambda = 4.89$A) has a density of 0.81 (the spectrograph was set to photograph $M\beta$). Hence, density is proportional to intensity on this plate[9] and microphotometric curves made from this plate will be undistorted.

Fig. 7 gives the microphotometric curves for the Bi(83) $M\alpha_1$ and $M\beta$ lines just mentioned. The curve for $M\alpha_1$ is at the top; the middle curve is that of $M\beta$, while the lower curves are $M\alpha_1$ and $M\beta$ superimposed by tracing the two upper curves, rotating the $M\alpha_1$ curve slightly to eliminate its uneven background. It may be readily seen that for Bi(83) the satellites of $M\alpha_1$ and $M\beta$ have roughly the same intensity, with the $M\beta$ satellites possibly a little more intense. This last fact is to be expected because of the higher probability of double ionization due to the Auger effect, since the intersection of the curve for the energy difference M_{III}-M_{IV} and the $N_{IV,\ V}$ ionization energy curve, lies nearer atomic number 83 than does the intersection of the curve for the energy difference M_{III}-M_V and the $N_{IV,\ V}$ ionization energy curve (see Figs. 5 and 6).

It is unfortunate that the $M\alpha_1$ satellite intensity maximum should lie in a region which is difficult for the x-ray spectroscopist to study completely because of the presence of several radioactive elements. However, Dr. L. G. Parratt has recorded ionization curves of several M-lines in the (1, +1) position with the two-crystal vacuum spectrometer. For Au(79) he finds a line decidedly asymmetrical near the base with sug-

gestive irregularities indicating satellite lines. The relative intensity of the $M\alpha_1$ satellites is apparently much less than the relative intensity indicated by the author's photometer record (Fig. 7) for Bi(83), $M\alpha_1$. This intensity difference is in agreement with predictions to be made from Fig. 5, since Au(79) is farther removed from the intersection of the curve for the energy difference M_{III}-M_V and the $N_{IV,\ V}$ ionization energy curve, than is Bi(83). Although quantitative comparison of the relative satellite intensities for these elements cannot be made from these data, because of the different types of instruments used, the qualitative conclusion stands. Furthermore, U(92), $M\alpha_1$ should have very faint satellites, since the Auger effect is very improbable (see Fig. 5). Preliminary measurements by Dr. Parratt on the U(92), $M\alpha_1$ line indicate less asymmetry at the base than in the case of the Au(79), $M\alpha_1$ line. This experimental agreement with the predicted intensity anomaly is suggestive, but requires further investigation for its final confirmation.

Conclusions

1. The experimental existence of an intensity anomaly for the satellites of $L\beta_1$ is demonstrated.

2. Satellite enhancement is studied, in line with the suggestion of Coster and Kronig, for the M-series, and is shown to agree qualitatively with existing data.

Acknowledgments

It is a pleasure to acknowledge Dean Richtmyer's continued interest in these studies, and to thank him for permission to use certain equipment granted him by the Heckscher Research Council of Cornell University.

The author wishes to thank Dr. Parratt for permission to mention his preliminary results on the $M\alpha_1$ satellites.

The writer also wishes to acknowledge helpful discussions with Dr. E. G. Ramberg.

The author desires to express his appreciation of the action of the Faculty of the Cornell University Department of Physics in extending research privileges.

AUGUST 1, 1936 PHYSICAL REVIEW VOLUME 50

Fine Structure in the K X-Ray Absorption Edge of Gallium*

W. W. Mutch, *Sloane Physics Laboratory, Yale University*†

(Received June 13, 1936)

The absorption of x-rays by a Ga foil in the region extending from the main K absorption edge of Ga toward shorter wave-lengths for a distance of about 250 volts has been investigated by the ionization method. The absence of any extended fine structure at room temperature is confirmed. The temperature of the Ga has been reduced to −67°C and −140°C, and a progressive appearance of extended fine structure has been noted as the temperature decreased. Checks have been made to prove the validity of the conclusions. The results of the investigation are presented in graphical and tabular form. A value of 1192.5 x.u. for the wave-length of the main K absorption edge of Ga is determined. This value is believed to be more accurate than the value of 1190.2 x.u. found in most tables.

Introduction

TWO distinct types of fluctuation have been noted in the values of x-ray absorption coefficients in the neighborhood of the main absorption discontinuities for various substances. These two types are distinguished by their energy separations from the main absorption edge, both occurring on the short wave-length side of the main edge. The fluctuations within energy separations of a few tens of volts of the main absorption edge have been called the Kossel type of fine structure. Those fluctuations occurring at energies between fifty and several hundred volts greater than the energy of the main edge have been called the Kronig type of fine structure. The existence of this extended fine

* Part of a dissertation presented to the Faculty of the Graduate School of Yale University in candidacy for the degree of Doctor of Philosophy.

† Now at Pennsylvania College for Women, Pittsburgh, Pennsylvania.

structure for crystals was explained theoretically by Kronig[1] as due to forbidden and allowed energy zones beyond the ionization potential of the atom, consequent upon the atom's location in a periodic array. Hanawalt noted[2] that this fine structure, in the case of the K edge of Fe, moved in slightly toward the main absorption edge, and gradually disappeared as the temperature of the absorbing screen was raised toward the melting point. This disappearance, and the non-appearance of any extended fine structure in the case of Ga[3] and other substances, at temperatures just below their melting points, was then explained by the broadening out and overlapping of the forbidden and allowed zones. This broadening out may result from the thermal vibrations of the atoms in the crystal lattice which are appreciable near the melting temperature.

It was suggested by Professor C. D. Cooksey that the K edge of Ga be investigated for the existence of extended fine structure at temperatures as low as could be obtained with the use of liquid air.

Apparatus

A Compton type double crystal spectrometer, made by the Société Génévoise, was modified for use as a simple Bragg spectrometer for this investigation. The two vertical collimating slits between the x-ray tube and the calcite crystal were 0.0025 cm wide, 0.3 cm high, and spaced 18 cm apart. A cleavage face of the crystal was placed accurately parallel to, and including, the crystal table axis. Observations of the positions of the crystal were made, through a micrometer microscope, on a precision circle attached to the crystal table. The Ga absorbing screen was supported between the two collimating slits. Observations of the intensity of the reflected x-ray beam were made with an ionization chamber and vacuum tube electrometer.

The source of x-rays was a demountable metal tube. The vacuum was maintained by the continuous operation of an Apiezon oil diffusion pump backed by a Megavac mechanical pump. For this work, the tube was fitted with a tungsten target, a General Electric medium focus filament, and an aluminum window 0.0023 in. thick. The filament was heated by current from storage batteries. The high potential was obtained from a transformer through a full wave Kenotron rectifier. Power was supplied to the transformer from a 500 cycle motor generator set. The constancy of the high potential was ensured by synchronous motor control of the speed of the motor generator, and by storage battery excitation of the generator.

The Ga for this investigation was kindly donated by Dr. Donald Cooksey. The analysis stated that the material was 99.8 percent pure Ga. The absorbing screen was formed by rolling the Ga between ordinary machine shop rolls. It was found necessary to keep the rolls and all tools which came in contact with the Ga cooled by contact with solid CO_2 to prevent the Ga from melting while being worked or handled. Foils of 0.002 to 0.0025 cm thickness were readily obtainable, and proved quite satisfactory as absorbing screens. These foils were supported between a piece of stiff paper and a piece of Cellophane, and mounted on a copper ring.

The cooling of the Ga foil was accomplished by passing across it a stream of vapor from boiling liquid air, after the manner of Cioffi and Taylor.[4] The copper ring carrying the Ga was mounted in a double walled cylindrical chamber provided with four cellophane windows in a line perpendicular to the axis of the chamber. The cold air was conducted from the Dewar flask boiler to within a cm of the absorbing screen in the inner section of the chamber by a double-walled, silvered, evacuated glass tube. To prevent the formation of frost in the x-ray path, the dry exhaust air was warmed and returned through the outer jacket of the double-walled chamber. It was found that the absorbing screen could be maintained steadily at temperatures as low as -150°C. Temperatures were measured with a copper-constantan thermal junction in contact with the copper ring supporting the Ga screen.

Measurements and Results

Preliminary observations were made over the tungsten emission spectrum in the wave-length region of the K edge of Ga. The β_9, β_7, β_2 and β_3 lines of the tungsten L group fall just on the long

[1] R. de L. Kronig, Zeits. f. Physik **70**, 317 (1931); **75**, 191 and 468 (1932).
[2] J. D. Hanawalt, Zeits. f. Physik **70**, 293 (1931).
[3] B. Kievit and G. A. Lindsay, Phys. Rev. **36**, 648 (1930).
[4] P. P. Cioffi and L. S. Taylor, J. O. S. A. **6**, 906 (1922).

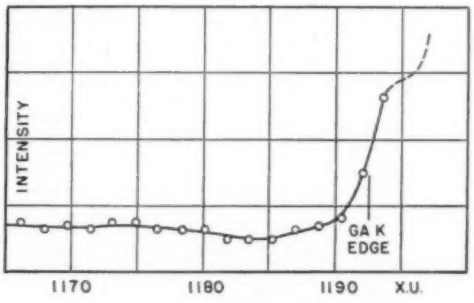

FIG. 1. K absorption edge of Ga at 20°C.

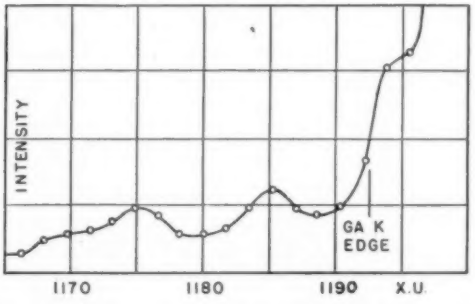

FIG. 2. Fine structure in the K edge of Ga at −67°C.

wave-length side of the K edge of Ga, and were used as reference points in determining wave-lengths.

In all runs, unless otherwise noted, the x-ray tube current was 24 milliamperes, and the peak voltage across the x-ray tube was approximately thirty kilovolts. A change of one percent in either of these quantities could be detected easily, and readings affected by observable changes were discarded.

Electrometer readings were taken by the rate of drift method. The zero rate of drift, i.e., the rate with the x-rays screened out, was carefully checked and found to be very constant. In the curves shown, the ordinates are proportional to the x-ray intensity as determined by subtracting the observed rate of drift from the zero rate.

Fig. 1 shows the results of a run taken over the K edge of Ga at 20°C. In agreement with the report of Kievit and Lindsay,[3] no fine structure is found. The wave-length of the edge is 1190.2 x.u. according to Duane, Blake and Hu.[5] There is no evidence in Fig. 1 of an edge at this point, and the conclusion that it is hidden in the side of the $L\beta_9$ line from the target, just to the long wave-length side of its expected position, is borne out in the later curves.

A run was taken over the region of the expected fine structure and extended to include the $L\beta_9$ line of tungsten with the absorbing screen at a temperature of −67°C. For this run, the x-ray tube current was 36 milliamperes, and the collimating slits were narrower than before, with the resolution consequently better. The resulting curve is shown in Fig. 2. Here two minima of absorption have appeared at separations from the main edge of 65 volts and 153 volts. Fig. 2 also shows the K edge of Ga clearly separated from the tungsten line.

Four runs were taken in the region of the fine

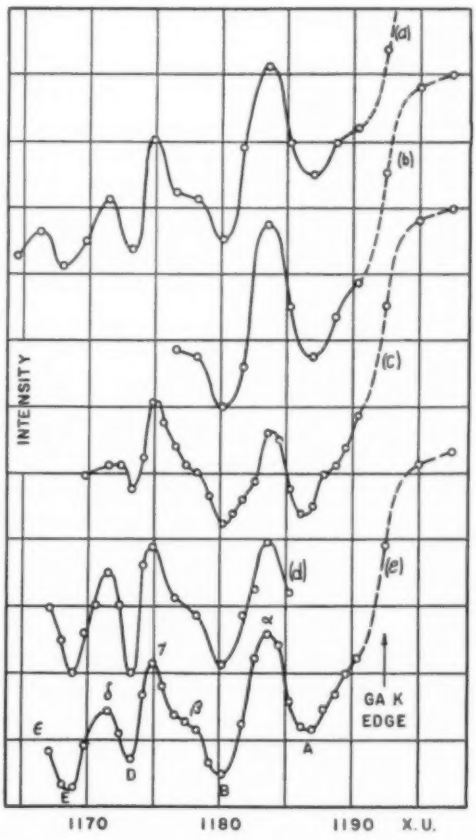

FIG. 3. Fine structure in the K edge of Ga at −140°C. a, b, c and d represent individual runs, and e is a composite of the four runs.

[5] W. Duane, F. C. Blake and K. F. Hu, Bull. Nat. Res. Coun. 1, 6 (1920).

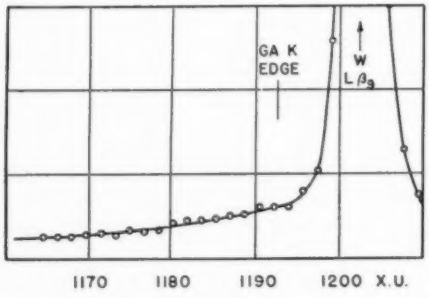

FIG. 4. Tungsten emission spectrum in the region of the K edge of Ga.

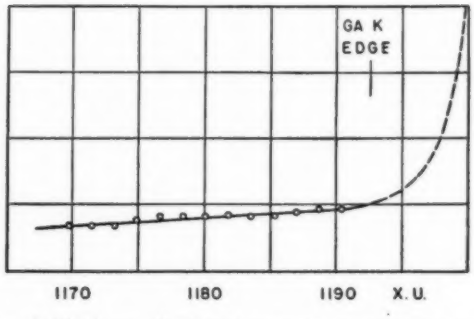

FIG. 5. Blank run, showing absence of fine structure from the Ga mounting at −140°C.

structure at −140°C, and the results are shown in Fig. 3a, b, c and d. Because of the difficulty of maintaining this low temperature steadily over the periods of three to five hours required to make complete runs, only one of the runs covers the entire range of the fine structure. Fig. 3e is a composite of the other four curves in Fig. 3. Since no attempt was made to take the four curves under the same conditions of electrometer sensitivity, measured intensities have been multiplied by arbitrary factors to give the best fit. Since the temperature and other conditions were essentially constant for the four runs, it is the author's belief that the curve of Fig. 3e is a better representation of the fine structure than any of the curves of individual runs.

Figs. 4 and 5 show the results of two control runs, taken to prove the absence of spurious effects. Fig. 4 shows the emission spectrum of the target over the region concerned, and shows a satisfactorily uniform continuous background of "white radiation." Fig. 5 shows the results of a blank run taken with the cooling system in operation and the Ga mounting in place exactly as for the runs illustrated in Figs. 1, 2 and 3, except that the Ga foil was removed. The complete absence of any fine structure in Fig. 5 is taken as conclusive evidence that the structure observed in the previous runs is due to absorption in the Ga foil.

Table I gives the positions of all the maxima and minima found near the main K edge of Ga.

Previous experiment and theory agree on the point that the position and shape of the fine structure characteristics depend on the crystal structure of the absorber. A comparison of the present results with published reports on the fine structures observed for various other absorbers fails to show any patterns resembling that found for Ga. Since Ga has an unusual and unique crystal structure (orthorhombic-pseudotetragonal) this lack of similarity is to be expected.

The data of Fig. 2 present an excellent opportunity to determine the position and wave-length of the main K edge of Ga. The wave-length so determined is 1192.5 x.u. This agrees with the value of 1192.9 x.u. reported by Kievit and Lindsay[3] and differs appreciably from the value of 1190.5 x.u. given in most tables. The position of the main edge is taken as the center of the linear portion of the absorption curve. The nearness of the tungsten emission lines makes the present measurement particularly simple and accurate. To obtain the accepted wave-length of 1190.5

TABLE I. *Maxima and minima near main K edge of Ga.*
Column (1) gives the designation of the particular characteristic, following the notation of Coster and Veldkamp;[1] column (2) gives the measured Bragg angle of reflection, θ; column (3) gives the wave-length as computed from the relation $\lambda = 2d \sin\theta$; column (4) gives the excitation potential as obtained from the relation $\lambda v = hc$; and column (5) gives the separation in volts of each characteristic from the center of the main edge.

(1)	(2) θ	(3) x.u.	(4) Volts	(5) Volts
K	11° 21′ 11″	1192.5	10356.4	
A	11° 17′ 49″	1186.7	10407.0	50.6
α	11° 16′ 4″	1183.7	10433.5	77.1
B	11° 13′ 59″	1180.1	10465.2	108.8
β	11° 12′ 44″	1177.9	10484.0	127.6
γ	11° 10′ 59″	1174.9	10511.5	155.1
D	11° 9′ 49″	1172.9	10529.7	173.3
δ	11° 8′ 59″	1171.5	10542.5	186.1
E	11° 7′ 24″	1168.7	10567.4	211.0
ϵ	11° 5′ 59″	1166.3	10589.7	233.3

[1] D. Coster and J. Veldkamp, Zeits. f. Physik **74**, 191 (1932).

x.u. the separation between the nearest tungsten line and the K edge of Ga would have to be 24 percent greater than that observed.

The writer wishes to express his appreciation to Professor C. D. Cooksey for suggesting the problem and for his direction throughout the investigation; to Dr. Donald Cooksey for the use of materials and certain valuable instruments; and to Professor L. W. McKeehan for much helpful advice and constructive criticism.

AUGUST 1, 1936 PHYSICAL REVIEW VOLUME 50

A Theoretical Investigation of the Fine Structure of X-Ray Absorption Edge of Gallium

R. SMOLUCHOWSKI, *Institute for Advanced Study, Princeton*

(Received May 14, 1936)

The fine structure of x-ray absorption edge of gallium is calculated theoretically on the basis of Kronig's theory. A method given by the author in a previous paper of calculating the fine structure in complicated crystals is applied for the first time to a non-cubic crystal (orthorhombic-pseudotetragonal). A quantitative comparison with experimental results shows a good agreement.

CHARACTERISTIC x-ray absorption is connected with the transferring of an electron from one of the inner shells of the atom to the outside of the occupied electronic levels; the minimum energy necessary for this act corresponds to the absorption edge. Quanta of higher energy than this minimum value eject the electron into the region of the so-called "free electrons," the probability of such a transition however is not a continuous function of the electronic energy (i.e., of the absorbed quantum). Namely on account of the presence of (a) unoccupied atomic levels and, for higher energies, of (b) forbidden and allowed energy zones, which arise in crystals (and in molecular gases) there appear in the energy spectrum of electrons regions of higher and lower transition probability. These give rise to the so-called Kossel[1] (case a) and Kronig[2] (case b) fine structure of x-ray absorption limits. In his theory, which has been checked in many ways on a quite extensive experimental material,[3] Kronig considers the ejected electron moving in a certain direction in the periodic field of the crystal lattice. For a certain direction not every energy value is allowed and the energy spectrum consists of alternate allowed and forbidden zones. In wave-mechanical picture this fact corresponds to the scattering of the wave associated with the ejected electron on the atoms of the lattice and the resulting interference of primary and of scattered waves. As a result of this the x-ray absorption coefficient for each direction is finite in certain intervals and zero in between. Since the position of these intervals depends upon direction of the movement of the electron one must take the average over all directions whereby only fluctuations ("discontinuities") of the absorption coefficient remain. A set of $(\alpha\beta\gamma)$-planes (α, β, γ-Miller indices) gives rise in this way to a minimum and a maximum of absorption coefficient, the first occurring on the short wave-length side and the latter at the same distance on the long wave-length side of the energy

$$W=(h^2/8\mu d^2)(\alpha^2+\beta^2+\gamma^2) \qquad (1)$$

(μ-mass of an electron) measured from the mean potential of the crystal (assumed to be cubic with the lattice constant d).

If we represent the potential in the crystal

---

[1] W. Kossel, Zeits. f. Physik **1**, 119 (1920).
[2] R. de L. Kronig, Zeits. f. Physik **70**, 317 (1931); **75**, 191 (1932); **75**, 468 (1932).
[3] D. Coster and J. Veldkamp, Zeits. f. Physik **70**, 306 (1931); **74**, 191 (1932); J. Veldkamp, Zeits. f. Physik **77**, 250 (1932); **82**, 776 (1932); Dissertation Groningen 1934; D. Coster and R. Smoluchowski, Physica **2**, 1, 1935; R. Smoluchowski, Dissertation Groningen, 1935; Zeits. f. Physik **94**, 775 (1935); **95**, 588 (1935); and others.

lattice as a Fourier series then the magnitude (intensity of electron wave reflection) of a discontinuity is proportional to

$$I_{\alpha\beta\gamma}=H_{\alpha\beta\gamma}(V_{\alpha\beta\gamma})^2, \qquad (2)$$

where $H_{\alpha\beta\gamma}$ is the abundance factor of the $(\alpha\beta\gamma)$-planes and $(V_{\alpha\beta\gamma})$ is the Fourier coefficient of the potential in the crystal. The occurrence of many closely lying discontinuities and the neglected interaction of electrons and of thermal agitation of the nuclei make it impossible for each discontinuity to show up individually in the absorption curve. One must rather find the accumulation centers ("gravity center") of the discontinuities in the energy scale and only these can be used for comparison with experiment.

It has been shown by the author[4] that in case of an alloy and of a complicated arrangement of atoms in the unit cell of the crystal the fine structure has to be calculated with the $V_{\alpha\beta\gamma}$ given by the formula

$$V_{\alpha\beta\gamma}=[ed^2/\pi(\alpha^2+\beta^2+\gamma^2)]$$
$$\sum_j[\exp -2\pi i(\alpha x_j+\beta y_j+\gamma z_j)]\cdot Z_j(1-F_j), \qquad (3)$$

where x_j, y_j, z_j are coordinates of the atom j in the unit cell, Z_j is its atomic number and Z_jF_j the atomic form factor in the Fermi approximation for heavier elements. This formula was found in good agreement with experimental investigations on several alloys with complicated structure (e.g., γ-brass) or very different atomic numbers of constituents (e.g., Cu Be).[5] In case of pure metals it simplifies and one can finally calculate only with the so-called structure factor

$$K_{\alpha\beta\gamma}=\sum_j[\exp -2\pi i(\alpha x_j+\beta y_j+\gamma z_j)]. \qquad (4)$$

The factor $1/(\alpha^2+\beta^2+\gamma^2)$ in (3) and the slow change of F_j with (α, β, γ) can be omitted since they make $V_{\alpha\beta\gamma}$ decrease monotonically with increasing energy a fact which has no appreciable influence on the final results. All quantitative comparison of theoretical fine structure with experiment was done up until now only for cubic crystals. This paper is the first attempt to make a theoretical calculation of fine structure for a non-cubic crystal, namely for the orthorhombic pseudotetragonal (space group V_h^{18} in Shoenflies' system[6]) type of crystal lattice. The fine structure of the K absorption edge of gallium which according to Laves[7] crystallizes in this lattice was recently investigated by Mutch[8] so that a direct comparison with experiment is possible.

The unit cell of gallium contains 8 atoms of which the positions are given by means of two parameters $p=0.080$ and $m=0.153$ and the identity periods are $a=b=4.506$A, $c=7.642$A. Formula (4) retains its validity in this case, in the application of formula (2) however one must be careful with the abundance factor $H_{\alpha\beta\gamma}$ since the permutation of indices does not always give equivalent planes. Taking this into account the main change occurs in formula (1) which has to be substituted by

$$W=(h^2/8\mu)[(\alpha^2+\beta^2)/a^2+\gamma^2/c^2]. \qquad (5)$$

Mutch's measurements were made in -140°C and -67°C so that one should calculate with lattice constants at these temperatures, these however are not known. Fortunately the thermal linear expansion coefficient α for Ga at room temperature is rather low (18×10^{-6}) so that even not taking into account the fact that α in general is smaller at low temperatures[9] the correction can be shown as negligible in view of

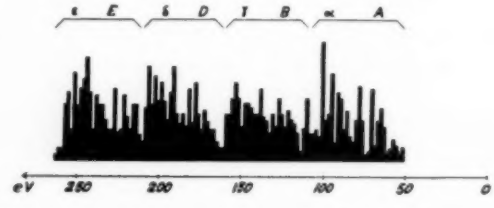

FIG. 1. Intensity of electron wave reflection *vs.* energy.

[4] R. Smoluchowski, Diss. Groningen, 1935; Zeits. f. Physik **94**, 775 (1935); **95**, 588 (1935).
[5] R. Smoluchowski, references 3, 4.
[6] See R. W. G. Wyckoff, *The Structure of Crystals*.
[7] F. Laves, Zeits. f. Kristallographie **84**, 256 (1933).
[8] W. W. Mutch, Phys. Rev. **50**, 197 (1936) (preceding paper).
[9] See, e.g., G. Borelius, *Handbuch der Metallphysik*, vol. I, part 1, page 224 (the value of α for Ga given there is wrong since 55 is the volume expansion coefficient for gallium).

TABLE I.

Group	Exper.	Theor.
$A-\alpha$	74	86
$B-\gamma$	142	139
$D-\delta$	190	191
$E-\epsilon$	230	236

the accuracy of comparison with measurements and of the experimental error. Moreover as can be seen comparing the fine structure at $-67°C$ and $-140°C$ the position of the maxima and minima which can be reasonably used as check of Kronig's theory that is, which are sufficiently far from the main edge are within experimental error the same in both curves (B and γ).

For actual calculation the formula (4) simplifies for this crystal lattice to

$$K_{\alpha\beta\gamma}=\cos\left[2\pi m\alpha+\pi/2(\alpha+\beta)\right]\cdot\cos\left[2\pi p\gamma-(\pi/2)(\alpha+\beta)\right], \quad (6)$$

where m and p are the parameters mentioned above. The values $I_{\alpha\beta\gamma}$ obtained with help of formula (2) and (6) for a set of planes which give rise to discontinuities lying between 50 and 260 volts and plotted against energy as given by (6) are shown in Fig. 1. One can distinguish four groups denoted $(A-\alpha)$, $(B-\beta)$, $(D-\delta)$, $(E-\epsilon)$ and obtain their centers of gravity (see above). In order to compare these with experimental results one must add to the values given by Mutch the energy difference between the mean potential in the crystal lattice and the first empty level. Since the experimental data necessary to calculate this magnitude are not known for Ga the value accepted is 10 volts which is the usual magnitude found experimentally in other metals and often applied with good results in similar cases.[10]

The maximum β occurring in Mutch's measurements has not been taken into account in our comparison since it is not very pronounced and the theoretical group $(B-\gamma)$ has sufficient breadth to account for the comparatively large distance between B and γ. The experimental and theoretical values (in eV) are compared in Table I. We see that the agreement is quite good if one takes into account the many approximations underlying the theoretical values. The group $(A-\alpha)$ is here as well as in all other comparisons not to be taken into consideration since the basic assumption of the theory (approximation from "free" electrons) is not valid in this region of fine structure.

[10] From measurements of electronic reflection we know how low the mean potential in the crystal lies in comparison with the outside potential; from the Richardson potential in the photoelectric effect we can obtain the energy necessary to remove from the crystal electrons of greatest energy. The difference between these two values gives us the desired quantity. See J. Veldkamp, Diss. Groningen 1934 and R. Smoluchowski, references 4.

Effects of Chemical Composition on X-Ray Lines

H. H. ROSEBERRY AND J. A. BEARDEN, *Rowland Physical Laboratory, Johns Hopkins University*

(Received May 28, 1936)

The influence of chemical combination with oxygen on the width, index of asymmetry and separation and ratio of peak intensities of the alpha-doublet of the elements Ti, Cr, Mn, Fe and Zn of the *K*-series emission lines has been studied with a double crystal spectrometer. The widths of the alpha-lines were increased 3 to 35 percent and the beta-lines were increased 4 to 30 percent except in two cases, namely that of the $K\alpha_1$-line of TiO_2, whose width decreased 3 percent, and that of the beta-lines of the oxides of Mn, whose width remained the same as that of the pure metal. No effect of chemical composition on the widths of the gamma-lines was observed. The $\alpha_1 \rightarrow \alpha_2$ separations were unaffected by chemical composition. The asymmetries of all the lines were unaffected with the exceptions of the alpha-lines of TiO_2, and the $K\alpha_1$- and the beta-lines of MnO and Mn_3O_4. The ratios of peak intensities of the alpha-lines were affected by changes of width caused by chemical composition such that the ratio of areas remained 2 : 1.

INTRODUCTION

THE effects of chemical combination on x-ray emission spectra have been the subject of numerous investigations[1–18] in the past few years. The effects found so far are: changes in frequency,[1, 2, 8, 10, 11, 13] in relative intensity,[9] in width,[9, 12, 14, 15, 16] of certain emission lines, and in some cases the appearance of new lines.[9] All of this work, with two exceptions, has been done with vacuum photographic spectrometers, with indefinite conclusion due in the main to the lack of resolving power either in the spectrometer itself or in the microphotometer used to analyze the photographic plates. A double crystal spectrometer was used by Wilhelmy,[16] who found that the Cu $K\alpha_1$-line from CuF_2 was much wider than that from pure copper, and by Parratt,[14] who examined two ($K\alpha_1$ and $K\alpha_2$) of the much studied sulphur lines. In none of the above cases have all the lines of a complete emission series been studied as a function of chemical combination under the same conditions of resolving power. In the present work the changes introduced in all the lines of the *K*-series (except Ti $K\gamma$) have been measured with a double crystal spectrometer for a number of substances sufficiently stable that they may be used satisfactorily as x-ray targets.

APPARATUS

Spectrometer

The double crystal spectrometer is of a precision type built by the Gaertner Scientific Corporation. The first crystal was mounted on a slide midway between the focal spot of the x-ray tube and the axis of the second crystal,[19] so that the wave-length region to be studied could be selected by simply adjusting the slide. The angular position of the second crystal was determined by reading the divided circle with two microscopes. Small displacements were measured by a worm-gear tangent screw and dial. Angular settings could be repeated with the tangent screw within 0.2 second of arc.

The ionization chamber was 6 cm in diameter, 13 cm long and made of steel to reduce alpha particle contamination.[20] The chamber was filled with pure argon at atmospheric pressure. The ionization current was measured by a Compton electrometer with a voltage sensitivity of 3 meters per volt. The peak of the weakest line measured

[1] Lindh and Lundquist, Ark. f. Matem. Astr. o. Fysik, Vol. 18, Nos. 14, 34, 35 (1924).
[2] Lundquist, Zeits. f. Physik **33**, 901 (1925); **60**, 642 (1930); **77**, 778 (1932); **89**, 273 (1934).
[3] Bäcklin, Zeits. f. Physik **33**, 547 (1925); **38**, 215 (1926).
[4] B. B. Ray, Phil. Mag. **49**, 168 (1925); **50**, 503 (1925).
[5] Ortner, Wien Sitzungsber. **II a 135**, 71 (1925); **136**, 369 (1927).
[6] Wetterblad, Zeits. f. Physik **42**, 603 (1927).
[7] Owens and Williams, Proc. Roy. Soc. **A132**, 282 (1931).
[8] Faessler, Zeits. f. Physik **72**, 734 (1931).
[9] Deodhar, Proc. Roy. Soc. **A131**, 647 (1931).
[10] Svensson, Zeits. f. Physik **75**, 120 (1932).
[11] Valasek, Phys. Rev. **43**, 612 (1933); **47**, 896 (1935).
[12] Yoshida, Inst. Phys. Chem. Res. Tokyo Sci. Rep. **421**, 298 (1933).
[13] Tanaka and Okuno, Phys. Math. Soc. Japan Proc. **17**, 540 (1935).
[14] Parratt, Phys. Rev. **45**, 364 (1934); **49**, 14 (1936).
[15] Siegbahn and Magnusson, Zeits. f. Physik **96**, 1 (1935).
[16] Wilhelmy, Zeits. f. Physik **97**, 312 (1935).
[17] Shearer, Phil. Mag. **20**, 504 (1935).
[18] Johnson, Zeits. f. Physik **95**, 93 (1935).
[19] Ross, Phys. Rev. **39**, 550 (1932).
[20] Bearden, Rev. Sci. Inst. **4**, 271 (1933).

gave an ionization current of 10^{-14} ampere. The average deviation from the mean reading at the peak of the line did not exceed 0.5 percent for the majority of the lines and for the weakest lines was approximately 2 percent.

Crystals and slits

The crystals were split from a large sample of perfectly clear Iceland calcite. The freshly cleaved surfaces gave a rocking curve width for the copper $K\alpha$-lines (1.54A) of 10.8 seconds, which is 1.2 seconds greater than the theoretical value of 9.6 seconds.[21] The crystals were ground, polished and etched[22] and then gave 9.8 seconds width and a percentage reflection of 55 percent. The alignment of the crystals was effected as previously described[23] using the $K\alpha$-lines of copper and titanium in the $(1-1)$ and the $(1+1)$ positions. This method makes the atomic planes rather than the cleavage planes parallel.[23] The measured physical resolving power of these crystals for the Cu $K\alpha$-lines was 11,000 in the $(1+1)$ position.

The first slit was 1.0 mm high (vertical projection of the focal spot), the second slit 10.0 mm high and the separation of the slits was 55 cm, giving a geometrical resolving power of 40,000. Since the crystals were always used in the first order where the measured physical resolving power is 11,000, the effective resolving power was determined by the perfection of the crystals and not by the geometrical resolving power.

X-ray tube

The water-cooled target was permanently mounted in a vertical position and arranged so that the glass body of the tube could be lowered over the target and the ground joint between the glass and target made tight with Apiezon sealing compound. This arrangement made possible the change of target material without disturbing the target's alignment with the crystals of the spectrometer. The target was cut at an angle of 10° with the horizontal and the focal spot thus acted as the first height limiting slit for the spectrometer. It has previously been shown[24] that satisfactory targets for accurate ionization chamber measurements can be made by pounding the desired material into the surface of the copper target. This method has proved entirely satisfactory for substances used in the present work.

In order that the source of x-rays be as constant as possible and that the oxides not be heated unnecessarily, the following procedure was adopted: the x-ray tube was assembled and connected to the diffusion pump. The tube (except the ground joint) was heated to about 500°C and then the target heated by bombardment to about 800°C. This process of alternately heating the glass and bombarding the target was repeated several times until the tube would operate with the target at 800°C without any evidence of gas. The tube was opened and the desired chemical or pure metal was quickly pounded into the surface of the target. The tube was re-assembled and evacuated. The previous baking-out process made it unnecessary to reheat the target. When the substance was properly pounded into the target the thermal contact was sufficient to prevent either noticeable heating or any chemical change of the target material with prolonged operation of the tube. As a further precaution against any decomposition, the power input to the tube was maintained at less than 50 watts except when measuring the gamma-lines, when about 350 watts were used.

The high voltage transformer was supplied with 60 cycle a.c. from a generator driven by a d.c. motor. The control arrangement which maintained the primary voltage constant to 0.1 percent has already been described.[25] The high voltage circuit was the balanced filament type[24] which corrects for changes of space charge, charges on the walls of the tube, and minute changes of pressure. Over a period of two or three hours the intensity was constant to better than one percent.

Experimental Procedure

The procedure for obtaining the contours of the various lines was as follows: The alpha-lines were observed first, recording the ionization current every second of arc in the vicinity of the

[21] Parratt, Phys. Rev. **49**, 280 (1936).
[22] Manning, Rev. Sci. Inst. **5**, 316 (1934).
[23] Bearden and Roseberry, Phys. Rev. **48**, 110 (1935).
[24] Bearden and Shaw, Phys. Rev. **48**, 18 (1935). In all tables the numbers in parenthesis are taken from this paper.
[25] Bearden and Shaw, Rev. Sci. Inst. **5**, 292 (1934).

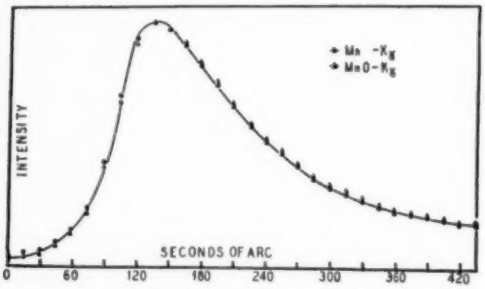

FIG. 1. Mn $K\gamma$ from targets of pure Mn and MnO. The two curves corrected for the effect of the β-line are superimposed with peaks matched. The width and asymmetry of the γ-line are not affected by chemical composition.

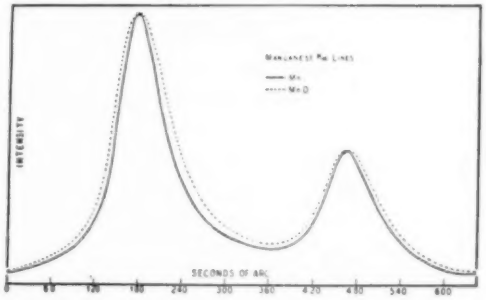

FIG. 2. Mn $K\alpha$ doublet from targets of pure Mn and MnO. The two curves are superimposed with peaks matched. The widths of the $K\alpha_1$-lines of Mn and MnO are 76.5″ and 93.7″ respectively, and the corresponding widths of $K\alpha_2$ are 89.3″ and 97.5″. The indices of asymmetries of the $K\alpha_1$-lines of Mn and MnO are 1.54 and 1.42 respectively, and of $K\alpha_2$, 1.17 and 1.21.

peaks. Then observations were repeated several times near the region of half maximum and at the peak of the line so that the width and asymmetry could be accurately determined. The same procedure was followed in the case of the beta- and gamma-lines. Observations on the alpha-lines were made consecutively without any changes of voltage and current through the tube, hence the ratio of the two peak intensities could be secured. Similarly consecutive observations were made on the beta- and gamma-lines, and the intensity ratio of the two peaks obtained. No correction for differential absorption due to the window of the tube or air path was made to obtain this ratio.

After the complete K-series had been finished, the alpha-lines were repeated to see if any chemical changes of the target material had taken place. The maximum deviation from the values of the widths as recorded in Table I did not exceed one second, though the curves were repeated after some 30 to 40 hours' operation of the tube.

The line widths and asymmetries of the K-series of the pure metals, copper, manganese, and titanium, were measured and found to be in excellent agreement with the results of Bearden and Shaw.[24] In the cases of iron, chromium, and zinc, new measurements were not made on the pure metals and the previous results[24] were used for comparison.

The base line of the alpha- and beta-lines was easily measured, and the widths, asymmetries and intensities were accurately determined. The base of the gamma-line had superposed upon it the foot of the intense beta-line. In the analysis of the gamma-line the following procedure was adopted. First, the curve for the pure metal and that of the compound were superimposed (with peaks matched) without any correction of base

TABLE I. *Effects of chemical composition on the widths of the emission lines of the K-series.*

Line.....	$K\alpha_1$			$K\alpha_2$			$K\beta$			$K\gamma$		
Target.....	Sec.	X.U.	Volts	Sec.	X.U.	Volts	Sec.	X.U.	Volts	Sec.	X.U.	Volts
Ti	80.9	1.06	1.74	109.3	1.43	2.34	109.8	1.46	2.87			
TiO_2	78.6	1.03	1.69	113.0	1.48	2.42	122.5	1.64	3.21			
Cr	(75.5)	1.03	2.43	(90.4)	1.23	2.90	(77.4)	1.07	3.05	(135.0)	1.86	5.38
Cr_2O_3	102.0	1.39	3.28	115.0	1.56	3.67	104.0	1.43	4.09	136.3	1.88	5.44
Mn	76.5	1.05	2.96	89.3	1.23	3.44	76.5	1.07	3.62	140.0	1.95	6.72
MnO	93.7	1.29	3.62	97.5	1.34	3.76	76.5	1.07	3.62	138.5	1.93	6.66
Mn_3O_4	100.2	1.38	3.88	103.3	1.42	3.98	76.3	1.06	3.61	140.0	1.95	6.72
Fe	(68.4)	.95	3.15	(80.1)	1.11	3.67	(73.2)	1.03	4.13	(119.0)	1.67	6.82
Fe_2O_3	85.2	1.18	3.92	84.8	1.18	3.88	85.2	1.19	4.81	118.5	1.66	6.79
Fe_3O_4	85.5	1.19	3.93	85.0	1.18	3.89	85.0	1.19	4.80	120.0	1.68	6.88
FeS	79.3	1.10	3.65	81.8	1.14	3.75	84.0	1.18	4.76	118.0	1.66	6.78
Zn	(36.9)	.527	3.18	(43.1)	.615	3.69	(63.5)	.911	6.73	(91.0)	1.30	9.83
ZnO	38.5	.549	3.32	42.6	.608	3.64	66.3	.951	7.03	92.0	1.32	9.91

TABLE II. *The effect of chemical composition on the indices of asymmetry and ratio of peak intensities.*

	INDEX OF ASYMMETRY				INTENSITY RATIOS	
	$K\alpha_1$	$K\alpha_2$	$K\beta$	$K\gamma$	α_1/α_2	β/γ
Ti	1.22	0.86	1.72		2.15	
TiO_2	1.01	1.00	1.76		2.43	
Cr	(1.37)	(1.03)	(1.53)	(2.54)	2.26[14]	
Cr_2O_3	1.36	1.03	1.54	2.58	1.92	40.1
Mn	1.54	1.17	1.37	2.35	2.20	50.0
MnO	1.42	1.21	1.75	2.36	2.16	52.1
Mn_3O_4	1.43	1.14	1.75	2.36	2.18	50.0
Fe	(1.61)	(1.26)	(1.75)	(2.44)	2.07[14]	
Fe_2O_3	1.61	1.24	1.79	2.46	1.85	32.9
Fe_3O_4	1.58	1.24	1.75	2.43	1.85	32.7
FeS	1.58	1.20	1.74	2.42	1.88	32.2
Zn	(1.12)	(1.33)	(1.48)	(3.02)	1.99[26]	
ZnO	1.12	1.33	1.46	3.05	1.74	34.4

line, to observe if the two contours fitted. The fit was in all cases within the error of observation. Second, the two curves were corrected for base line taking into account the effect of the beta-line, and third, as a final check, the two corrected curves were superimposed. The widths and asymmetries of the gamma-lines recorded in Table I are from the corrected curves. In Fig. 1 the corrected gamma curves of pure manganese and manganese oxide are superimposed showing how closely the two contours matched. In Fig. 2 the curves of the alpha-lines of pure manganese and manganese oxide are superimposed to illustrate the broadening due to chemical combination.

RESULTS

Widths of lines

There are recorded in Table I the effects of chemical composition on the full widths at half-maximum of the various lines of the K-series measured in the (1+1) order. The alpha-lines are not resolved into components because of the uncertainty as to how this resolution is to be affected, since there is not sufficient information on the shapes of the individual lines for this purpose. In general, the alpha-lines showed the largest broadening effect, the beta-lines being considerably less influenced. The gamma-lines exhibited no change in width within an estimated observational error of five percent. This high observational error results from the difficulty in determining the base line accurately.

The data concerning the effect of chemical combination on asymmetry (the ratio of the part of the full width at half maximum lying to the long wave-length side of the maximum ordinate to that on the short wave-length side) and the intensity ratios of the peaks of the various lines are given in Table II. The asymmetries of all the lines were unaffected with the exceptions of the alpha-lines of the TiO_2, and the $K\alpha_1$- and the beta-lines of MnO and Mn_3O_4. In both of these cases when the asymmetry of one line increases that of the other decreases.

TABLE III. *The alpha-doublet separation of the pure metals and their compounds.*

	Seconds	X.U.	$\Delta\lambda$ X.U.
Ti	139.5	3.65	
TiO_2	140.0	3.67	0.02
Cr	(143.0)	3.89	
Cr_2O_3	143.7	3.91	0.02
Mn	142.8	3.93	
MnO	143.5	3.96	0.03
Mn_3O_4	142.5	3.94	0.01
Fe	(141.2)	3.93	
Fe_2O_3	141.5	3.95	0.02
Fe_3O_4	141.7	3.95	0.02
FeS	141.2	3.93	0.00
Zn	(134.0)	3.82	
ZnO	133.7	3.81	0.01

Williams[26] has shown that in the present spectral region the correction to the intensity ratio $K\alpha_1$ to $K\alpha_2$ or $K\beta$ to $K\gamma$ for differential absorption in the target and windows is within the accuracy of observation; therefore no attempt was made to make these corrections. In the case of the beta to gamma intensity ratio which was secured from the corrected curves, no effect of chemical combination was observed. For the alpha-lines the ratio varied depending on the change of width involved; i.e., an increase of width was accompanied by a decrease of the intensity ratio, and *vice versa*. With the exceptions of the oxides of manganese this increase or decrease of the intensity ratio of the alpha-lines was very pronounced.

Alpha-doublet separation

The alpha-doublet separations obtained in the present work for the pure metals and their compounds are given in Table III. Because of the high resolving power of the double crystal spectrometer and the greater accuracy of the ionization method of recording the intensity distributions in wave-length, the doublet separa-

[26] Williams, Phys. Rev. **44**, 140 (1933).

tion as obtained is more reliable than former data secured by photographic methods. The angular distance between the two peaks could be repeated with an accuracy of one second (=0.03 X.U.). Within this experimental deviation the separation of the alpha doublet was unaffected by chemical composition.

Discussion

Titanium

The pure metal has a cubic crystal form and the oxide used (TiO_2, spectroscopically pure rutile) has a tetragonal crystal form. The results obtained in the case of TiO_2 were different from those found for the other chemical compounds, in that the $K\alpha_1$-line showed a *decrease* of width of 3 percent, while the $K\alpha_2$-line showed an *increase* of width of 3 percent, and the beta-line showed an increase of width of 11 percent. The indices of asymmetry for Ti $K\alpha_1$ for the pure metal and the oxide were respectively 1.22 and 1.01 and for Ti $K\alpha_2$ 0.86 and 1.00. Hence a decided effect of chemical composition is noted on the asymmetries of these lines.

Chromium

The pure metal has a cubic crystal form, while the crystal form of the oxide Cr_2O_3 is hexagonal. The $K\alpha_1$-line was broadened 35 percent, the $K\alpha_2$-line was broadened 27 percent, and the beta-line was broadened 34 percent. No effect was noted for the gamma-line, its width and asymmetry remaining the same as that for the pure metal.

Iron

The crystal forms of iron and Fe_3O_4 are cubic, and those of Fe_2O_3 and FeS are hexagonal. The $K\alpha_1$-lines of Fe_2O_3 and Fe_3O_4 were both broadened 25 percent, and the $K\alpha_1$-line of FeS was broadened 16 percent. The $K\alpha_2$-lines of the two oxides were broadened 6 percent and that of the sulfide 2 percent. The beta-lines of the oxides were broadened 16 percent, and that of the sulfide 14 percent. In the case of the lines of Fe_2O_3 and Fe_3O_4 where the same percent of broadening was experienced, there is represented an example in which the broadening of a line cannot be correlated with the crystal structure, for the crystal forms of these two oxides are different. The widths of the gamma-lines from the oxides and the sulfide remained the same as that of the pure metal within experimental error. No change of asymmetry was observed for any of the K-series lines.

Manganese

The crystal forms of the pure metal and MnO are cubic and Mn_3O_4 is tetragonal. The striking result in this case is that no broadening was observed for either the beta- or gamma-lines of any of the compounds. The $K\alpha_1$-line of MnO was broadened 22 percent and that of Mn_3O_4 30 percent. The $K\alpha_2$-line of MnO was broadened 9 percent and that of Mn_3O_4 was broadened 16 percent. The asymmetries of the $K\alpha_1$-lines of the oxides changed slightly but no effect was noted in the case of the other lines.

Zinc

The crystal form of the pure metal and that of the oxide are hexagonal. Only a small broadening of the lines was noted in this case. The $K\alpha_1$- and beta-lines broadened 4 percent and the $K\alpha_2$-line broadened 1 percent. The gamma-line was unaffected.

The question of just how atomic environment affects the energy states of the emitter and changes the widths of the lines as observed here is not obvious. In some way the lifetime of the excited state appears to be changed, but just why the electrons in the L-shell are those which are usually affected is not clear, when one would expect the electrons in the outer shells to be affected by chemical combination more than the internal electrons. Other factors which may need to be considered in framing a satisfactory theory are: the Auger effect, the role played by valence forces, the effect of field potentials on the energy levels, and the probability distributions for the different levels.

We are greatly indebted to the Naval Research Laboratory for the generous loan of the Gaertner double crystal spectrometer used in the present investigation. The sample of spectroscopically pure TiO_2 was supplied by the Titanium Alloy Manufacturing Corporation.

The Infrared Absorption of CS_2 at 4.57μ

J. A. SANDERSON, *The Johns Hopkins University, Baltimore, Md.*

(Received August 6, 1935)

The rotational structure of the infrared absorption band of CS_2 lying at 4.577μ has been partially resolved. Average values of B and B' were found to be 0.112 and 0.111, while the separation of the P and R branches of the band is 13.3 cm^{-1}. The best representation of the positions of the rotational lines is by means of the relation $\nu = 2184.50 + 0.224M - 0.00025M^2$. The location of the center of the band at 2184.5 cm^{-1} does not agree with previous determinations of 2179 cm^{-1} and 2167 cm^{-1} by Bailey and Cassie.

INTRODUCTION

RECENT developments in the theory of the infrared spectra of polyatomic molecules have made measurements on the absorption bands of some of the simpler molecules desirable. A number of triatomic molecules have been investigated, and one of these, CO_2, has been completely solved.[1] It has been definitely established that the CO_2 molecule is linear and symmetric. In view of the success with CO_2 it seemed of interest to examine the spectrum of CS_2 since this molecule has the same symmetry characteristics as CO_2. This paper is the report of an attempt to resolve the rotational structure of the CS_2 absorption band lying at 4.57μ.

The infrared absorption spectrum of CS_2 was first mapped by Bailey and Cassie[2, 3] and by Dennison and Wright.[4] The Raman spectrum was first studied by Krishnamurti.[5] The results of these investigations are shown in Table I in which the assignment of frequencies is due to Bailey and Cassie.[3]

Of the various infrared absorption bands, the one lying near 4.6μ is most suitable for study under high dispersion, since it is found in a region of the spectrum which is relatively free from atmospheric absorption, and in which reasonably large energies are available.

TABLE I. *Infrared and Raman bands of CS_2.*

Origin	Wave-length	Frequency cm^{-1}	P–R Separation cm^{-1}	Reference
ν_2	25.2	396.8	16.4	4
ν_1 (Raman)	15.3	655.5		5
$\nu_3-\nu_1$	11.391	878	13	2
ν_3	6.566	1523	12	2
	4.591	2179	12.0	2
$\nu_3+\nu_1$	4.615	2167	13.3	3
	4.577	2184.5	13.3	This paper
$\nu_3+2\nu_2$	4.292	2330		2

APPARATUS AND METHODS

This band has been investigated using a Pfund stigmatic spectrometer[6] equipped with a 4800 line/inch echelette grating which concentrated at 4.3μ. Elimination of overlapping higher order spectra was effected by the use of a filter prepared by evaporating selenium onto rocksalt at low pressure.[7]

As a source of energy a Globar heater was used. Globar is a carborundum product which is widely used for heating elements in electric furnaces. It possesses the characteristic that the intensity of the radiant energy of wave-length 2μ is much weaker than the 2μ energy from a Nernst glower, while for longer wave-lengths its emission is comparable with that of the Nernst glower. This property aids materially in the purification of the spectrum.

The heater elements have been constructed by grinding down the central portion of a 3-inch length of Globar $\frac{5}{16}$ inch in diameter to a diameter of $\frac{3}{16}$ inch, leaving about $\frac{1}{2}$ inch at each end of the stick unaltered in size so that excessive heating of the contacts will not occur. On account of the extreme brittleness of the elements it is necessary that they be mounted quite loosely.

[1] Adel and Dennison, Phys. Rev. **43**, 716 (1933).
[2] Bailey and Cassie, Proc. Roy. Soc. **A132**, 236 (1931).
[3] Bailey and Cassie, Proc. Roy. Soc. **A140**, 605 (1933).
[4] Dennison and Wright, Phys. Rev. **38**, 2077 (1931).
[5] Krishnamurti, Ind. J. Phys. **5**, 109 (1930).
[6] A. H. Pfund, J. Opt. Soc. Am. and Rev. Sci. Inst. **14**, 337 (1927).
[7] A. H. Pfund, J. Opt. Soc. Am. **23**, 375 (1933).

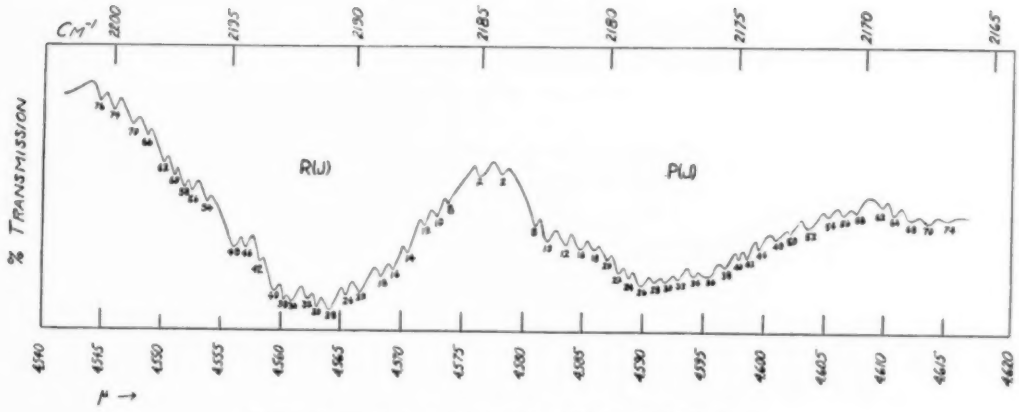

FIG. 1. Transmission curve for the 4.57μ band of CS_2 vapor.

In one type of mounting which has been successful the upper end of the element is clamped in a block of aluminum by means of a set screw, while the lower end dips into an aluminum cup which is filled with molten tin. Good electrical contact is thus provided, and when the element cools it takes a strain-free position in the tin. A heater constructed in this manner is readily adaptable to enclosure in a water jacket and provides a constant source of energy which will perform for several months without attention.

Energies were measured by means of a radiometer, the vanes of which were coated with zinc black. The instrument was mounted on a Mueller[8] vibration-free support, and deflections read on a scale at 3 meters distance were easily repeated.

The CS_2 vapor was enclosed in a glass cell 10 cm long closed at the ends by polished rocksalt windows which were held on by shellac. The cell was evacuated and pure CS_2 allowed to distill into it, care being taken to see that no free liquid condensed on the windows or walls of the cell.

Even with the most sensitive radiometer it was possible to devise it was necessary to use much wider slits than good practice dictates. The slits were of about the same effective width as the average separation of the rotational lines in the spectrum, namely 0.45 cm^{-1}. Use of slits of this relative width introduces many uncertainties into the location of the positions of the lines and impairs the resolving power of the instrument to a great extent, but there can be no doubt that the spectrum which was obtained is due to CS_2. Repeated measurements were made, and average values of the positions of the lines were taken. No lines are recorded which did not appear in all runs. All readings were taken first with the cell in the light path and then with the cell replaced by compensating rocksalt plates, the ratios of the radiometer deflections so obtained being plotted against wave-length. No lines appeared when measurements were made with an empty cell, thus disposing of the possibility that an interference spectrum was under observation. The absorption curve is shown in Fig. 1.

Discussion of Results

The numerical data are presented in Table II. Twenty-seven lines in the R branch and thirty in the P branch have been resolved. Due to the antisymmetrical nature of the wave function in the sulphur nuclei, alternate rotational lines are missing. Since both the oxygen and sulphur nuclei obey the same statistics, the missing lines in the CS_2 spectrum are those for which the J of the lower state is odd, as is the case for CO_2. Column 1, Table II, gives the values of J in the initial, or lower, state; Columns 2 and 3 give the observed frequencies of the lines in the R and P branches. Columns 4 and 5 show the frequency differences for the upper and lower vibrational states represented by

[8] R. Mueller, Ann. d. Physik **1**, 613 (1929).

$$R(J-1)-P(J+1)$$
$$=[F'(J)-F(J-1)]-[F'(J)-F(J+1)]$$
$$=F(J+1)-F(J-1)=(4J+2)B,$$
$$R(J)-P(J)$$
$$=[F'(J+1)-F(J)]-[F'(J-1)-F(J)]$$
$$=F'(J+1)-F'(J-1)=(4J+2)B',$$

where $F(J)=A+BJ(J+1)$, $B=h/8\pi^2Ic$, and primes refer to the upper state. Values of B and B' are given in Columns 6 and 7. The average values of these quantities are $B=0.112$ and $B'=0.111$. These values represent one-fourth of the separation of the rotational lines in the P and R branches of the band.

The positions of the lines in the band are reasonably well represented by the formula

$$\nu=2184.50+0.224\,M-0.00025\,M^2,$$
$M=J+1$ for lines in the R branch,
$M=-J$ for lines in the P branch.

The average deviation of the calculated positions of the lines from the measured positions is ± 0.14 cm^{-1}.

TABLE II. *Data on R and P branches in CS_2 spectrum.*

Initial J	$R(J)$	$P(J)$	$D(J+1)$	$D'(J)$	B	B'
2	2185.17	2184.28				
4						
6						
8	2186.26	2182.83	4.10	3.43	.107	.100
10	2186.74	2182.16	5.15	4.58	.112	.109
12	2187.20	2181.59		5.61		.112
14	2187.75		6.73		.108	
16	2188.42	2181.02	7.92	7.40	.113	.112
18	2188.80	2180.50	8.83	8.30	.113	.112
20		2179.97				
22	2189.76	2179.59	10.50	10.17	.111	.110
24		2179.26				
26	2190.34	2178.83	12.17	11.51	.110	.109
28	2190.82	2178.17	13.08	12.65	.110	.109
30	2191.44	2177.74	14.22	13.70	.112	.112
32	2191.88	2177.22	15.30	14.66	.114	.112
34		2176.58				
36	2192.50	2176.04	17.01	16.46	.113	.112
38	2192.86	2175.49	17.96	17.37	.113	.113
40	2193.39	2174.90	18.82	18.49	.113	.114
42	2193.80	2174.57	19.80	19.23	.113	.113
44		2174.00				
46	2194.57		21.23		.111	
48	2195.00	2173.34	22.18	21.66	.112	.111
50		2172.82				
52		2172.14				
54	2195.97	2171.50	25.08	24.47	.113	.112
56	2196.47	2170.89	26.01	25.58	.113	.113
58	2196.98	2170.46		26.52		.111
60	2197.32		27.89		.113	
62	2197.80	2169.43	28.84	28.37	.113	.113
64		2168.96				
66	2198.52		30.27		.112	
68		2168.25				
70	2199.01	2167.69		31.32		.111
72						
74	2200.00	2166.80		33.20		.111
76	2200.40					

TABLE III. *Moment of inertia and internuclear distance in CS_2.*

	$I\times10^{-40}$ gm cm^2	r_0 A.U.
From doublet separation	262	1.57
From $B'=0.111$	249	1.53
From $B=0.112$	247	1.52

In their first survey of the band under consideration, Bailey and Cassie,[2] using a prism spectrometer, located the center at 2179 cm^{-1} and found the separation of the P and R branches to be about 12 cm^{-1}. In a subsequent study of the same band by means of a grating spectrometer the center of the band was found to lie at 2167 cm^{-1}, and the $P-R$ separation was found to be 13.3 cm^{-1}.[3] The results of the present investigation of the band are in agreement with the doublet separation of 13.3 cm^{-1} found by Bailey and Cassie, but the center of the band has been found to lie at 2184.50 cm^{-1}. The wave-length measurements have been very carefully checked, and no obvious source of error has been located.

Values of the moment of inertia of the molecule obtained from the doublet separation and from the average values of B and B', and values for the internuclear distance are given in Table III.

The value for r_0 obtained by Wierl[9] from electron diffraction experiments is 1.6 A.U.

In conclusion, the writer wishes to thank Professors A. H. Pfund and G. H. Dieke for valuable assistance in various phases of the problem.

[9] R. Wierl, Physik. Zeits. **31**, 1028 (1930).

Positive Ray Analysis of Ions from a High Frequency Spark

SHENG-LIN CH'U, *Ryerson Physical Laboratory, University of Chicago*

(Received August 7, 1935)

This paper gives the analysis by the Thomson parabola method of the positive rays of various materials produced by the high frequency spark method developed by Dempster. The spark materials investigated may be classified into three groups, i.e., metals of high melting point, metals of low melting point and minerals. It was found that almost all the ions obtained were atomic and that most of the elements gave multiply charged ions. The change of charges during the passage from the accelerating field to the analyzing field was also observed. Ions of the elements which exist ordinarily in the gaseous state were obtained from the solid compounds of which these elements form constituents. Helium ions were obtained from the radioactive mineral, cleveite ($UO_2 \cdot UO_3 \cdot PO \cdot ThO_2$). From the experiments thus far performed, the high frequency spark method has been shown to be able to give strong sources of multiply charged ions of almost all the elements.

IN a previous paper A. J. Dempster[1] has discussed various forms of spark sources for positive ions, and pointed out the possibility of obtaining charged ions from a high frequency oscillatory discharge between metal electrodes in a high vacuum. This paper forms an extension of those experiments and gives the analysis by the Thomson parabola method of the ions formed by sparks between electrodes of a great many elements.

The mounting of the spark electrodes is shown in Fig. 1. The two electrodes are held in position by means of two sylphon bellows and three screws attached to each of the bellows between *AB* and *BC* so that by adjusting the screws the upper electrode can be moved with respect to the lower one, and in addition the whole spark gap moved with respect to the circular aperture S_1. The lower electrode is attached to the metallic part of the spark chamber and the upper one is insulated by means of a thick wall glass tube. The two metallic disks between which the ions are accelerated are held parallel by three alsimag insulators kindly supplied by the American Lava Company, so that the apertures S_1, S_2 and S_3 (Fig. 1) once adjusted will remain in a straight line throughout the experiments. These two disks forming a unit are screwed onto the cylindrical chamber and can be detached for changing the electrodes. The whole spark chamber is mounted on the analyzing chamber by three threaded rods of linen Bakelite between *C* and *D*. The glass tube forming the wall of the vacuum space is waxed to the metal part with picein wax. A large side tube is connected for exhausting. Holes are also made in the metal cylinder inside the glass tube to facilitate the evacuation and serve as windows through which the spark may be observed. The Tesla circuit is arranged in a compact form and immersed in a five-gallon earthenware jar filled with oil.

The analyzing chamber with the spark chamber attached is shown in Fig. 1. The chamber is a brass casting, and the axis of the spark chamber and the collimating system is inclined at an angle such that the direct beam hits close to the upper edge of the photographic plate. The aperture S_3 at the end of the collimating tube has a diameter of 0.1 mm. The other two, S_1 and S_2 mentioned before, are of $\frac{1}{2}$ and $\frac{1}{4}$ mm diameter respectively. The analyzing fields lie just beyond the aperture S_3. The magnetic pole pieces are fastened on a brass frame which is made to fit inside the chamber. The upper and lower brass walls of the chamber in contact with the pole pieces are cut out and iron pieces inserted so that an electromagnet can be placed outside the chamber. The negative terminal of the deflecting potential is connected to a thin brass plate which is attached to the lower magnetic pole, and insulated by a piece of amber; the upper magnetic pole piece which has metallic contact with the wall of the chamber serves at the same time as the positive electric plate. It was found necessary to shield the battery and the leads in order to avoid fluctuation of potential while the oscillating circuit is functioning. The photographic plate holder was each time waxed onto the chamber with picein wax. A wide tube shown in the

[1] A. J. Dempster, Rev. Sci. Inst. **7**, 46 (1936).

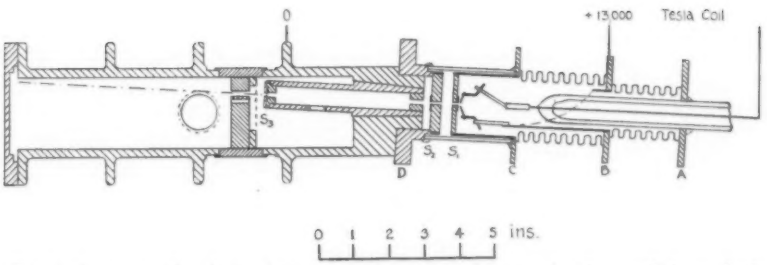

FIG. 1. Apparatus for the analysis of ions from a spark source by the parabola method.

diagram by a circle serves to evacuate the chamber.

A constant accelerating potential applied across the gap between S_1 and S_2 is obtained from a rectifier (FP-85) together with a large capacity condenser and a choke. The average current through the spark as measured by a thermocouple ammeter was between 0.1 and 0.25 ampere.

The materials thus far investigated may be classified into three groups, namely, (1) metals of high melting point, (2) metals of low melting point, below 1000°C, and (3) minerals. With the materials of the first group, electrodes were prepared by cutting a short rod of the metal, about 5 or 6 mm long and 1 mm in diameter. The materials of the second group were put in nickel tubes of about 1 mm diameter, which were then fixed into the electrodes in the same way as the metal rods of the first group. Some soft metals such as lithium and barium were simply pressed into the nickel tube. Some, such as tin and lead, were melted in the tube by heating. The titanium metal is very brittle, so that it is difficult to cut out a thin rod. Also because of its reaction with any metal upon heating, a thick wall nickel tube was used and filled with powdered metal. Minerals were usually ground into powder and then put into the nickel tube. The nickel tubes filled with the material were used only as the lower electrode, the upper one being simply a nickel rod.

The pressure under which the spark was produced was about 10^{-5} mm. With an accelerating potential of about 13 kv, positive ray pictures were obtained by an exposure of two to three minutes with Schumann plates. Examples are given in Fig. 2.

With this arrangement of apparatus, ions were all produced in the spark region where the electric field was low, due to the intense ionization in the spark, and were then accelerated across a constant high potential of 13 kv. Ions of the same value of e and m would therefore have the same energy when entering the analyzing fields and would have the same deflections. Thus the patterns obtained consist of discrete spots instead of continuous parabolas. Analysis of the pattern can be made by means of the general consideration given below.

It was originally shown by J. J. Thomson[2] that deflections of the path of ions passing through electric and magnetic fields perpendicular to the direction of motion are given respectively by $x=AeE/mv^2$ (1), and $y=BeH/mv$ (2), where A and B are constants. Eliminating v from (1) and (2), one gets $y^2=(B^2H^2/AE)(e/m)x$ (3), showing that particles of the same value of e/m but different v lie on the same parabola. As the particle may be multiply charged, one may put $e=ne_0$ where e_0 is the electronic charge. Now if we consider a particle having a charge ne_0 during acceleration and $n'e_0$ during deflection, (1) and (2) become $x=A(n'e_0/m)(E/v^2)$ (4) and $y=B(n'e_0/m)(H/v)$ (5). Also $\frac{1}{2}mv^2=Vne_0$ (6). Substituting the v from (6) into (4) and (5), one gets $x=A(E/2V)(n'/n)$ (7) and $y=BH(e_0/2V)\times(n'/nm)$ (8). From (8) and (9), when n is eliminated, $y^2=(B^2H^2/AE)(n'e_0/m)x$, and when n' is eliminated, $y=(BH/AE)(2Ve_0/nm)x$. Therefore for a given mass m, spots of the same n' but of different n lie on a parabola and spots of same n but of different n' lie on a straight line passing through the origin. A theoretical pattern for a constant m is shown in Fig. 3.

[2] J. J. Thomson, *Rays of Positive Electricity*, 2nd ed., pp. 16–21.

Now in general a particle may retain its charge or lose it partly or completely by capturing electrons during its passage from the accelerating gap to the deflecting fields. The converse phenomenon, that is an increase of charge, was not observed.

For different values of m, the same pattern will be repeated with only a shift of y value, x will be the same for all values of m as shown by (7).

Along the line A (Fig. 3), $n=n'$ for each point, then (7) and (8) become $x=AE/2V=$constant, and $y=BH(e_0/2V)(n/m)$, or $y^2m/n=K$ (9). Thus by measuring the y distance along the line A and taking into consideration the fact that points of low value of n or n' always appear strong, one can easily identify the elements corresponding to points on the photographic plates and assign the proper number of charges.

Almost all the ions were atomic except that sometimes a weak trace of the hydrogen molecule ion appeared. Isotopes of light elements such as lithium and boron were clearly resolved.

Most of the elements gave multiply charged ions. Hydrogen, lithium, sodium and potassium had only singly charged ions, beryllium and barium were singly and doubly charged, boron and aluminum singly, doubly and triply charged and carbon with all charges up to four. These phenomena agree with other experiments in showing the existence of the easily ionized valence electrons in atoms. But elements which possess more than four valence electrons did not give higher multiplicity of charge. This is perhaps due to the comparatively high ionization potential of the remaining electrons.

The materials examined are listed below. The various charged ions found are given, followed by the changes of charge observed, the figures in brackets (nn') indicate an ion of n' charges, with the energy of an ion originally accelerated with n charges.

Iron treated with hydrogen Fe^+ Fe^{++} Fe^{+++} H^+ H_2^+ O^+ O^{++} C^+ C^{++} C^{+++} Fe (31)(21)(32)

Steel Fe^+ Fe^{++} Fe^{+++} C^+ C^{++} C^{+++} O^+ O^{++} N^+ Fe (41)(31)(21)(42)(32)(43)

Cu and Al Alloy Cu^+ Cu^{++} Cu^{+++} Al^+ Al^{++} Al^{+++} O^+ C^+ Cu and Al (31)(21)(32)

Speculum metal Cu^+ Cu^{++} Cu^{+++} Cu^{++++} Sn^+ Sn^{++} Sn^{+++} Sn^{++++} O^+ C^+ N^+ Cu and Sn (41)(31)(21)(42)(32)(43)

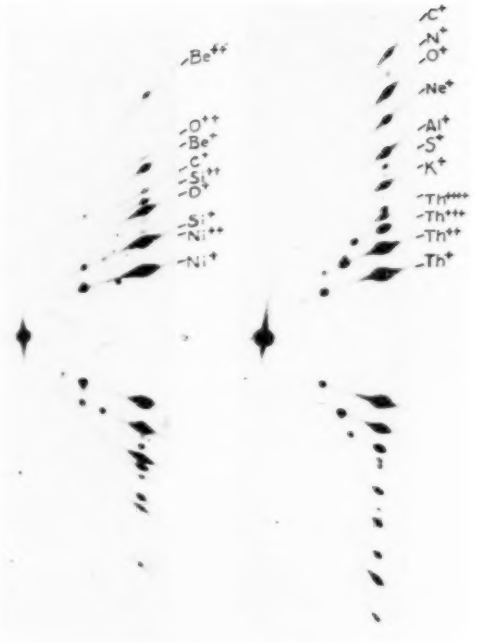

FIG. 2. (a) Ions from beryl, (b) ions from thorium.

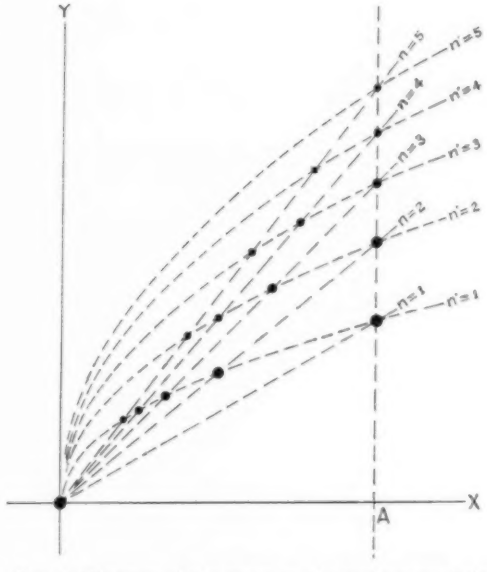

FIG. 3. Diagram of the spots on the various parabolae due to ions analyzed with n' charges, when they were originally accelerated as ions having n charges.

Titanium metal Ti^+ Ti^{++} Ti^{+++} Ti^{++++} O^+ O^{++} C^+ C^{++} Ti (41)(31)(21)(32)
Thorium metal Th^+ Th^{++} Th^{+++} Th^{++++} K^+ Cl^+ S^+ Al^+ O^+ O^{++} N^+ N^{++} C^+ C^{++} $^{20}Ne^+$? Th (31)(21)(42)(32)(43)
Nickel (tested with other materials) Ni^+ Ni^{++} Ni^{+++} Ni^{++++} Ni (31)(21)(32)
Pencil core C^+ C^{++} C^{+++} C^{++++} Na^+ K^+ Fe^+ Si^+ or Al^+? C (31)(21)
Lithium metal $^6Li^+$ $^7Li^+$ ($^6Li^{++}$ $^7Li^{++}$) (very weak) O^+ N^+ C^+
Beryllium metal Be^+ Be^{++} O^+ O^{++} C^+ N^+ N^{++} H_2^+ Be (21)
Barium metal Ba^+ Ba^{++} Ba^{+++} Tl^+ Y^+ Sc^+ O^+ O^{++} C^+ N^+ N^{++} Ba (31)(21)
Cerium metal Ce^+ Ce^{++} Ce^{+++} H^+ H_2^+ H_3^+ Ce (31)(21)(32)
Tellurium metal Te^+ Te^{++} Te^{+++} $^{21}Ne^+$? Te (31)(21)
Tin Sn^+ Sn^{++} Sn^{+++} Sn^{++++} O^+ C^+ Sn (41)(31)(21)(42)(32)(43)
Lead Pb^+ Pb^{++} O^+ O^{++} C^+ C^{++} Pb (31)(21)(32)
Ferro-boron Fe^+ Fe^{++} Fe^{+++} $^{10}B^+$ $^{10}B^{++}$ $^{10}B^{+++}$ $^{11}B^+$ $^{11}B^{++}$ $^{11}B^{+++}$ O^+ O^{++} N^+ N^{++} Na^+ K^+ Fe (31)(21)(32)B (31)(21)
Boron carbide and Uranium oxide $^{10}B^+$ $^{10}B^{++}$ $^{10}B^{+++}$ $^{11}B^+$ $^{11}B^{++}$ $^{11}B^{+++}$ C^+ C^{++} C^{+++} U^+ U^{++} U^{+++} O^+ O^{++} Na^+ K^+ B (31)(21)(32) U (21)(32) O (21)
Spodumene $LiAl(SiO_3)_2$ $^6Li^+$ $^7Li^+$ O^+ O^{++} O^{+++} Si^+ Si^{++} Si^{+++} Na^+ K^+ Rb^+ Cs^+ Si (21)
Uranium oxide U_3O_8 U^+ U^{++} U^{+++} O^+ O^{++} O^{+++} C^+ C^{++} Na^+ K^+ U (31)(21)(32)
Beryl $Be_3Al_2(SiO_3)_6$ Be^+ Be^{++} Si^+ Si^{++} O^+ O^{++} O^{+++} N^+ N^{++} C^+ C^{++} Be (21) Si (31)(21)(32)
Goethite FeO(OH) H^+ H_2^+ Fe^+ Fe^{++} Fe^{+++} O^+ O^{++} O^{+++} C^+ C^{++} Fe (31)(21)(32)
Manganite MnO(OH) H^+ H_2^+ O^+ O^{++} C^+ Mn? (not observed)
Cleveite $UO_2 \cdot UO_3 \cdot PbO \cdot ThO_2$ He^+ H^+ H_2^+ O^+ O^{++} O^{+++} U^+ U^{++} U^{+++} C^+ C^{++} U (31)(21)(32).

Oxygen and nitrogen were present almost on every plate due to the residual air in the system and carbon also sometime appeared due to grease vapors. These gas ions usually gave a short line rather than a sharp spot. Ions of the elements which exist ordinarily in the gaseous state can also be obtained from the solid compounds of which those elements form constituents. Thus some of the minerals tested were compounds containing hydrogen and oxygen, often oxides with water of crystallization. Ions of the latter two elements were strongly shown on the plates.

Hydrogen ions can also be obtained from the metals which absorb this gas. Iron, which had been treated with hydrogen at high temperature, kindly supplied by Mr. P. P. Cioffi of the Bell Laboratories, gave strong spots of hydrogen. It was found that cerium metal served also as a strong source of hydrogen, singly charged ions of H_1, H_2 and H_3 were all present. The metal evidently absorbs large quantity of hydrogen gas. But care must be taken not to drive off the absorbed gas by preliminary heating in the vacuum. It was found that a second photograph gave much weaker hydrogen spots than the first one. With both of these sources H_1 always appeared strongest.

To get strong positive rays from inert gases with the spark method is still somewhat of a problem. An attempt was made to get helium ions from radioactive minerals which presumably contain helium gas. It was found that cleveite ($UO_2 \cdot UO_3 \cdot PbOThO_2$) gave a comparatively strong trace of helium at the first photograph, but a very weak one at the second.

The high frequency spark method has thus been shown to be able to give strong sources of multiply charged ions of almost all the elements.

The writer wishes to express his most sincere thanks to Professor A. J. Dempster who proposed this problem and has given constant guidance and inspiration throughout the investigation. He also wishes to thank Dr. A. E. Shaw for suggestions and help during the construction of the apparatus.

The Energy Distribution of Secondary Electrons from Columbium

L. J. HAWORTH, *Department of Physics, University of Wisconsin*

(Received May 18, 1936)

Energy distribution curves of secondary electrons from an outgassed columbium target have been obtained with the same apparatus as in similar studies on molybdenum. The results from Cb are qualitatively similar to those from Mo. "Discrete loss" and "fixed energy" groups of secondary electrons are observed at energies which are in most cases slightly less than the corresponding ones in the case of Mo. The number of elastically reflected electrons was also studied as a function of primary energy. The curve shows marked similarity to that obtained from Mo, the peaks again being at somewhat lower energies in the case of Cb. It is shown that the lower values of the energies involved in the various phenomena in the present case are to be expected because of the lower atomic number of Cb and because of its larger lattice constant.

IN a previous investigation[1] it was found that the energy spectrum of secondary electrons from a thoroughly outgassed molybdenum target bombarded with relatively low energy primary electrons exhibited two types of fine structure: (1) three "discrete loss" peaks at energies certain fixed amounts less than that of the primary electrons; (2) three "humps" in the curves at definite secondary energies independent of the primary energy. The efficiency of elastic reflection of the primary electrons as a function of the primary energy was also investigated. The curve plotted from these data also exhibited many peaks and irregularities. Possible interpretations of the results in terms of x-ray and optical levels and of the banded structure of the allowed energies of the conduction electrons were discussed.

In the present paper are described the results of similar experiments using columbium as a target material. This metal was chosen for various reasons. It is next below molybdenum in the periodic table and has the same crystal structure. Furthermore a sample of columbium which had been thoroughly outgassed was kindly made available by Professor H. B. Wahlin who had used it in his thermionic studies of that metal.[2]

A small amount of data obtained some years ago from a target of rhodium is also included.

[1] L. J. Haworth, Phys. Rev. **48**, 88 (1935). An error in this paper has recently been called to the author's attention. The integration limits of curve *a*, Fig. 5, were zero to 6 volts rather than zero to 10 volts as there stated.

[2] H. B. Wahlin and L. O. Sordahl, Phys. Rev. **45**, 886 (1934).

Apparatus and Procedure

The energy distribution of secondary electrons was determined by magnetic analysis using the apparatus already described,[1] with a few minor improvements.

The part of the tube containing the Faraday collector, the amplifying vacuum tube and the grid circuit of the latter were more carefully shielded than before, this time by five grounded layers of copper and tinfoil separated from each other by 1 cm layers of insulating material. The remainder of the apparatus, research tube, leads, rheostats, meters, batteries, etc., was surrounded by single copper and tinfoil shields. All elements of the tube except the Faraday collector were grounded through shielded $4\mu F$ paper condensers. With these precautions it was found that the amplifier was comparitively steady even when severe electrical disturbances were taking place in other parts of the laboratory.

The additional steadiness thus obtained allowed the use of a more sensitive amplifier, which in turn made possible an increase in resolving power by narrowing the analyzer slits.

The Cb furnished by Professor Wahlin was in the form of a long thin ribbon 2.5 mm in width. This was cut into short pieces which were then laid side by side with a slight overlap and spot welded together at the ends. The foil thus formed was laid on the face of the molybdenum target cylinder previously used and protruding edges were bent over and wired.

The outgassing of the columbium in the present research tube extended over some 1500 hours during which period a high vacuum was maintained continuously. As both the target and

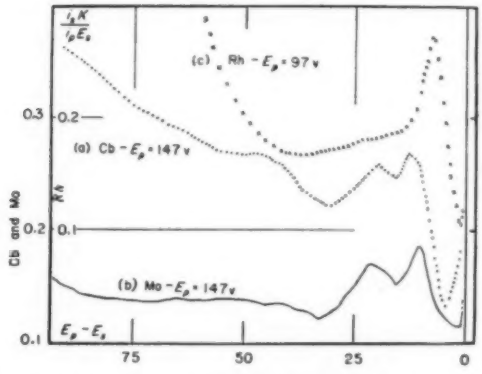

FIG. 1. Discrete loss peaks. Experimental points are indicated on curves *a* and *c*.

the cylinder supporting it had been previously well degassed the process proceeded more rapidly than had new materials been used. At the end of 1000 hours of heating the pressure in the system was 3×10^{-7} mm Hg when the target was hot (1700°K) and 2.5×10^{-8} when it was at room temperature. At this point the ionization gauge unfortunately failed. The McLeod gauge continued, however, to register zero throughout the investigation and it is believed that the vacuum continued to be at least as good as indicated above.

The rhodium, in the form of a thin ribbon filament,[3] was outgassed only 200 hours, after which the filament burned out. Only a very limited amount of data was obtained before this failure.

RESULTS

The number of secondary electrons per primary electron was plotted as a function of secondary energy, proper corrections being made for dispersion by dividing the secondary/primary ratio by the secondary energy.

The distribution curves obtained were qualitatively very similar to those from molybdenum, as to both general form and fine structure. The general shape of the curves is well illustrated by Fig. 2, curves *a*, *b*, *c* of the previous paper.[1]

Discrete loss peaks appeared at energies 12.6, 19.5, and approximately 44 volts less than that of the primary electrons (curve *a*, Fig. 1). The peaks in the case of columbium are somewhat less intense than and a few volts removed from the corresponding ones at 10.6, 22 and 48 volts in the case of molybdenum which are shown in curve *b* for comparison. The peak at 44 volts on the columbium curve is much narrower than is the broad band centering around 48 volts on the molybdenum curve.

Fixed energy groups appear at energies of 9, 21 and 31 volts on an absolute scale (curve *a*, Fig. 2) as compared to 11, 24 and 35 volts in the case of molybdenum (curve *b*). The magnitudes of the irregularities are much less in the case of columbium than in that of molybdenum. This is not necessarily of any great significance as the columbium was probably not as gas free as was the molybdenum and it was observed in both cases that very small amounts of gas were sufficient to entirely mask this effect. It should be mentioned in this connection that no observations were taken at low secondary energies during the later stages of the outgassing. It had been intended to repeat these observations later but an accident to the tube prevented. The 9 volt fixed energy group may have suffered an apparent loss in intensity on account of its position on the curve near the large maximum at 4.5 volts.

The number of elastically reflected secondary electrons is plotted as a function of primary energy for both columbium and molybdenum in Fig. 3. Each curve is marked by a large permanent decrease in the number of elastically reflected electrons as the primary energy is

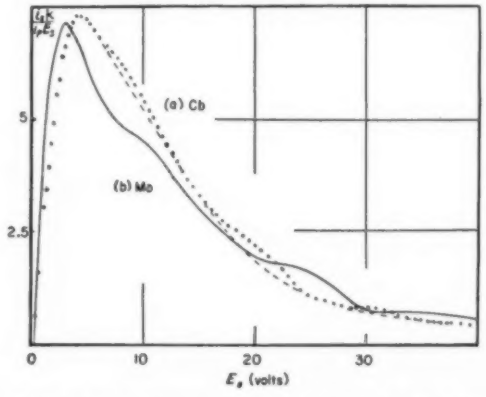

FIG. 2. Low energy secondary electrons showing fixed energy groups. Dots (curve *a*) are experimental points. The dashed line indicates the probable background curve.

[3] The first form of target described in reference 1.

TABLE I. *Energies (in volts) of the various maxima of Fig. 3.*

Cb	2.5	5.0	9.5	12.0	18.5	25.3	32.0	49.0	——	81.5 ——
Mo	3.6	7.6	12.0	——	20.8	28.8	——	50.7	78.5	—— 101

increased beyond a certain point (about 25.5 volts for Cb, 29 volts for Mo), and by a number of maxima and irregularities, principally at low energies. There seems to be a certain correspondence between most of the irregularities of the two curves as indicated by Table I, the peaks occurring at somewhat lower energies in the case of columbium than do the corresponding ones in the case of molybdenum. None of the four peaks[4] which apparently occur for only one metal are very large. The peak at 78.5 for molybdenum was observed in the case of only one specimen out of three well outgassed specimens studied. In fact, it was not the most thoroughly outgassed of the three and was not the one illustrated in Fig. 3. An irregularity similar to the one occurring at 32 volts on the columbium curve was observed at about 34 volts in the case of incompletely outgassed molybdenum but was made to disappear by more thorough heat treatment.

The relative heights of the peaks on the two curves are not the same. In this respect the results from columbium resemble those from an incompletely outgassed molybdenum target more nearly than they do those of curve *b* in Fig. 3.

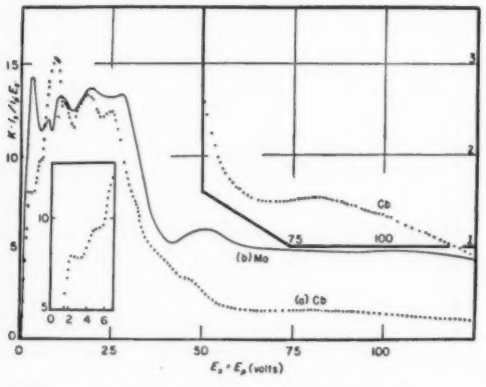

FIG. 3. Elastically reflected (full velocity) secondaries as a function of primary energy.

[4] The words "peak" and "maximum" are here used to describe any irregularities which indicate an abnormally large number of secondaries in the region in question.

Rhodium. The curves obtained from the rhodium specimen were similar in general form to those from the other two metals but the fine structure, in so far as it was investigated, was different. Only one discrete loss peak was observed, that at an energy loss of 7.7 volts. As seen by curve *c*, Fig. 1, it is much greater in magnitude[5] than any of the peaks of the other two metals.

The outgassing of the rhodium was not complete enough to enable one to expect much evidence of fixed energy groups. There was, however, some indication of such a group in the neighborhood of 8 volts.

The efficiency of elastic reflection was not investigated in the case of rhodium.

DISCUSSION

Tentative explanations of some of the results of this type of experiment are possible in terms of the allowed energy states for electrons within a metal.

A discussion of the general form of the distribution curves was given in the previous report[1] and will not be repeated here.

It has been shown[1] that the discrete loss peaks are to be expected from the metallic theory as the excitation processes within the metal should to a large extent be more or less discrete in nature. It is not possible at this time, however, to assign the peaks to any specific excitation processes.

There should be some sort of correlation between the discrete loss peaks and the irregularities of the elastic reflection curve. As the primary energy is increased beyond the values necessary for the excitation processes responsible for the discrete loss peaks there should be sharp decreases in the efficiency of elastic reflection. Any attempt at correlation is, however, complicated by the effects of electron "diffraction." An attempt at a sorting out of these two effects was given for molybdenum. Although a similar analysis is possible in the case of columbium it is not unique and so will not be given.

[5] Note the reduced scale of ordinates for curve *c*. It should be stated that slight changes in apparatus geometry somewhat affect the relative intensities for the various metals in all of the curves of this paper. Such differences, however, probably do not amount to more than a few percent

It has been pointed out that most of the irregularities of curve *a* Fig. 3 occur at lower energies than the corresponding ones of curve *b*. This is to be expected in general, whatever the explanation. As the lattice constant is greater for columbium (3.29A) than for molybdenum (3.14A) the spacing of the allowed and disallowed energy bands will be less in the former than in the latter. Thus energy transfers between zones should involve smaller amounts of energy. For the same reason the energies at which diffraction peaks occur will be less, for it is in reality these zones, or rather their counterparts in momentum space, which are responsible for this phenomenon. Furthermore, the lower atomic number of Cb will cause the energies involved in the excitation of optical and x-ray states to be smaller than in the case of molybdenum.

In the case of molybdenum the sharp decrease in the number of elastically reflected electrons which occurs when the primary energy is increased beyond 29 volts was interpreted as being due to the excitation of the $N_{II, III}$ x-ray states. On the curve for columbium this occurs at an energy approximately 3.5 volts less than the similar decrease on the molybdenum curve. This is approximately the same difference as that which exists between the $N_{II, III}$ term values for the two metals as given by Siegbahn.[6] ($N_{II, III} = 38$ volts for molybdenum, 35.6 volts for Cb.)

No certain connection can be found between the fixed energy groups and either the discrete loss peaks or the irregularities of the elastic reflection curve. It is noticeable, however, that the large maximum at the low energy end of the distribution curves occurs at a higher energy in the case of columbium than in that of molybdenum, which may be connected with the fact that the energy loss involved in the first discrete loss peak is greater in the case of columbium.

The fixed energy groups found at 11 and 33 volts on the molybdenum distribution curves were interpreted as being the result of the banded structure of the allowed energy states above the conduction levels. It was pointed out that their positions were in agreement with certain peaks in the fine structure of x-ray absorption curves which Kronig[7] has explained in this way. Although no x-ray data are available for columbium the corresponding groups at 9 and 32 volts have energies lower by just about the amount that one would expect from a comparison of the lattice constants.

The fixed energy group at 21 volts may arise from a similar cause but it seems more likely that it results from the photoelectric action of soft x-rays emitted on the return (in steps) to the normal state of atoms in which the $N_{II, III}$ levels are excited. Again the difference in the energies involved in the two cases is in the right direction and of approximately the right magnitude to agree with this hypothesis.

The author is indebted to Mr. L. D. P. King for aid in the performance of certain phases of the work.

[6] M. Siegbahn, Zeits..f. Physik **88**, 559 (1934).

[7] R. de L. Kronig, Zeits. f. Physik **75**, 191 (1932).

Nuclear Spins and Magnetic Moments of Rb^{85} and Rb^{87}

S. MILLMAN* AND M. FOX, *Columbia University*

(Received May 27, 1936)

The atomic beam method of "zero moments" has been applied to measure the nuclear spins and h.f.s. separations, $\Delta\nu$, of the $^2S_{\frac{1}{2}}$ states of Rb^{85} and Rb^{87}. We find the spin of Rb^{85} to be 5/2 and that of Rb^{87} 3/2, in agreement with the most probable values given by Kopfermann. With the value of $\Delta\nu$ for sodium as a standard we were able to measure the $\Delta\nu$'s of the Rb isotopes with a precision of 1 percent. We find these values to be 0.1018 cm^{-1} for Rb^{85} and 0.229 cm^{-1} for Rb^{87}, as compared with Kopfermann's values of 0.105 cm^{-1} and 0.240 cm^{-1} respectively. The magnetic moments calculated from the modified Goudsmit formula, are 1.44 nuclear magnetons for Rb^{85} and 2.92 for Rb^{87}. The ratio of magnetic moments, μ_{87}/μ_{85}, is found to be 2.026, with a precision of 0.2 percent. The $\Delta\nu$ for Cs was also measured with a precision of 1 percent. The result, 0.307 cm^{-1}, is in excellent agreement with the value 0.3067 cm^{-1} of Granath and Stranathan.

INTRODUCTION

THE nuclear spins and h.f.s. separations of the $^2S_{\frac{1}{2}}$ states of Li^7, Na, K^{39}, K^{41} and Cs have been measured in this laboratory by the method of atomic beams.[1, 2, 3, 4, 5] The h.f.s. separations of Li, Na and K were determined with a precision of 1 percent while that of Cs was good to only about 4 percent. These nuclear properties of Rb^{85} and Rb^{87} have never been measured by this method. Results obtained for the nuclear spins of the Rb isotopes by spectral methods have not been altogether decisive. From intensity measurements of the hyperfine structure patterns of the resonance lines Jackson[6] concluded that the most probable values for these spins are 3/2 for Rb^{85} and 5/2 for Rb^{87}, although other possibilities were not excluded. Kopfermann,[7] working on the spark spectrum of Rb, applied the interval rule and obtained results which indicated that the most probable values were 5/2 for Rb^{85} and 3/2 for Rb^{87}, but the values 6/2 and 7/2 for Rb^{85} could not be excluded. It seemed desirable to determine decisively the nuclear spins of the Rb isotopes by the method of atomic beams, and also to obtain the h.f.s. separations of the normal states of Rb^{85}, Rb^{87} and Cs with the same precision as that obtained for Li^7, Na, K^{39} and K^{41}.

METHOD

The method of determining the nuclear spins of the Rb isotopes and for measuring the h.f.s. separations for Rb and Cs was that of the "zero moments" as used for other alkali atoms and described in detail by Cohen[2] and Millman.[3] In the present investigation however, the magnetic field was not calculated from the geometry of the apparatus but was calibrated by means of the zero moment peak of sodium.[4]

APPARATUS

The apparatus used in the work on Li, Na, and K^{39} [3, 4] had to be modified to permit the use of very high currents in the field wires. The length of the field wires was increased to 115 cm and was divided into two sections. The section nearest the oven was made 33 cm long and the one nearest the detector 75 cm long. In the space of 7 cm between the sections the collimating slit was placed. In order to carry through the investigation on Rb it was necessary to send currents as high as 1500 amp. through the field wires, and our batteries were such that this could not be done with both sections of the wires in series. External connections to the field wires, which were easily interchangeable, permitted the use of either the short section of the field alone in the case of high currents, or of both sections to form one long field, in the case of lower currents. The maximum current that could be sent through the long field of 115 cm was about 900 amp. This was sufficient to provide the magnetic fields required for the two zero moment peaks of Rb^{85}. The peak of Rb^{87} required the high currents and it was in

* John Tyndall Fellow.

[1] Rabi and Cohen, Phys. Rev. **46**, 707 (1934).
[2] Cohen, Phys. Rev. **46**, 713 (1934).
[3] Millman, Phys. Rev. **47**, 739 (1935).
[4] Fox and Rabi, Phys. Rev. **48**, 746 (1935).
[5] Manley, Phys. Rev. **49**, 921 (1936).
[6] Jackson, Proc. Roy. Soc. **A139**, 673 (1933).
[7] Kopfermann, Zeits. f. Physik **83**, 417 (1933).

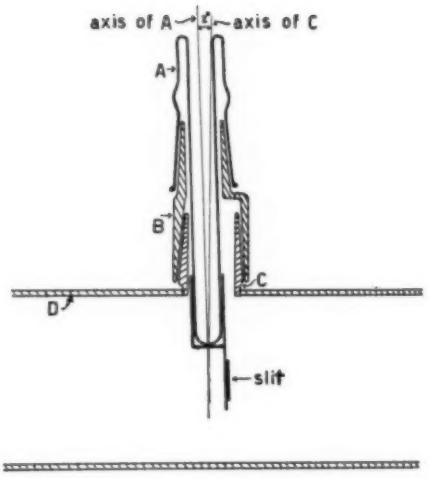

FIG. 1. Slit mount. *A*, standard No. 30 Pyrex female gd. joint; *B*, brass collar; *C*, standard No. 40 brass male gd. joint; *D*, portion of apparatus cylinder.

the location of this peak that the short section of the field was used. The decrease in resolution as a result of shortening the field length did not matter because of the high gradients which accompany the high fields.

The height of the beam was limited by stops to 2 mm, over which height the field was constant to about 0.5 percent. Four slits were placed along the path of the beam. The first was a wide fore slit of 0.1 mm separating the oven chamber from the receiving chamber. The second was 0.035 mm wide and was placed at the oven end of the short section of the field. The third, 0.030 mm wide, was the collimating slit. It was situated in the place between the two sections of the field. The fourth, 0.035 mm wide, was placed at the end of the longer section of the field. The second and fourth slit were included in the arrangement to eliminate scattered atoms from the detector. The collimating slit was mounted eccentrically on a ground joint which was in turn mounted on a second ground joint with axis inclined at an angle of 2 degrees to that of the first. A schematic diagram of this arrangement is shown in Fig. 1. If the brass collar *B* is kept fixed and the ground joint *A* turned, the distance of the slit from the plane of the wire axes is changed. If the collar is rotated and *A* held in place, the orientation of the slit with respect to the beam plane is varied. By the term beam plane is meant the plane defined by the oven slit and the center of the collimating slit. With the aid of the atomic beam the collimating slit can be brought into the beam plane more accurately than by optical means alone. The second and fourth slits, as well as the one mil tungsten detector were mounted in the same manner as the collimating slit. The fore slit was made movable in a direction normal to the beam plane by means of a screw coupled to the slit holder through the oven chamber. The pegs which supported the oven were fixed to a dovetail slide that could be moved in the same manner as the fore slit. These motions enabled us to set the beam plane parallel to the plane of the field wire axes and at any desired distance from it.

PROCEDURE

The Rb and Cs used in this work were distilled under vacuum from a mixture of freshly cut calcium shavings and the chlorides of these alkali metals. The metals were collected in small glass bulbs which were sealed off under vacuum and dropped directly into the oven. To prevent oxidation of the metal the bulb was broken in an atmosphere of nitrogen in the process of forcing the lid into the oven.

The beam was first detected with only the fore slit to define it. The collimating slit was brought in and its orientation with respect to the beam plane varied in small steps by means of the brass collar. For each collar position the maximum beam intensity obtained with various detector collar positions were recorded. The greatest maximum intensity thus obtained corresponded to the collar positions for which the collimating slit and detector were in the plane of the beam. With the collimating slit and detector fixed in the optimum positions the second slit and later the fourth slit were brought into the beam plane in a manner similar to that outlined for the collimating slit. The magnetic field was then turned on and a zero moment peak located, first using the whole field and then only the short section. If the two current readings for the same peak were not the same the beam plane was not parallel to the plane of the field wire axes. The slits and detector were then moved as required until the desired parallelism was achieved.

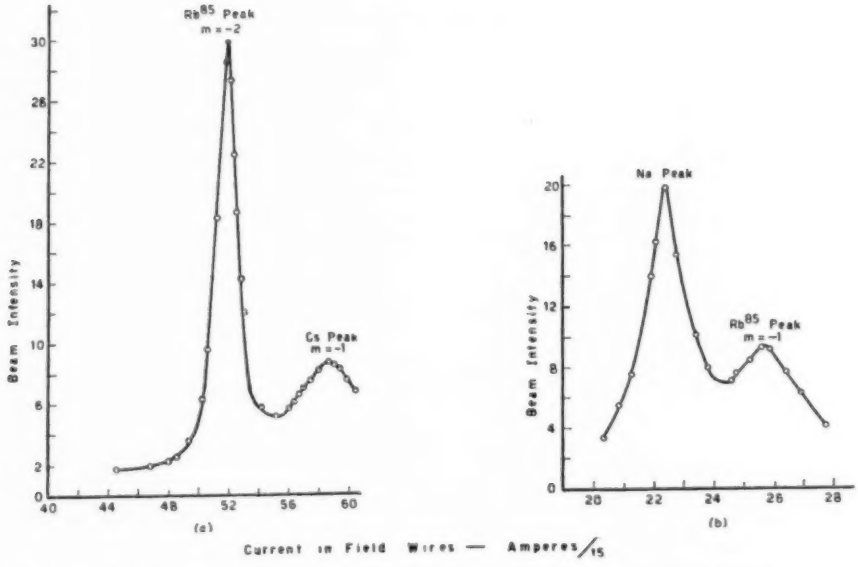

FIG. 2. (a) Variation of beam intensity with field in the region of $m=-2$ peak of Rb^{85} and $m=-1$ peak of Cs. (b) Variation of beam intensity with field in the region of $m=-1$ peak of Rb^{85} and the Na peak.

A Leeds & Northrup type K potentiometer was used to read the potential drop across a 50 mv, 1500 ampere shunt in the field wire circuit. It was not necessary to know the resistance of this shunt accurately since our measured values of the $\Delta\nu$'s depend only on ratios of currents. To obtain the ratio of currents for any two zero moment peaks, the current was first set for maximum intensity of one of the peaks and then for that of the other alternately for a series of readings taken over a period of about 30 minutes. It was found necessary to take into account the warping of the field block due to the rise in temperature of the field wires, which amounted in the most extreme case to about 16°C. Thermometers were placed in the water line so as to read the temperature of the water which came out of each wire. Since each wire had its own water inlet and outlet the flow in each could be regulated to adjust the temperature of each wire. In comparing the currents corresponding to two zero moment peaks the water flow through the wires was regulated so that the temperature of the exit water was the same for both current values. This eliminated errors due to temperature changes in the shape of the field wires.

Runs were taken with mixtures of Na and Rb in the oven in order to find the ratio of the $\Delta\nu$'s of Na and Rb^{85}. The zero moment peak of Na and the lower field peak of Rb^{85} occur at only slightly different values of the field, but separated sufficiently so that they are clearly resolved. When the oven temperature was about 200°C the beam was almost entirely Rb, and during each run the zero moment peaks of Rb^{85} were located many times over a period of a few hours. As the oven temperature was slowly raised the Rb beam increased in intensity at first and then decreased when very little of the metal was left in the oven. At about 350°C the sodium began to appear in the beam. Fig. 2b is a plot of the intensity pattern in the neighborhood of the Na and Rb peaks. At the time these data were taken the Rb was rapidly disappearing from the beam. After the Rb was completely boiled off the Na peak was located many times. It was found that the current readings did not vary over a period of several hours by more than 0.3 percent. Mixtures of Cs and Rb were also put into the oven to get the ratio of their $\Delta\nu$'s. The higher field peak of Rb^{85} and the lowest field peak of Cs occur at only slightly different values of the

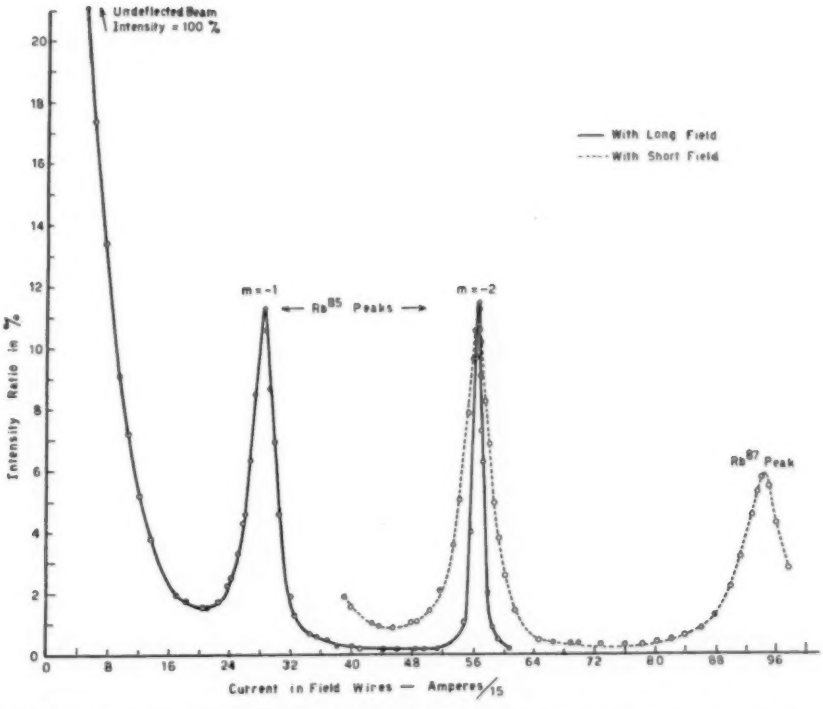

FIG. 3. Variation of beam intensity with field at the position of zero deflection. 1 amp. =0.85 gauss.

field and the same procedure was followed in locating these peaks as described above. Fig. 2a is a plot of the intensity pattern in the region of these peaks.

RESULTS AND DISCUSSION

Fig. 3 is a plot of the beam intensity at the position of zero deflection as a function of the current in the field wires. The solid line portion of the curve was obtained with the whole field. As previously stated sufficient current could be obtained with this arrangement to get the two peaks of Rb^{85}. For regions beyond 900 amperes the short section of the field was used. The broken line portion of the curve, obtained with this section of the field, shows the peak due to Rb^{87}. The region of the second peak of Rb^{85} was investigated with this arrangement for the purpose of comparing the $\Delta\nu$'s of the two isotopes and also to aid us in determining the spin of Rb^{87}. The first two peaks are of approximately equal intensity and are due to Rb^{85}. The current ratio for these peaks was accurately determined to be 2:1 to 0.2 percent. The fact that there are two peaks having the field ratio 2 : 1 immediately shows that the nuclear spin is 5/2 for Rb^{85}. The intensities of these peaks is in good agreement with theory. Since Rb^{85} is prevalent to about 72 percent the intensity of each peak should be 1/6 of 72 percent or 12 percent. The experimental intensities obtained from a great number of settings gave a value of 11.6 percent.

The value of $\Delta\nu$ for the ^2S state of Rb^{85} can be obtained at once from the knowledge of the current ratio of the first Rb peak and the Na peak. This ratio was found to be 1.139 ± 0.002. Since

$$x=2\mu_0 H/hc\Delta\nu \qquad (1)$$

for any alkali atom in the ground state, and the value of x at a zero moment peak is known when the spin is known, we have

$$\Delta\nu/\Delta\nu_0=(H/H_0)\times(x_0/x), \qquad (2)$$

where $\Delta\nu_0$, H_0 and x_0 refer to the atom used as a

standard and H/H_0 is the observed current ratio. Taking the value 0.0596 cm^{-1} for the $\Delta\nu$ of Na as given by Fox and Rabi,[4] and since x_0 is 1/2 for the Na peak and x is 1/3 for the first Rb peak, we obtain for the h.f.s. separation of $^2S_{\frac{1}{2}}$ state of Rb^{85} the value

$$\Delta\nu_{Rb^{85}} = 0.1018 \text{ cm}^{-1}.$$

The precision of this measurement is limited by the precision of the Na measurement, which is 1 percent.

The third peak in Fig. 3 is the only one due to Rb^{87}. Although it was not possible to investigate this curve at very much greater fields on this apparatus, it is known from some unpublished work of Paul Rosenberg in this laboratory that there are no other peaks in the region of higher fields. Rosenberg, working on the apparatus used by Cohen[2] in his Cs investigations, was able to investigate the region of fields higher than the Rb^{87} peak and found no trace of any additional peaks although it was possible to resolve them in case any were present. From this consideration it follows at once that the spin of the Rb^{87} nucleus is either 2/2 or 3/2. The following evidence shows that the value 3/2 is the correct one. Since Rb^{87} is prevalent to about 28 percent the intensity of the peak should be 7 percent if the spin is 3/2, while for 2/2 it should be 9.3 percent. The experimental value of this intensity is 6.4 percent in agreement with theory for a spin of 3/2.

Another method for determining the spin of one of two isotopes, when the spin of the other is known, and when each of the isotopes have at least one clearly resolved zero moment peak, was suggested by Rabi and first used by Manley[5] in determining the nuclear spin of K^{41}. For our case the method consists of replotting the curve in the region of the Rb^{87} peak of Fig. 3 by multiplying the abscissa of each experimental point in the curve by the value of the magnetic moment of the atom corresponding to this current, and comparing this with a similarly replotted curve of the second peak of Rb^{85}. Since the magnetic moment of the atom is a function of the nuclear spin we will get different curves for the Rb^{87} peak for different values of the spin. Now the force on an atom in an inhomogeneous magnetic field is proportional to the product of the magnetic moment of the atom and the field gradient (or current in the field wires). Hence if the intensity at the zero deflection position is due solely to atoms of one magnetic state the fraction of remaining intensity will depend on the product of magnetic moment

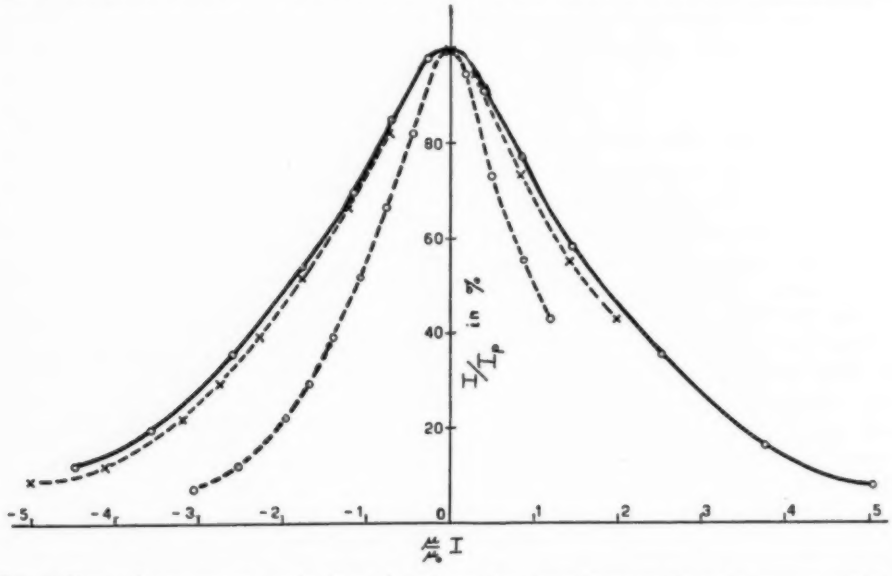

FIG. 4. Shape of zero moment peaks when plotted as a function of force on the atom. ——o——Rb^{85}, $m=-2$; ——×——Rb^{87}, $i=3/2$; - - -o- - -Rb^{87}, $i=2/2$.

and current, and on other quantities such as oven temperature, beam shape, etc. that are common to both isotopes. Thus, calling the peak intensity I_p and the intensity at points close to the peak I, if the ratio I/I_p is plotted as a function of the product of current and magnetic moment, the experimental curves in the region of the Rb^{87} peak and of the second peak of Rb^{85} should coincide for a correctly chosen value for the spin of Rb^{87}. This was done in Fig. 4. The curves fit well for an assumed spin of 3/2 for Rb^{87} and not for a spin of 2/2.

It may be mentioned that this method of analysis would limit the spin of the Rb^{87} nucleus to 3/2 even if one were not certain of the nonexistence of peaks beyond the Rb^{87} peak under discussion. If the spin of Rb^{87} were 4/2 or greater the peak would have to be the first zero moment peak. It can easily be shown that for an assumed spin of 5/2 the curve plotted as in Fig. 3 would coincide with the one plotted for an assumed spin of 2/2, and that for any other spin greater than 3/2 the curve would lie inside the curve given for 2/2 and would certainly not fit the Rb^{85} curve.

The value of $\Delta\nu$ for the $^2S_{\frac{1}{2}}$ state of Rb^{87} is obtained from equation (2) using Rb^{85} as the standard. The experimental ratio of the current at the Rb^{87} peak to that of the second peak of Rb^{85} is 1.688 ± 0.2 percent. The value of x_0 for the second peak of Rb^{85} is 2/3 and the value of x for the Rb^{87} peak is 1/2 for a spin of 3/2. This gives for Rb^{87}

$$\Delta\nu_{Rb^{87}}=0.229\ \text{cm}^{-1}.$$

Here again the precision is limited by that of our standard to 1 percent.

The results obtained for the nuclear spins of the two isotopes agree with the most probable values cited by Kopfermann,[7] but the values for the $\Delta\nu$'s of Rb^{85} and Rb^{87} are lower than his values of 0.105 and 0.240 cm^{-1}. It may be remarked in reference to the correctness of the value 3/2 for the nuclear spin of Rb^{87} that, if the spin were assumed to be 2/2, the $\Delta\nu$ would turn out to be 0.343 cm^{-1}. Such a disagreement is far beyond Kopfermann's experimental error.

The ratio of the $\Delta\nu$'s for the two isotopes as well as the ratio of the magnetic moments is established very accurately from these experiments. They are

$$\Delta\nu_{Rb^{87}}/\Delta\nu_{Rb^{85}}=2.251\pm0.2\ \text{percent},$$

$$\frac{\mu_{87}}{\mu_{85}}=\left(\frac{\Delta\nu_{87}}{\Delta\nu_{85}}\right)\left(\frac{[2I/(2I+1)]_{87}}{[2I/(2I+1)]_{85}}\right)$$
$$=2.026\pm0.2\ \text{percent}.$$

TABLE I. *Values of nuclear spins and magnetic moments.*

	Nuclear spin	$\Delta\nu$ of $^2S_{\frac{1}{2}}$	μ
Li^7	3/2	0.0267 cm^{-1}	3.20
Na	3/2	0.0596	2.08
K^{39}	3/2	0.0154	0.397
K^{41}	3/2	0.00853	0.220
Rb^{85}	5/2	0.1018	1.44
Rb^{87}	3/2	0.229	2.92
Cs	7/2	0.307	2.82

Cs

The h.f.s. separation of the $^2S_{\frac{1}{2}}$ state of Cs is obtained from Eq. (2) in the same way as for the Rb isotopes. The ratio of the current in the first Cs peak to that of the second Rb^{85} peak is found to be 1.131 ± 0.002. With the values 2/3 for x_0 of Rb^{85} and 1/4 for x of Cs, we obtain

$$\Delta\nu_{Cs}=0.307\ \text{cm}^{-1}$$

in excellent agreement with the value 0.3067 ±0.0004 obtained by Granath and Stranathan,[8] who have made extremely precise measurements of this quantity by hyperfine structure methods.

Table I contains the nuclear spins and $\Delta\nu$'s of the $^2S_{\frac{1}{2}}$ states of Li^7, Na, K^{39}, K^{41}, Rb^{85}, Rb^{87} and Cs as measured by atomic beam methods as well as the magnetic moments calculated from the modified Goudsmit[9] formula.

The moments are not to be considered as having the same precision as that of the $\Delta\nu$'s, since it is not yet known how reliable the modified Goudsmit formula is. However the ratio of moments for two isotopes can be considered reliable to 0.2 percent under the present view of the cosine law of interaction between nuclear and electronic spins.

We are indebted to Professor I. I. Rabi for his continued interest in this work and for helpful discussions.

[8] Granath and Stranathan, Phys. Rev. **48**, 725 (1935).
[9] Goudsmit, Phys. Rev. **43**, 636 (1933); Fermi and Segrè, Zeits. f. Physik **82**, 729 (1933).

The Force at an Anchored Cathode Spot

LEWI TONKS, *Research Laboratory, General Electric Company, Schenectady, N. Y.*

(Received April 30, 1936)

The steadying effect of a metallic anchor for the cathode spot of a mercury-pool arc has been used to make measurements on the force at the cathode. Two methods have been used. One was based on the depression of the meniscus edge carrying the cathode line, due to the pressure on it. This measured only the horizontal component which was exerted on the liquid and gave 19 dynes/amp. The other used a torsion pendulum to measure the total horizontal force component and gave 33 to 43.5 dynes/amp. over the current range zero to 10 amp. This was supplemented by a determination of the direction of the force based on the deflection of the cathode line by a magnetic field, giving 35 to 66 dynes/amp. for the resultant in the same current range. The results show interaction of current streams from different emitting areas to increase the force, and are not inconsistent with other determinations.

THE measurement of the force against a liquid mercury-arc cathode is inherently difficult. The force is probably not normal to the general liquid level but is more likely to be perpendicular to small portions of that surface which, due to the violent agitation, make considerable angles with the horizontal. And when, as seems to happen occasionally,[1] a spot plunges quite beneath the surface, the matter looks still more hopeless.

Recourse to confining the spot to a small area of mercury surface as Kobel has done[2] may well increase the pressure through the constriction of the arc path above the spot, although the arc tube could be designed so as not to do this. There is an additional objection to Kobel's method which will appear later.

An anchored[1] cathode spot gives a more stable and better defined condition thereby lending itself the better to measurements. Incidentally, the equality of arc drop between free and anchored spot arcs probably means that the results for the anchored spot are applicable to the free spot.

MEASUREMENTS USING THE DEPRESSION OF THE MENISCUS EDGE

Two methods were available. Direct observation of the cathode line formed at the junction of mercury with a vertical Mo strip immersed in it showed that as the arc current was increased, the meniscus edge and cathode line were depressed. By measuring the lowering of the line as the current was varied and applying the theory of the meniscus shape, it was possible to calculate the force per cm at the cathode line.

Consider in Fig. 1 the Mo sheet A against which the mercury meniscus M rises to tangency at point Q at height y_0 above the free liquid surface. Let the angle between the meniscus and the vertical at any point be θ, the height be y, the pressure against the liquid be P. Then

$$\sin\theta = 1 - y^2/\alpha - \gamma^{-1}\int_0^y P dy, \qquad (1)$$

where $\alpha = 2\gamma/\rho g$, γ = surface tension, ρ = density.

For simplicity we suppose first that P is constant between θ_0, at the meniscus edge, and θ_1, corresponding to some point below the edge, and that it is zero beyond; and second, that the trace of the meniscus seen in the figure is circular between θ_0 and θ_1, the radius of curvature being r. With these assumptions

$$\int_0^{y_0} P dy = -Pr\int_{\theta_1}^{\theta_0} \cos\theta d\theta$$

$$= Pr(\sin\theta_1 - \sin\theta_0). \qquad (2)$$

If we denote the width of the pressure strip between θ_0 and θ_1 by w, then

$$w = r(\theta_1 - \theta_0), \qquad (3)$$

whence, combining,

$$\int P dy = Pw(\sin\theta_1 - \sin\theta_0)/(\theta_1 - \theta_0). \qquad (4)$$

Applying Eq. (1) to the meniscus at y_0 and y_1, respectively, we then have,

[1] L. Tonks, Physics **6**, 294, 298 (1935).
[2] E. Kobel, Phys. Rev. **36**, 1636 (1930).

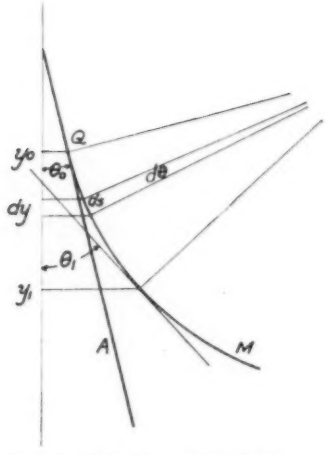

FIG. 1. Analysis of meniscus shape.

$$y_0^2/\alpha = 1 - \sin\theta_0 - (Pw/\gamma)\frac{\sin\theta_1 - \sin\theta_0}{\theta_1 - \theta_0}. \quad (5)$$

$$y_1^2/\alpha = 1 - \sin\theta_1. \quad (6)$$

Suppose, further, that w is so small that y_0 does not differ appreciably from y_1. Subtraction leads to

$$Pw = \gamma(\theta_1 - \theta_0), \quad (7)$$

giving the force per unit length at the cathode spot in terms of θ_0, the angle of the anchor, and θ_1 as determined from Eq. (6), where y_1 is the observed height of the cathode line.

It is to be noted first that any force against the anchor itself will not be counted; second, that the force is assumed to be highly localized; and third, that it is certainly pulsating corresponding to the passage back and forth of the small emitting areas which compose the cathode line. The last consideration, however, would be without influence on the validity of the results if there were no consequent motion of the liquid. Actually such motion is small and mainly confined to the narrow zone occupied by the cathode line.

The second limitation can be lifted by not adopting such definite suppositions. We note that quite generally, aside from any constant radius of curvature of the liquid or localization of P,

$$Pdy = P\cos\theta ds.$$

Eq. (1) then becomes

$$y_0^2/\alpha = 1 - \sin\theta_0 - \gamma^{-1}\int P\cos\theta ds$$

in place of Eq. (6). Thus y_0^2 varies linearly with the integral so that

$$\int P\cos\theta ds = -\gamma\Delta y_0^2/\alpha,$$

where Δy_0^2 is the change in y_0^2 from its value for zero current.

The experiment was tried in the simple tube, shown in Fig. 2, which had been constructed for another purpose. The mercury contained a trace of Al to aid in wetting the Mo strip S, which projected through the Hg surface when the tube was tilted back slightly (8°). The cathode line occupied the whole 3-cm-long front side of straight portion of S for the current range used.

The angle of tilt, θ_0, was measured by reflecting light from the Hg-wet Mo surface. The cathode line and mercury level heights were measured with a cathetometer. The meniscus height for zero current was found by observing the height at which surface curvature ceased, using the reflection of a movable light source.

From this height, which was 0.24 cm above the pool level, and from θ_0, the surface tension of the

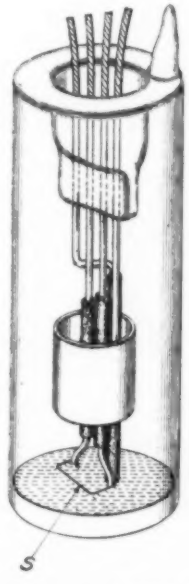

FIG. 2. Tube for measurement of depression of meniscus by cathode line.

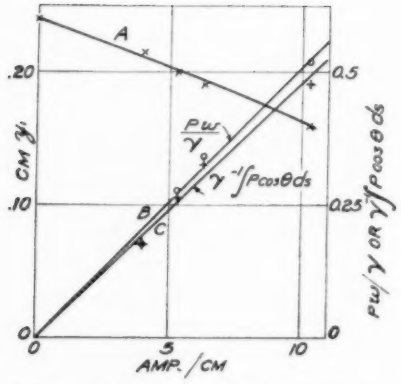

FIG. 3. Results of meniscus depression measurements.

mercury was found through α in Eq. (6). It came out to be 450 dynes/cm, which is acceptable within the limits of accuracy of this experiment and of uncertainty in the true value.

The depression of the cathode line with increasing current density is shown as Curve A in Fig. 3. Currents up to 31 amp. were used. The corresponding values of Pw/γ are plotted in Curve B as calculated from Eqs. (6) and (7). They show a linear variation of Pw/γ of 0.051 amp.$^{-1}$ cm, and differ only slightly from the more rigorous $\int P\cos\theta ds/\gamma$ represented by Curve C. This is no justification for the correctness of the assumptions underlying the calculation of Pw/γ, for a large pressure, exerted where the liquid had become almost horizontal, would not cause a large discrepancy. Using $\gamma=450$ dynes cm^{-1} as determined above, the force on the cathode by this method is found to be

$$Pw/i=23 \text{ dynes/amp.},$$

where i is the arc current.

MEASUREMENTS OF THE FORCE AGAINST AN ANCHOR

The second method used was to measure the force against the anchor itself. This force includes not only that exerted directly on the exposed anchor surface, but also the $\int P\cos\theta ds$ of the first method. This is demonstrable either on the general ground of momentum balance or by an analysis of the hydrostatic pressures on the two sides of the anchor.

An experimental tube with the anchor hung from a simple gravity pendulum was built but deemed unsatisfactory because of the change in relation between anchor and Hg surface with deflection.

Finally a torsion pendulum was built in which a cathode spot, anchored at either of two symmetrically placed vanes, V_F or V_B of Fig. 4, caused a deflection of the mirror M against the torsion of the tungsten wires W_1 and W_2. Here the vanes always maintained the same position relative to the liquid surface. Two vanes were used because, while the moment arm of either was uncertain, the sum of the two, which became effective when both vanes were used in succession and the sum of their torques taken, was measurable and fixed. The glass ring R served to steady the rotating system with respect to the mercury surface. The mica disk extending across the whole tube kept the arc glow away from the mirror where its light would interfere with observations of the deflected light beam. The elastic constant of the system was determined by the oscillation method. The torsion wires were of tungsten 0.0178 cm in diameter and each 3 cm long, and the constant was 9.90×10^3 dynes cm/radian. V_F was 1.00 cm and V_B 1.08 cm in the clear. They were cleaned electrolytically in a H_2SO_4 bath, then hydrogen fired at 1200°C. They were mounted on the suspension without handling and then each was coated on one side, the back, with aquadag to prevent the cathode line from forming there; and in addition stripes 1 to 2 mm wide were painted along the vertical edges on the fronts of the vanes to confine the cathode line to the plane portion of the anchors.

The assembled tube was baked out on the pump for one hour at 500°C. Because of their unfavorable position, the vanes could only be heated to dull redness with the high-frequency coil, but the anode was brought almost to whiteness repeatedly. Despite the poor heating of the anchors, the spot anchored without undue difficulty. A permanent magnet helped by keeping the free spot in the vicinity of the vane on which it was to settle. The tube was run with 15 amp. from each vane in turn until a sticking vacuum was obtained; then the tube was sealed off.

A preliminary tube of similar design contained two anodes, one, A_1, in the azimuth of V_B, the

other, A_2, 90° from it. In that tube it was determined that the cathode force was independent of the position of the anode. Changing the temperature of a water bath surrounding the cathode pool between 15°C and 33°C had no appreciable effect on the observed force.

On this same tube the cathode line was subjected to a magnetic field of some 25 gauss from an electromagnet. The magnet was supported in various positions with respect to the meniscus so that the field lay parallel to the edge, vertical, or horizontal and perpendicular to the edge. The field affected the position of the cathode line along the meniscus, thus changing the moment arm and consequently the deflection. After making the obvious correction, a small change in deflection remained with the parallel orientation, which could be explained by electrodynamic forces within the mercury. Other smaller differences are thought not to be significant.

In using the final tube it was noticed that when the arc current was suddenly stopped in order to confirm the zero following a deflection reading, the light beam consistently overshot the zero by several mm and only returned to the original zero in the course of a minute. The discrepancy increased with arc current. It was due to the convection currents set up in the mercury by the vapor blast from the cathode line. Their effect was to decrease the deflection, and by just the amount of the zero deflection. Accordingly, deflections were measured from the deflected zero to which the beam returned temporarily.

In this way deflections of the torsion system were measured for a series of arc currents, with the spot anchored on each vane for each current value. It was not possible to control which vane the spot would anchor on when it was started with the spark coil, but in several starts it would go to the desired vane in one of them. With each reading, a record was made of the "center of gravity" of the cathode line with respect to the vane itself in order that a more accurate value of the moment arm might be used in the calculations. This was desirable because it often happened that the whole available vane width was not occupied, particularly at the lower currents. Measurements were made from 1.5 amp., the lowest current which was sufficiently stable, up to 10 amp., the largest current that the tube was designed for.

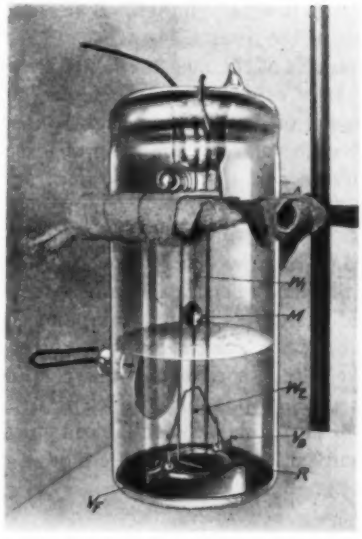

FIG. 4. Torsion tube.

To use the compensation afforded by the double vane, the simple theory of the deflecting system, for an assumed axis displaced from the actual axis, was worked out. Since readings on the two vanes were not taken with equal currents, those at nearly equal currents were paired and the deflections corrected on the assumption that for the small differences involved, deflection was proportional to current. The force to be measured, f, is given by

$$f = i(L_1/i_1 + L_2/i_2)/l$$

and the error, δ, in axis position by

$$\delta = L_1/f - l_1 = l_2 - L_2/f$$

where L_1 and L_2 are the observed torques (given directly by deflections) on the two vanes, i_1 and i_2 the corresponding arc currents, $i(\sim i, \sim i_2)$ is the current to which f applies, l_1 and l_2 are the assumed radial distances of the two cathode lines, and l is the distance between the cathode lines on the two vanes. The analysis of the data on these lines gives values of δ ranging from $+0.08$ to -0.08 cm, compared to a value of l averaging 5.5 cm. This shows that the analysis is not justified by the accuracy of the measure-

ments, but it sets a limit of 3 percent to the accuracy of the results.

The results of the measurements are shown in Fig. 5. It is evident that the force (horizontal component, of course) rises slightly faster than linearly with current. The ratio of force to current increases from 33 dynes/amp. at zero to 42.5 at 10 amp. It must, of course, be current density, rather than total current which is significant. But the observations of cathode line length which had been made during the course of the readings were too uncertain, and the distribution of spots along the line were too uneven to make direct correlation between force and current density possible. Suffice it to say that above 8 amp. the full available meniscus edge was occupied, a matter of 0.7 cm on V_F and 0.9 cm on V_B.

Measurement of the Direction of the Cathode Force

It has already been noted that the force here measured is only a horizontal component. It was observed, however, in applying the magnetic field to the cathode line in the earlier tests, that when the field direction was turned from the horizontal through the current flow direction to parallelism with the anchor, the displacement of the cathode spot reversed. Thus, at some position of the field intermediate between these two extremes, the cathode line was undisplaced. It is to be expected that the line of action of the mechanical force on the cathode coincides with the mean direction of current flow near the cathode. By deflecting this current, the magnetic field creates a force component parallel to the meniscus edge which moves the cathode line to one side or the other. The cathode line will be unaffected only when the field lies in a neutral direction coincident with that of the current, and this neutral direction is the direction of the cathode force itself. Knowledge of the neutral angle makes the calculation of this force from its horizontal component possible.

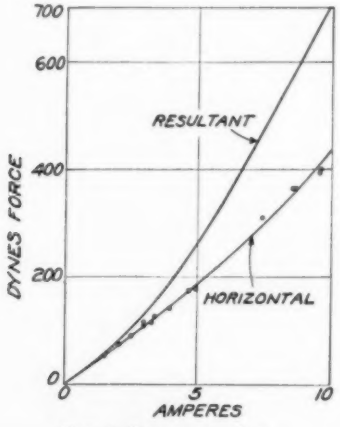

Fig. 5. Force on anchor.

In order to measure this direction, the simple arc tube shown in Fig. 6 was constructed. The Mo vane, 2 cm long by 1 cm wide, was tipped at 45° to the tube axis to permit a wide range of angles between anchor and pool by tilting the tube and using both sides of the anchor. The anchor was centered in the spherical bulb so that with the bulb half full of mercury the mercury surface always cut the anchor at the same level.

The Mo anchor was cleaned electrolytically in a H_2SO_4 bath, next it was hydrogen fired, then coated along the oblique edges with aquadag in order to confine the cathode line to the plane surface. The assembled tube, of hard glass, was baked out at 500°C for one hour; the Mo anode was repeatedly heated to whiteness by induction; the anode was thoroughly degassed; the mercury was distilled in; and the tube was run with a free spot until anchoring had been achieved on both anchor faces. The tube was run with 10 amp. until a sticking vacuum was obtained, then it was sealed off the pumping system.

The field for the actual tests was that from an old instrument magnet mounted on a horizontal shaft whose center line bisected the center line between N and S poles perpendicularly. The other end of the shaft carried an angular scale from which the orientation of the magnetic field was read. The experimental tube was mounted off the poles of the magnet and adjusted so that the meniscus edge lay in the extension of the center line of the shaft. The pool surface and a straight wire passing from pole to pole through two holes in the centers of the pole faces were useful in making the alignment and in determining the angular scale reading for a horizontal field. By sighting across vane and

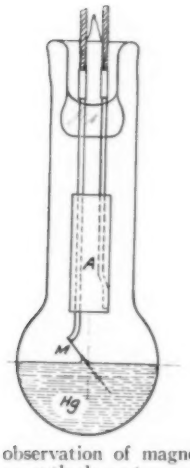

FIG. 6. Tube for observation of magnetic deflection of cathode spot.

wire, the angle φ between vane and liquid, as shown in Fig. 7, was then found.

Two distances between anchor center and pole ends, 27 and 43 mm, were used, resulting in field strengths of 36 and 17 oersteds, respectively. At a given anchor angle and current value, the two neutral positions of the field were determined alternately several times. The average angle ψ between neutral direction and that of anchor was calculated for each position, and the pairs of values were plotted, joined by a vertical line, in Figs. 7 and 8. Tests at one or two anchor angles indicated that the effect of water cooling was to decrease the difference between the two values of a pair. In view of the rapid evolution of Hg vapor from the cathode spot, it is unlikely that a difference in pressure of a few microns in the body of the tube, such as is occasioned by an increase in temperature, would affect the phenomena at the cathode. Accordingly, a difference in direction of current flow on this account is not to be expected. The sense of the magnetic field will, however, affect the flow of current through the body of the tube, which, in turn, can influence the neighborhood of the cathode spot. Such an effect appears very definitely in Fig. 8 between 5 and 7 amp. on the 90° curve. Besides the pairs of readings which are continuous with the lower current readings and lie near 45°, there is a set at 12° to 23° corresponding to a peculiar glow distribution which sometimes occurred with the field in one sense. Another cause for different

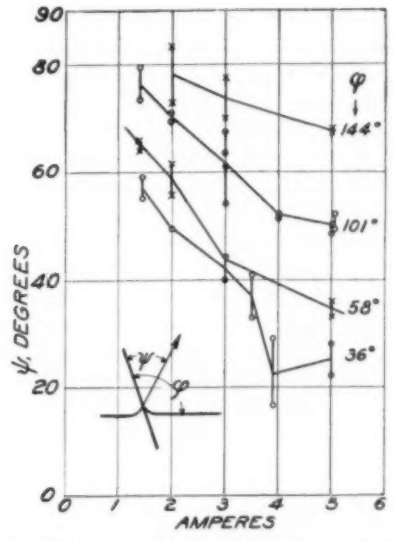

FIG. 7. Neutral magnetic field angles at about 36 oersteds.

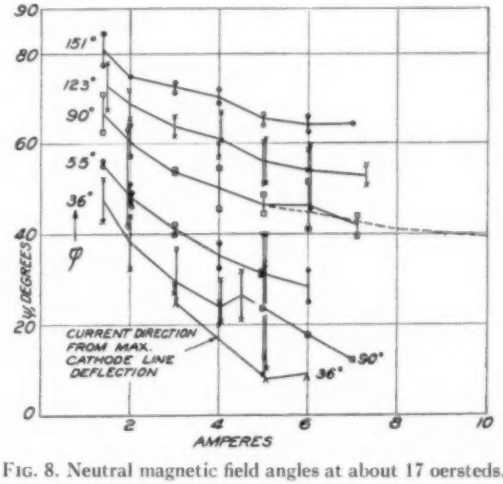

FIG. 8. Neutral magnetic field angles at about 17 oersteds.

angle values for the pair lies in the dissymmetry of the magnetic field which undoubtedly existed under the experimental conditions.

A few field angle readings were made for the extreme deflection of the cathode line using an anchor angle of 36°. The points designated in this way in Fig. 8 were then calculated on the assumption that the current direction lay at right angles to the magnetic field. But the deflected spot was far from horizontal so that the whole phenomenon would have to be referred to a different

set of axes. It is therefore reasonable that the points found this way do not agree with those determined by a null deflection method.

The decrease in angle between neutral direction and anchor plane as the current increases reflects the depression of the meniscus edge and shows the effect of the cathode surface immediately adjacent to the cathode line in directing the current flow. If this were the only factor, affecting the flow in the region where the cathode pressure develops we should, however, find that the various curves for different anchor angles coincided; since the shape of the meniscus at the anchor is but slightly affected by the anchor angle. For instance, the assumption used in Eq. (2) leads to an almost coincident set of curves independent of anchor angle, except for a small region at the larger current values.

The decrease in ψ with anchor angle undoubtedly arises from effects at some distance from the meniscus edge, which tend to make the current pass midway between the two surfaces bounding the region. This requires an interaction between the current elements from the different elementary emitting areas so that the whole cathode phenomenon cannot be considered as the simple sum of individual elementary processes.

Calculation of the Resultant Cathode Force

The neutral magnetic field angles found for the 90° anchor angle can now be applied to the force data. Since it had not been possible to reach 10 amp. in the magnetic deflection tests because of spot freeing with the field applied, the 90° curve of Fig. 8 was extrapolated as shown by the dashed line. Dividing the horizontal force component as given by Fig. 5 by the sin ψ from Fig. 8 the resultant shown in Fig. 5 was found.

The force is seen to increase more than proportionally to the current. From a value of 35 dynes/amp. at small currents it rises to 66 at 10 amps. Apparently each emitting area of the cathode line exerts not only a pressure arising from it alone but also an additional force arising from the interaction of the currents from the neighboring areas, already evidenced above.

This action, taking place at a greater distance from the meniscus edge than that due to the individual spot, is consistent with the behavior of the neutral angle with increasing current.

If we ascribe the force F of 35 dynes/amp. arising from a single emitting area to the pressure of plasma electrons[3] we have

$$F=2.74(1-f)T_e^{\frac{1}{2}},$$

where $(1-f)$ is the fraction of the arc current carried by ions at the cathode and T_e is the electron temperature. Corresponding to an electron temperature of 20,000° this calls for a positive ion fraction of 9 percent, for 40,000° it calls for 6 percent. These values are within limits set by other considerations.

A preliminary experiment on the rate of vaporization q from an anchored cathode spot has given the very rough value of 2×10^{-4} g coulomb^{-1}. This is 12 times Kobel's value, but there is good reason for believing it to be the more reliable. Now the reaction from the cathode force must be the momentum carried toward the anode by particles leaving the cathode plasma. Thus their average velocity, neglecting angular distribution, must be F/q. If we suppose these particles to acquire this velocity as ions in the cathode plasma, the voltage through which they would have to be accelerated is

$$V=300(m/2e)(F/q)^2=3.2 \text{ v}$$

for $F=35$, $q=2\times10^{-4}$. It does not seem at all unreasonable that there should be a potential maximum of this order of magnitude in the plasma at the cathode and that the degree of ionization within the plasma should be high. Kobel's value of q would lead to a voltage difference of over 400 v.

The force value of 66 dynes/amp. at the largest current used, with the indication that still higher values occur for more concentrated emission, is at variance with Kobel's[2] value of 40 for a surface supposedly completely covered by a cathode spot. Anchoring experiments indicate, however, that possibly half or two-thirds of Kobel's arc current was coming from a cathode line at the edge of his small cathode pool. The large horizontal component of the corresponding force would not appear as a hydrostatic pressure and would, therefore, go undetected, thus ex-

[3] L. Tonks, Phys. Rev. **46**, 278 (1934).

plaining his lower experimental result for the concentrated cathode condition.

Working with a poorer vacuum and using solid cathodes, Easton, Lucas and Creedy[4] have found considerably lower force values than these, though in the same order of magnitude. Two copper cathodes gave 7 and 5.5 dynes per amp. respectively and zinc gave 14. Their curves bend upward slightly.

Summary

The horizontal component of the force at a cathode line between mercury and a vertical anchor has been measured, first roughly by the depression of the meniscus edge, then more accurately by means of a torsion system.

The orientations of a magnetic field which deflected the cathode line neither one way nor the other were determined as current and anchor angle were varied.

Assuming that these neutral directions gave the directions of the resultant cathode force, this resultant was calculated from the horizontal components and was found to vary from 35 dynes amp.$^{-1}$ at low currents from the 1-cm wide vane to 66 dynes amp.$^{-1}$ at 10 amp.

Both the neutral angle experiment and this result show that the effects of concentrating emission at the cathode line are not simply additive.

[4] Easton, Lucas and Creedy, Elec. Eng. **53**, 1454 (1934).

AUGUST 1, 1936 PHYSICAL REVIEW VOLUME 50

The Separation of Gaseous Isotopes by Diffusion

DEAN E. WOOLDRIDGE AND W. R. SMYTHE, *California Institute of Technology*

(Received May 16, 1936)

The design and use of a 34-member apparatus of the Hertzian type for the separation of gaseous isotopes by diffusion are described. Results of tests of the speed of various types and numbers of separation members are given. Tests on mixtures of carbon dioxide and argon at a few millimeters pressure give the same results as tests on the neon isotopes. The equilibrium time, from ten to fifteen hours, and the separation factor, 80, of a 24-member apparatus, working on mixtures of such gases, are found to be independent of the initial mixing ratios. Results obtained with the 34-member apparatus on methane, to concentrate C^{13}, and on nitrogen, to concentrate N^{15}, are shown to be in reasonable agreement with appropriate theory. Methane containing 16 percent of $C^{13}H_4^1$, and nitrogen containing 6 percent of $N^{14}N^{15}$, instead of the normal 1 percent and 0.6 percent, respectively, have been produced.

IN this laboratory[1] an apparatus has been constructed similar to that described by Hertz,[2] which utilizes the difference in the thermal velocities of molecules of different weights to separate the isotopes of a gas. In principle, the apparatus works as follows. The mixture of gaseous isotopes it is desired to separate is circulated through a series of porous-walled tubes by diffusion pumps, as shown in Fig. 1. The tubes, which are alternately short and long, are surrounded by individual Pyrex jackets, connected to the low-pressure side of mercury diffusion pumps, as shown in the figure. The gas which diffuses through the wall of a long tube is pumped back into the system at a point just to the right of the adjacent short tube. Now this gas will be a little richer in the lighter isotopes than that which passed on toward the left. Similarly, the portion of this gas which diffuses through the wall of the adjacent short tube on the right will be still lighter, and so on. Thus, on the average, there is a net transfer of the lighter isotopes toward the right, or "light" end of the apparatus, while the

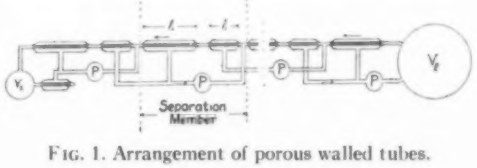

FIG. 1. Arrangement of porous walled tubes.

[1] Norman Bridge Laboratory of Physics, Pasadena.
[2] G. Hertz, Zeits. f. Physik **79**, 108 (1932).

heavier isotopes tend to gather in the reservoir provided at the left, or "heavy" end.

Since the system is closed, an equilibrium must eventually be reached. Hertz has treated the case of a mixture of two isotopes. He showed[2] that, in equilibrium, the ratio of the density of the heavy molecules to that of the light molecules increases from one separation member to the next by a factor

$$q=f^{\mu}/(1-(1-f)^{\mu}),$$

where $f=1/(2+l_2/l_1)$; $\mu=(m_l/m_H)^{\frac{1}{2}}$.

"q" he has called the "separation factor" of a single member. For an apparatus of m members, the separation factor is obviously q^m. This result was derived for the usual case, in which the relative abundance of the heavier isotope is small. He also assumed, in his derivation, that no backward diffusion occurs, either along the tubing or through its walls. If l_1 is made too small, gas passes from one separation member to the next chiefly by diffusion along the tubes, and a different relation applies.[3] In general, the speed of separation is less for an apparatus with $l_1=0$, but it has been thought to give a higher separation factor.

In our preliminary tests of various types of separation members, an apparatus with two pumps was constructed. Unglazed pyrometer tubing, obtained from the Stupakoff Laboratories in Pittsburgh, Pa. has been used throughout the work done here; it can be sealed directly to Pyrex. The circulating pumps were, initially, ordinary first-stage mercury diffusion pumps. The apparatus had end volumes of 3 liters and 200 cc at the light and heavy end, respectively. Mixtures of nitrogen and carbon dioxide, at pressures of from 3 to 15 mm, were used in this early work. The composition of the gas in V_s was followed continuously during the diffusion process by means of a Pirani gauge, which had been calibrated previously at various pressures by known nitrogen-carbon dioxide mixtures. More precise single analyses were made by measuring the pressure before and after freezing out the carbon dioxide in liquid air.

We found, early in this work, that ordinary high vacuum mercury pumps are not suitable for circulating gas at pressures of several millimeters of mercury. Tests of several pump designs led to the adoption of a single-stage pump having a flat boiler, to prevent bumping, a condenser of length 6 inches and I.D. $\frac{3}{8}''$, and a jet of O.D. $\frac{9}{32}''$, set $\frac{1}{16}''$ down into the condenser. With such a pump, the pressure outside a porous tube in the diffusion apparatus can be maintained at less than $\frac{3}{4}$ mm when that inside is 12 mm. This requires a mercury vapor pressure of 6 cm in the boiler of the pump. In operation, enough heat is supplied to the pumps, by Bunsen burners, to maintain a mercury column in each of about 8 cm.

The care taken to develop adequate pumps was justified, not only by the attainment of greater speed of separation, but by the elimination of the surprisingly large decrease in the separation factor caused by failure of the pumps to maintain a negligible pressure outside the porous tubes. If y represents the ratio of this pressure to that inside the tube, the usual expression for q must be modified by replacing μ by μ', where

$$\mu'=\mu[1+y(1-\mu)].$$

Since q is quite sensitive to small changes in μ, this correction may be quite appreciable, even if y is only about 0.1.

Separation members were constructed and tested for which:

1.	I.D. = 5.0 mm;	O.D. = 7.0 mm
a.	$l_1=12''$;	$l_2=12''$
b.	6	12
c.	4	12
d.	2	12
e.	0	12
2.	I.D. = 5.5 mm;	O.D. = 8.0 mm
a.	$l_1=1''$;	$l_2=12''$
b.	1	18
c.	$1\frac{1}{3}$	12
d.	$1\frac{1}{3}$	18
e.	2	24
3.	I.D. = 2.95 mm;	O.D. = 4.32 mm
a.	$l_1=1\frac{1}{3}''$;	$l_2=12''$

All tubes were made of the same material (Stupakoff E–42 tubing).

The measurements showed that, when running on a carbon dioxide-argon mixture (of initially equal proportions) at 6 mm pressure, the apparatus required an equilibrium time not measurably greater for case 1d than for 1a, whereas for

[3] Harmsden, Zeits. f. Physik **82**, 589 (1933).

TABLE I. *Comparison of the experimental results with theory in the case of a mixture of carbon dioxide and argon.*
t is the time the diffusion has been in progress. R_s is the ratio of the pressure of carbon dioxide and argon in the sample removed from V_s. R_l is the ratio of the pressures of argon and carbon dioxide in the sample removed from V_l. $Q(=R_sR_l)$ is the separation factor of the apparatus.

t	R_s	R_l	Q
Run 1: $p=6.9$ mm			
0	1/2.7	2.7	1
6.5 hrs.	10.0	5.0	50
26	14.8	5.75	85
Run 2: $p=6.80$ mm			
0	1/10	10	1
8	1.57	48	75
30	1.50	59	88
The gas of this run was then allowed to stand in the system for 15 hours, then circulation was recommenced:			
0	?	?	
10	1.11	70	78
28	1.04	72	75
Run 3: $p=6.60$ mm			
0	1/50	50.0	1
11	0.21	350	74

case 1e it was four times as great. This led to the use of separation members having a low, but not actually zero, value of f. In its final form the apparatus has units of all five types listed under "2" in the foregoing. These units have almost identical characteristics.

Later, runs were made with systems of five and ten members, to compare their equilibrium times. For these comparisons types 2c and 2d were used. A $10\frac{1}{2}$ mm run on a carbon dioxide-nitrogen mixture (of initially equal proportions) was completed in 30 minutes using five members, and in 90 minutes using ten. The final separation factors were at least 7.5 and 50, respectively. For these tests, V_l was 5 liters and V_s was 200 cc.

Apparatus of more than ten separation members was tested with mixtures of carbon dioxide and argon. Analyses were made by pressure measurements before and after freezing out the carbon dioxide. The mass ratio 40 : 44 for mixtures of such gases is exactly that of the neon isotopes. Before using the results of tests made with this mixture, it seemed advisable to see if this separation factor was the same as that obtained with the neon isotopes. With 14 members, 11 mm runs on carbon dioxide-argon mixtures (of initially equal proportions) gave a separation factor of 8 or 9. Similar runs on neon gas were made and four analyses of the end-products, using a mass-spectrometer,[4] agreed in assigning a value of between 6 and 10 to the separation factor, the average being 7. The agreement between these results seemed to justify the simpler method of testing. It should be remarked here that the results obtained with carbon dioxide-argon mixtures are always consistent with those obtained in the actual separation of isotopes, provided that the pressure of the carbon dioxide-argon runs is not over 10 or 11 mm. At higher pressures the separation factor drops rapidly, probably because of the setting in of viscosity effects which invalidate the simple diffusion ideas on which the theory of the apparatus has been founded. It seems likely that similar viscosity effects should appear in actual isotope separations, but so far no evidence for this has been found, for pressures up to 12 mm.

Table I affords a comparison of the experimental results with theory, and gives an idea of the time of equilibrium of the apparatus, for various initial mixing ratios of the component gases. These data were obtained with carbon dioxide and argon in an apparatus of 24 separation members, for which V_l was 5 liters and V_s was 300 cc. The apparatus contained five members of type 2a, five of type 2b, five of type 2c, five of type 2d, and four of type 2e. In Table I "t" shows the length of time the diffusion has been in progress; "R_s" denotes the ratio of the pressures of carbon dioxide and argon in the sample removed from V_s and analyzed; "R_l" is the ratio of the pressures of argon and carbon dioxide in the sample removed from V_l and analyzed; "Q" is the separation factor of the apparatus, i.e., $Q=R_sR_l$. Each analysis of R_s and R_l involved the removal from each end of the system of enough gas to fill a 600 cc volume to a pressure of from 0.5 to 1.0 mm of mercury.

Such data clearly show that neither the separation factor nor the equilibrium time depends appreciably on the initial mixing ratio of the gases, for carbon dioxide-argon mixtures in the 24 member apparatus. These measurements give the separation factor to be about 80, and the time of equilibrium to be of the order of 10 to 15 hours. The calculated separation factor for this apparatus is 73. The apparent greater than 100

[4] D. D. Taylor, Phys. Rev. **47**, 666 (1935).

percent efficiency signifies little, since small errors in the lengths of some of the porous tubes could easily account for this difference, if indeed it is real.

But one is ordinarily interested, not in Q, but in the enrichment factor, E, which is the ratio of the relative abundance of the heavier isotope in V_s, after equilibrium is reached, to that in the gas initially admitted to the system. If E is to approach Q, it is evident that V_l should be large compared with the volume of the rest of the system, so that R_l is nearly constant. Even though V_l is 22 liters in the final diffusion apparatus, E is always quite appreciably less than Q. It can be shown that, when equilibrium has been reached:

$$x_0/P=(-b+(b^2-4ac)^{\frac{1}{2}})/2a,$$

where $a=q^{m+1}-1$; $b=rq^{m+1}+1-(p_0/P)t(q^{m+1}-1)$;

$$c=-(p_0/P)t$$

and $$r=(V_s+V_e)\rho^{m+1}/V_l;$$

$$t=[V_l+\rho^{m+1}V_s+v(1-\rho^m)/(1-\rho)]/V_l,$$

while

$$V_e=v\frac{[(q^{m+1}-1)/(P/x_0)+1]}{(\rho q)^{m+1}}\sum_{n=1}^{m}\frac{(\rho q)^n}{(q^n-1)/(P/x_0)+1}$$

where x_o is pressure of heavy isotope in V_l; P is total pressure in V_l; p_o is pressure of heavy isotope in gas when separation was started; m is number of separation members; q is separation factor for one member; ρ is factor by which total pressure in nth separation member from V_l exceeds that in $(n-1)$st member (always less than 1); v is volume of a separation member.

In practice, it is necessary to solve for x_o/P and V_e simultaneously, by successive approximations. All other quantities are known except v, the volume of a separation member. This cannot be determined from geometrical considerations alone because the gas pressure in the pump boilers, and its effective contribution to v, is not known. For the data in Table I, an assumed value of 110 cc for v fitted all the experimental results, so this value has been used in subsequent computations.

The present apparatus has 34 members, five more members of type 2b, and five of type 2d having been added. A 22-liter Pyrex bulb is used for V_l and a 300 cc or 400 cc one for V_s. The pressure gradient in this apparatus depends on the pressure in V_l. When this pressure is 10 or 11 mm, the pressure in V_s is only 6 or 7 mm; when p_l is 8 mm, p_s is about 4.

The porous tubes used are somewhat hygroscopic, so that preliminary flushings to remove water and absorbed gas must usually precede a separation run. The run itself is generally performed at a pressure (in V_l) of 10 or 11 mm. Somewhat arbitrarily, 24 hours of circulation has been fixed upon as ample and convenient for a separation process. Ordinarily, several 300 cc samples are removed from V_s, at 24-hour intervals, for each filling of the system. This removal is facilitated by using a magnetically operated mercury cut-off to shut off V_s from the diffusion system while its contents are being pumped into storage bulbs by a mercury diffusion pump like those in the diffusion apparatus.

During the separation process the spectrum in a small capillary discharge tube sealed into V_s is watched through a small pocket spectroscope for the appearance of impurities. When any real concern is felt as to the extent of impurities in the final sample, a molecular weight determination is made by means of a quartz fiber gauge,[5] into which a small amount of the contents of V_s may be admitted. If, as is often the case, the gas initially admitted to the diffusion system contains several tenths of a percent of heavy impurities, it is necessary to remove this by a preliminary separation run. This, of course, decreases the enrichment factor.

Occasionally we have used multiple diffusions to increase the effective enrichment factor of the apparatus. This involves collecting gas from the heavy end of the system at the end of several diffusions and reintroducing this, together with enough ordinary gas to fill the system, for the final separation process. Another scheme tried has been that used by Hertz[6] in his work on heavy hydrogen. He ran a discharge tube continually in his diffusion apparatus, in order to break up the H^2H^1 molecules and form, by recombination, H^2H^2 molecules. This device might be useful whenever the gas being worked with is

[5] Haber and Kirschbaum, Zeits. f. Elektrochemie **20**, 296 (1914).

[6] Hertz, Naturwiss. **21**, 884 (1933).

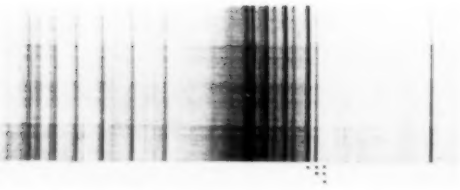

FIG. 2. Photograph of the Swann bands of C_2 showing an enrichment factor of about 16 in C^{13}. The single dot marks the head of the λ4737A $C^{12}C^{12}$ band; the double dot, the head of the λ4744A $C^{12}C^{13}$ band; the triple dot marks the corresponding $C^{13}C^{13}$ band head. (Photograph taken by F. A. Jenkins.)

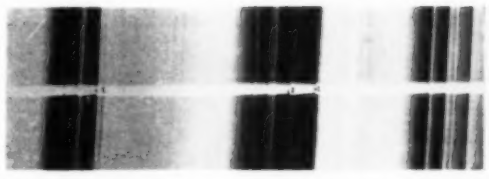

FIG. 3. Photograph of a part of the band system of N_2 in the λ3000A region. Upper photograph, ordinary N_2; lower photograph, with nitrogen enriched in the N^{15} isotope.

of the form X_2—i.e., H_2, N_2, O_2, etc. It can be shown that ordinarily (when the separation factor is not too high) the use of a discharge tube in this way can result in doubling the separation factor.

DESCRIPTION OF RESULTS

Results obtained in separations performed with this apparatus on methane, to concentrate C^{13}, and on nitrogen gas, to concentrate N^{15}, have been reported in recent issues of the *Physical Review*.[7, 8] In Fig. 2 is reproduced a photograph of an intensity plate taken by F. A. Jenkins, of the Physics Department of the University of California, of the Swann bands of C_2. The discharge was produced in argon containing some of the methane gas which had been run through the 34 member diffusion apparatus described herein. The single dot marks the head of the λ4737A $C^{12}C^{12}$ band, the double dot the head of the λ4744A $C^{12}C^{13}$ band, while the triple dot marks the corresponding $C^{13}C^{13}$ band head, which can be seen in the lower steps of the photograph. Microphotometer measurements yielded a value of 3.3 ± 0.2 for the relative intensities of the $C^{12}C^{12}$ and $C^{12}C^{13}$ bands. The intensity of the $C^{13}C^{13}$ band (three dots), which could also be measured, was consistent with this. The relative intensity of these bands, in normal carbon, is 53 : 1.[9] The enrichment factor of the process which produced this heavy gas was, therefore, about 16. This was an occasion on which heavy gas was lost by preliminary purification runs, while this was compensated for by a multiple diffusion process such as described in the foregoing, wherein two preliminary runs were employed. The result is in as good agreement with the theory as could be expected, in view of the quantitative uncertainties of this method.

In Fig. 3 are shown photographs, also taken by Jenkins, of part of the band system of N_2, in the λ3000A region. The upper photograph is of a discharge in gas containing ordinary N_2; the lower is of a discharge in gas containing N_2 which had been run through the diffusion apparatus. Single dots mark $N^{14}N^{14}$ band heads, double dots the corresponding $N^{14}N^{15}$ heads. Measurements[10] of the intensities of the normal and isotope bands of nitrogen have assigned a value of 175 : 1 to this ratio, for ordinary gas. The corresponding ratio was found by Jenkins to be 16.5 : 1 for the enriched gas. Three preliminary diffusions were employed in the work with nitrogen. Theory and experiment check as well as can be calculated, on the assumption that the efficiency of the diffusion process is 100 percent.

More recently, oxygen has been treated in this way, but no measurements of the results have yet been made. For the near future, work on argon is projected, to concentrate A^{36}.

Acknowledgments are due Dr. F. A. Jenkins, for the photographs and analyses of band spectra reproduced here; to Dr. D. D. Taylor, for assisting in the mass spectrometric measurements on neon; and to Drs. B. N. Sage and W. N. Lacey, of the Chemistry Department of the California Institute of Technology, for supplying us with the pure methane gas used in some of this work.

[7] Wooldridge and Jenkins, Phys. Rev. **49**, 404 (1936).
[8] Wooldridge and Jenkins, Phys. Rev. **49**, 704 (1936).
[9] F. A. Jenkins, Proc. Koninklijke Akademie van Wetenschappen Te Amsterdam, **35**, 10, 1212 (1932).
[10] Murphy and Urey, Phys. Rev. **41**, 141 (1932).

The Effect of Temperature, Degree of Thoriation and Breakdown on Field Currents from Tungsten and Thoriated Tungsten

A. J. AHEARN, *Bell Telephone Laboratories*

(Received June 1, 1936)

Electron field currents from thoriated tungsten, with different degrees of thoriation, were found to be independent of temperature. The characteristic field current curve was found to be independent of the degree of thoriation of a thoriated tungsten filament. An electrical breakdown, a sudden discontinuity in the characteristic field current curve at which the current increases from small values usually considerably less than a microampere to a few milliamperes, occurs with thoriated tungsten and pure tungsten cathodes. This breakdown raises the field current curve to higher currents by an enormous factor. Current increases by factors from 10,000 to 10,000,000 were usually obtained. With pure tungsten no change in the thermionic activity of the cathode results from the breakdown; with thoriated tungsten the thermionic emission is increased; i.e., a partial thoriation of the filament occurs. Heat treatment at about 1300°K following breakdown generally further increases the field currents from thoriated tungsten but produces no such effect with pure tungsten. The high field currents following breakdown can be erased by heating the cathode to about 2600°K for a few minutes. The value of the breakdown field is independent of the temperature and the degree of thoriation of a thoriated tungsten cathode. The application of the usual breakdown voltage with the filament as anode produces none of the usual effects of breakdown. Breakdown does not occur if a sufficiently high resistance is inserted in the circuit. In general, successive breakdowns occur at increasingly higher values of the applied field. None of this progression can be attributed to a conditioning of the anode. A definite part of this progressive increase in the breakdown field can be attributed to glass surfaces when they are exposed to the discharge. The highest electric field that could be applied to a cathode without breakdown occurring was about 4.7×10^6 volts/cm. The evidence favors the following conclusions: The electric field applied to the cathode rather than the applied voltage is the more important factor in producing breakdown. The anode has no effect on the breakdown. When the shielding of glass surfaces is adequate, the breakdown is determined primarily by conditions at the cathode.

INTRODUCTION

MANY years ago it was discovered that electrons are emitted from a seemingly cold cathode when a sufficiently high voltage was applied. There was at first some question whether the onset and subsequent rise of this "cold discharge" depended primarily on the applied potential or upon the electric field applied to the surface of the cathode. Later experiments, in which the electrode separation in a given tube could be varied at will, showed definitely that the discharge was determined by the applied electric field at the cathode rather than by the applied voltage. For this reason this cold discharge of electrons is designated quite frequently by the term "field currents."

In field current experiments small fluorescent spots are often observed on the anode. By means of a magnetic field they can be moved about. This shows that field currents are not emitted uniformly over the surface of the cathode but consist chiefly of pencils of electrons from a few minute areas. These active areas probably consist of surface irregularities such that the applied electric field is there much greater than the average value over the surface of the cathode.

Whereas a thermionic current increases *very slowly* with the applied field, the logarithm of the current being proportional to the square root of the field in the Schottky effect, the field current emission varies very rapidly with the applied field. The functional relationship between current and field is quite different from that of the Schottky effect. Here the logarithm of the emission is proportional to the reciprocal of the applied field. Thus the variation of field currents with the applied field is of exactly the same form as the variation of thermionic currents with temperature.

The earliest experiments agreed that there was no large effect of temperature on field currents. It was found that the measured current remained unchanged as the temperature was raised from room temperature to about 1000°K. However, it was observed that a further increase in temperature to 1100°K resulted in an increase in the measured current by about 30 percent. One school of investigators interpreted this as a real

field current temperature effect while others maintained that this increase was due merely to the onset of the thermionic emission. It has since been definitely established that, when the thermionic emission correction is properly made, there is no evidence whatever for any effect of temperature on field currents from clean surfaces of tungsten and molybdenum. In view of the experimental fact that field currents from clean surfaces of metals are independent of temperature, it is important to know whether or not this independence extends to the case of composite surfaces. To this end temperature experiments were made with thoriated tungsten and are presented in Part I of this paper.

Little work has been done on the effect of the work function of the cathode on the field currents therefrom. In work of this kind it is important to be able to alternately increase and decrease the work function of the cathode by sizable amounts in order to distinguish between a real effect of the work function and a simple aging of the filament. Experiments of this sort are described in Part II.

In general, once a given field has been applied to a filament, so long as this value is not exceeded, a reversible current *vs.* field curve is obtained. When this value of the field is exceeded a new reversible curve results usually corresponding to somewhat smaller current values. However, when the applied field is extended to 1 or 2×10^6 v/cm a sharp discontinuity occurs involving enormous changes in the field currents. Experiments dealing with these breakdown effects are described in Part III.

PART I

The Effect of Temperature on the Emission of Electron Field Currents from Thoriated Tungsten

Introduction

In an earlier publication[1] results on the effect of temperature on the emission of electron field currents from molybdenum and tungsten were presented. In this work, the thermionic emission, particularly its onset, was separated from the field current emission by extrapolating high temperature emission measurements. Extensive measurements over a wide range of conditions showed that: (1) between 300°K and 1400°K, at which temperature the thermionic emission became perceptible, the electron field currents are independent of temperature to within 5 percent; (2) between 1400°K and about 1600°K the data are consistent with the assumption that the measured current consists of the thermionic current plus the field current which is independent of temperature; (3) beyond about 1600°K the field currents were completely masked by the thermionic currents. Thus from clean surfaces of tungsten and molybdenum there is no evidence of any field current temperature effect as great as 5 percent.

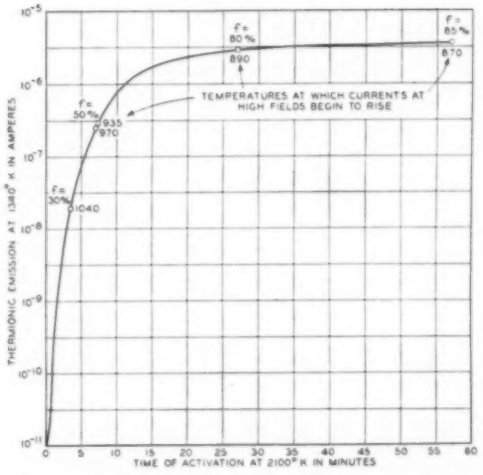

FIG. 1. Thermionic activation of thoriated tungsten filament. Field current *vs.* temperature measurements were made at the indicated points on the curve, the thermionic current becoming perceptible at the indicated temperatures.

Results

In this section, using the same technique of measurement and analysis of data, results on the effect of temperature on electron field currents from thoriated tungsten are presented. The filament was flashed at about 2800°K and then activated by operating at about 2100°K for about 60 minutes as shown in Fig. 1. This served to raise the thermionic emission at 1340°K by a factor of about 400,000. At the different states of activation[2] given by the plotted points in Fig. 1,

[1] Ahearn, Phys. Rev. **44**, 277 (1933).

[2] In this paper the degree of thoriation is given by values, reference 3, of f which are *approximately* proportional to the percentage of surface covered with thorium.

[3] Brattain and Becker, Phys. Rev. **43**, 428 (1933).

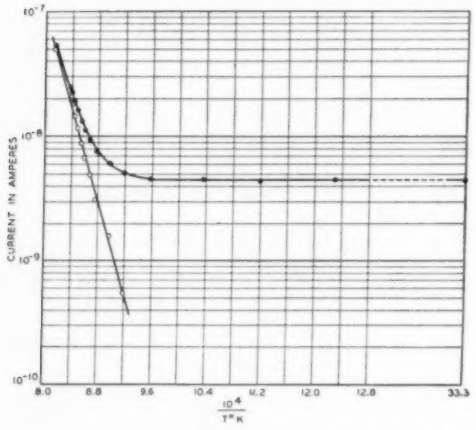

FIG. 2. Emission current *vs.* temperature data for thoriated tungsten filament. $F=5.7\times10^5$ v/cm. $f=28$ percent.

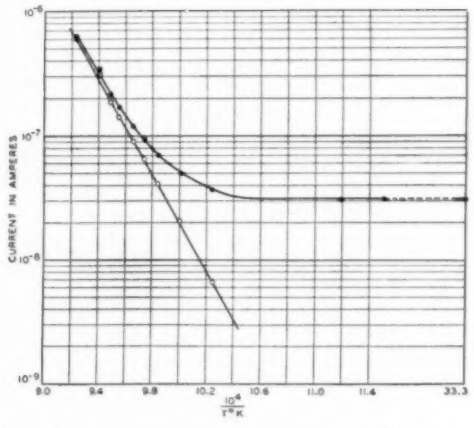

FIG. 3. Emission current *vs.* temperature data for thoriated tungsten filament. $F=9.3\times10^5$ v/cm. $f=80$ percent.

for different values of the applied field, emission current *vs.* temperature measurements were made. In all, measurements were made in the range of applied field from 4.4×10^5 volts/cm to 9.3×10^5 volts/cm. Figs. 2 and 3 give typical sets of data and show the effect of temperature. In Fig. 2 one sees that the measured currents are independent of temperature up to about 1040°K. The points marked by open circles (○) are obtained by subtracting the room temperature value of the field current from the observed currents at the higher temperatures. If the field current is independent of temperature these difference currents should be the values of the thermionic emission and should therefore, according to the Richardson thermionic emission law, fall on a straight line. They do satisfy a straight line relation very well as shown and one can assume that the increase in the observed current is due entirely to the thermionic emission. The data of Fig. 3 and all similar data taken at the various points on Fig. 1 show the same result.

Summary

The results therefore may be summarized as follows: Measurements were made over the range of applied field from 4.4×10^5 v/cm to 9.3×10^5 v/cm. The degree of thoriation f as varied from about 30 to 100 percent. At temperatures, indicated at the different points of Fig. 1, below which the thermionic emission is imperceptible, the field current (i.e., the measured current) is independent of temperature to within 5 percent. Over the temperature range employed, where the thermionic current does contribute to the measured emission, the data are all consistent with the assumption that the field current is independent of temperature. Thus, in complete agreement with the results on clean surfaces of molybdenum and tungsten, there is no evidence for any field current temperature effect with thoriated tungsten.

PART II

THE VARIATION OF THE FIELD CURRENT CHARACTERISTICS WITH THE DEGREE OF THORIATION OF THORIATED TUNGSTEN

Introduction

Having found that, so far as the effect of temperature of field currents was concerned, thoriated tungsten was not unlike clean tungsten and molybdenum, it was of some interest to see how the field current characteristics varied as the thermionic work function of the thoriated tungsten was varied. This point was studied by measuring the field current characteristic, i.e., the field current *vs.* applied field curve, of one mil thoriated tungsten filaments where by the proper heat treatment different amounts of thorium were accumulated on the filament surface thus varying its work function. The experimental tube is described elsewhere.[1]

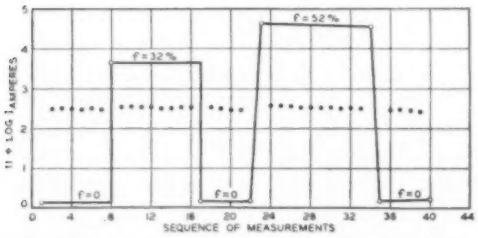

FIG. 4. Field current *vs.* degree of thoriation data for thoriated tungsten filament. ○—thermionic current at 1340°K; ●—field current at 300°K and $F=6.5\times10^{5}$ v/cm. Field current measurements at 30 second intervals.

Results

Typical results are given in Figs. 4 and 5. In Fig. 4, the filament was flashed at about 2800°K for a few seconds after which a thermionic current of about 1×10^{-11} ampere was obtained at 1340°K as shown by measurement No. 1. This current is about the value characteristic of clean tungsten and it can be assumed that now the filament surface is nearly free of thorium, i.e. f is about equal to zero percent. The filament was then cooled to room temperature and a field of 6.5×10^{5} v/cm applied, several current measurements being made at about 30-second intervals. Next by the appropriate heat treatment of the filament, enough thorium was accumulated on the surface to increase the thermionic emission by a factor of about 4000, i.e., f equals 32 percent as shown by measurement No. 8. Another series of field current measurements was then made. These are shown by points 9 to 16. By the proper heat treatment, the thermionic emission was now reduced to the original clean tungsten value and the cycle of measurements was repeated. In this case the thermionic emission was increased by a factor of about 40,000 i.e., f equals 52 percent. One immediately sees that the enormous changes in the thermionic activity are accompanied by little or no change in the magnitude of the field current. The average value of the field current corresponding to the low thermionic activity is 3.0×10^{-9} ampere ±5 percent while that for the high thermionic activity is 3.5×10^{-9} ampere ±5 percent. In view of the average deviations given, it is uncertain that this 16 percent increase is significant. The data do show that the field currents are nearly constant and independent of the degree of thoriation from f equal to 0 to about f equal to 50 percent.

TABLE I. *Constants of field current characteristic (log I vs. 1/f at 300° K).*

f in %	Slope		Intercept Current in amperes at $1/F=1.1\times10^{-6}$ cm/volt	
0		−2.63		3.5×10^{-8}
72	−2.53		3.0×10^{-8}	
0		−2.56		2.9×10^{-8}
0		−2.65		3.5×10^{-8}
43	−2.56		3.2×10^{-8}	
0		−2.63		2.9×10^{-8}
0		−2.67		3.5×10^{-8}
64	−2.72		3.6×10^{-8}	
0		−2.98		3.7×10^{-8}
Averages and average deviations	−2.68±3%		−2.69±4%	3.3±6% 3.3±9%

Table I summarizes further measurements on the same filament in which current *vs.* field measurements were made with widely different states of thermionic activity. The slopes and intercepts of the straight lines which result from plots of the logarithm of the emission *vs.* the reciprocal of the applied field are given along with the percentage of the surface covered with thorium. The filament is thermionically activated and deactivated repeatedly, through the values of f given. The average values for the slopes and for the intercepts of the field current character-

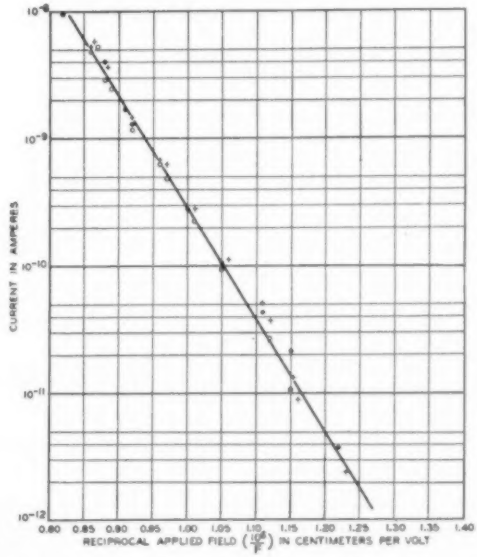

FIG. 5. Field current *vs.* applied field data as a function of degree of thoriation. Run 1 (●) $f=100$ percent; Run 2 (○) $f\sim0$ percent; Run 3 (+) $f=73$ percent.

istic curves accompanying the high thermionic activity state are not significantly different from those for the case of clean tungsten thermionic activity. Thus the field current independence of thermionic activity at the particular value of the field shown in Fig. 4 is shown to be quite general over the range of field investigated in Table I.

Fig. 5 shows similar results obtained with another one-mil thoriated tungsten filament. In Run 1 the filament is thoriated to f equals 100 percent. In Run 2 (f equals 0), a nearly clean surface of tungsten is presented. Again in Run 3, by the appropriate heat treatment, the filament is again thoriated to f equals 72 percent. The single straight line satisfies the three sets of data reasonably well.

The data of Fig. 4 show that at a given value of applied field, the field current is, to within a few percent, independent of the degree of thoriation of the cathode. The data of Table I and Fig. 5 show that this independence holds quite generally over the entire range of applied fields studied and for all values of f from zero to 100 percent or to fully thoriated tungsten.

Discussion of results

This experimental fact that the field currents from thoriated tungsten are independent of the degree of thoriation of the filament can be interpreted in three different ways: (1) The field currents are independent of the work function of the emitting surface; (2) the minute areas which emit the field currents never become thoriated; i.e., throughout the cycle of experiments these areas are clean tungsten surfaces; (3) these minute areas originally become thoriated and in the above cycle of experiments they remain unchanged. Interpretation No. 1 if proved to be correct is of fundamental importance in any theory dealing with the mechanism of field emission. If interpretation No. 2 or 3 is correct then the results are significant only in a more practical way.

One might hope to choose between the last two cases by comparing the field current curves for the thoriated tungsten filaments with those for pure tungsten. The second interpretation would be favored if the field current characteristic curves for the two metals were about the same, but if there was a significant difference appropriate to the difference in the work function of thoriated tungsten and clean tungsten, then the third interpretation would be favored.

In practice, such a comparison of field current curves for different metals can be very deceiving. The two thoriated tungsten filaments studied gave widely different characteristic curves. Likewise different pure tungsten filaments gave different characteristic curves. Moreover the characteristic curve for a given pure tungsten filament varied through a considerable range depending on its treatment. Hence from the present work it is not possible to state whether the characteristic curves for the two metals are the same or are significantly different.

These experimental observations are not in agreement with somewhat similar work of other investigators. Gossling,[4] De Bruyne,[5] and Stern, Gossling and Fowler[6] found that with tubes in which the anode was coated with sodium phosphate or barium azide the passage of a glow discharge, i.e., the bombardment of the cathode by ions of sodium or barium, tends to increase the field current emission. This current increase is attributed to a decrease in the work function of the cathode due to the adsorption of the ions. It was implicitly assumed that the ion bombardment resulted in no pitting of the cathode surface. Stern, Gossling and Fowler explicitly assumed that this ion bombardment produced no change in the potential gradient form factor of the cathode. On this basis, they associated the shift of the field current curves with changes in the work function of the cathode due to adsorption of sodium or barium. No direct measurements of work functions or work function changes were made in any of these experiments. The observed shifts in the field current curves can be equally well explained by changes in the potential gradient form factor of the cathode due to pitting, etc. Therefore proof that field currents depend on the work function of the cathode is lacking.

Unpublished experiments by Langmuir, Dushman and Hull[7] are briefly described in which, with an activated thoriated tungsten filament

[4] Gossling, Phil. Mag. **1**, series 7 (1928).
[5] De Bruyne, Phil. Mag. **7**, series 5 (1928).
[6] Stern, Gossling and Fowler, Proc. Roy. Soc. **A124**, 699 (1929).
[7] Compton and Langmuir, Rev. Mod. Phys. **2**, April (1930).

with 30 kv applied, small field currents are emitted, which are rapidly increased to a much greater value by the thermionic emission resulting from the heating of the anode and the resulting back radiation. This effect apparently does not occur with an unactivated thoriated tungsten filament. It is not clear however that this is evidence that field currents from a thoriated tungsten filament are a function of the degree of thoriation, due to the confusing effect of the thermionic emission which varies so rapidly with the degree of thoriation.

Quarles[8] using a high frequency impulse voltage method measured the electric field needed at the surface of a mercury cathode to initiate a vacuum spark which is known to be initiated by field currents. The contact potential between the mercury cathode and a platinum filament was varied in an uncontrolled way through about 0.7 volt. The assumption is made that the work function of the platinum filament remained constant and that the contact potential changes therefore represent changes in the work function of the mercury surface. On this basis, it is found that the field necessary to initiate the vacuum spark increased linearly with these increases in the work function of the mercury surface. Earlier experiments by Beams[9] show that the breakdown potential with a mercury cathode depended on the purity of the surface.

Subject to a possible uncertainty in the interpretation of the contact potential changes the experiments of Quarles show fairly definitely that the field required to produce a vacuum spark which is known to be initiated by field currents, varies with the cathode work function. It follows from this that field currents from the mercury cathode depend on the work function thereof *only* if they comprise the entire cathode emission that is responsible for the vacuum spark.

Thus we have so far no clear cut case showing whether or not field currents are a function of the cathode work function. Information on the proper interpretation to be applied to the author's experiments could doubtless be obtained by depositing a few or several layers of thorium, or other suitable element, from an external source onto the cathode surface. If as suggested earlier, the negative results of the present experiments occur because the field current emission areas did not become thoriated, one might succeed in thoriating them in this way.

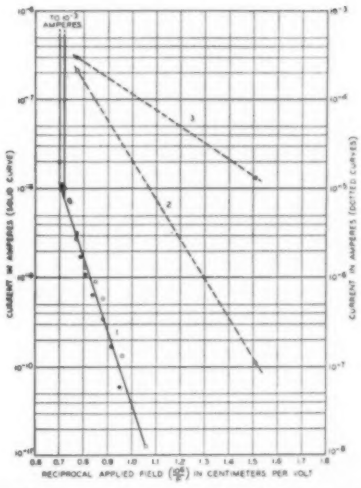

FIG. 6. Field current *vs.* applied field data for thoriated tungsten showing breakdown. Curve 1 (○) $f=4$ percent; Curve 1 (●) $f=0$ percent; Curve 2 (○) $f=20$ percent; Curve 3 (●) $f=13$ percent. 1.0×10^8 ohms resistance in anode circuit.

It seems very likely that using the electron microscope one could determine whether the areas active in field current emission were thoriated or were clean tungsten and whether or not they remained unchanged in the thoriation and dethoriation cycles of the above experiments. One could then choose between the above three interpretations of the experimental fact that the field currents are independent of the degree of thoriation of the filaments.

PART III

ELECTRICAL BREAKDOWN WITH THORIATED TUNGSTEN AND PURE TUNGSTEN

Description of breakdown

In extending the experiments on the effect of thoriation in the last section to higher fields a sharp discontinuity occurred as illustrated in Fig. 6. Between 1.0×10^6 v/cm and 1.3×10^6 v/cm the curve 1 was reversible but at 1.4×10^6 v/cm the current suddenly rose from 1×10^{-8} ampere to about 1×10^{-3} ampere. This discontinuity in the field current characteristic curve

[8] Quarles, Phys. Rev. **48**, 260 (1935).
[9] Beams, Phys. Rev. **44**, 803 (1933).

will be referred to as a "breakdown." On reducing the field, curve 2 is obtained which is approximately reversible. Noting the different current scales for curves 1 and 2, one sees that the breakdown has resulted in raising the characteristic curve by the enormous factor of 100,000 or more. Reducing the applied field to zero and heating the filament to about 2650°K for 40 seconds reduced curve 2 back to curve 1, the original pre-breakdown value. Again a reversible curve was obtained until a field of about 1.4×10^6 v/cm was applied at which point breakdown again occurred, the field current rising from about 1×10^{-8} ampere to about 1×10^{-3} ampere. The characteristic now given by curve 3, the currents being as much as 10,000,000 times greater than before breakdown. Heating the filament at 2650°K for a short time again reduced curve 3 approximately to that of curve 1.

Before the data of curve 1 were taken, a thermionic measurement showed that f equaled 4 percent approximately, i.e., the filament was only very slightly thoriated. Further tests showed that this value of f remained unchanged before the first breakdown occurred. However after this breakdown, the value of f was increased to 20 percent. In other words, now the thermionic emission at 1340°K was about 500 times greater than that of clean tungsten. The 2650°K heating of the filament employed to reduce curve 2 to curve 1 also reduced the value of f to about zero. Again, before breakdown, the thermionic emission remained unchanged but after breakdown the value of f was raised to 13 percent.

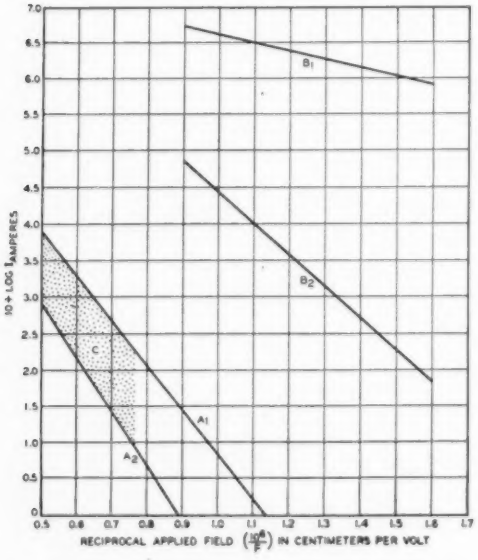

FIG. 7. An example of the range of breakdown fields and field current curves for a thoriated tungsten filament.
A_1 to A_2 Range of field current curves before breakdown.
B_1 to B_2 Range of field current curves after breakdown.
C The fields at which breakdown occur and the field currents just before breakdown fall in this dotted area.

Thus the breakdown produces two effects. It raises the field current characteristic curve on the current axis by an enormous factor. It increases the thermionic activity of the cathode by substantial amounts. Experiments with pure tungsten described later do not give an increase in thermionic activity following breakdown. Hence it follows that the increase with thoriated tungsten is due to a partial thoriation.

Range of field current increase following breakdown

In Fig. 6 one sees that the second breakdown shifted the characteristic curve 3 to higher current values than curve 2 which followed the first breakdown. One must not conclude however that successive breakdowns shifted the characteristic curve to increasingly higher current values. Many cases of breakdown have been observed in which the observable conditions were identical, i.e., the same characteristic curve before breakdown, the same breakdown field and current, the same thermionic activity of the filament, etc. Nevertheless the characteristic curves after successive breakdowns would be scattered at random over a wide range. Fig. 7 shows the range over which the curves after breakdown varied for a thoriated tungsten filament from which the data of Fig. 6 were obtained. In all about fifty breakdowns were observed with this filament before it was broken by a breakdown. For the same series of breakdowns the range of variation of the characteristic curve before breakdown is also given in Fig. 7. This variation did not proceed in any regular way with successive breakdowns but was quite random.

Neglecting the relatively small range over which the curve before breakdown varied, one sees that following breakdown, the characteristic curve may be raised to higher currents by a factor

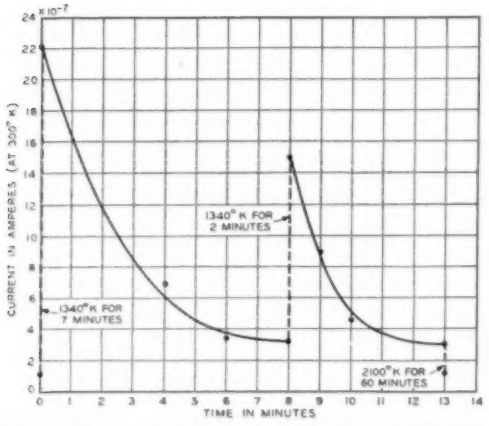

FIG. 8. Field currents from thoriated tungsten at $T=300°K$ and $F=6.5\times10^5$ v/cm.

anywhere between about 10,000 and about 1,000,000.

Degree of thoriation affected by breakdown

Just as there was wide variation in the amount by which the characteristic curve in Fig. 7 was shifted to higher currents by the breakdown, so there was considerable variation in the degree of thoriation produced by the breakdown. Whereas with f equal to zero before breakdown, it was found to range anywhere between zero and 50 percent after breakdown, values of f between 12 and 23 percent being most common. This must not necessarily be interpreted to mean that this thoriation is uniformly distributed over the surface. The above most commonly obtained values of f would be explained merely by assuming that 0.01 percent to 0.1 percent of the filament surface became fully thoriated by the breakdown.

There was no correlation between the magnitude of the thermionic activity increase and that of the field current curve shift to higher currents.

The effect of heat treatment of filament after breakdown

In connection with Fig. 6 it was stated that after each of the two breakdowns the characteristic curve was reduced to the low current values obtained before breakdown simply by heating the filament to 2650°K for less than a minute. This result could sometimes be attained at much lower temperatures. In a very few cases a temperature of 1340°K for a few minutes was sufficient. In many cases 2100°K for a minute or so was enough. In practically every case a temperature of about 2600°K for a couple of minutes was sufficient to restore approximately the characteristic curve obtained before breakdown.

A typical curve for the effect of low temperature heating of the thoriated tungsten cathode after breakdown is shown in Fig. 8. 1340°K for seven minutes raised the field current by a factor of about twenty. Leaving the voltage on, however, erased most of this gain. Again heating at 1340°K for two minutes gave an increase by a factor of five but the current decayed rapidly. In contrast to the increase in field current following the 1340°K heating, a temperature of 2100°K for one hour reduced this current slightly. A still higher temperature treatment in this case was necessary to reduce the current to the pre-breakdown value.

Similar low temperature treatments at 1340°K and 1640°K of a pure tungsten filament after breakdown gave no increase in field current. As stated already, treating the thoriated tungsten filament at 1340°K *before breakdown* does not change the field current at all. This low temperature effect is therefore closely associated with the breakdown phenomena and it may be an indication of an effect of thoriation on field currents in contrast to the thoriation experiments described earlier in this paper.

Range of breakdown fields

The second breakdown illustrated in Fig. 6 occurred at about the same value of the average applied field as the first one. In general as a filament was repeatedly taken through breakdown, the required field increased in an irregular way to higher values. In Fig. 7 the range through which the breakdown fields progressed is shown for that particular thoriated tungsten filament.

Table II summarizes the range of fields (and the corresponding applied voltages) over which

TABLE II. *Breakdown fields for pure and thoriated tungsten filaments.*

Cathode Material	Cathode Diameter, mil	Field Range, v/cm	Voltage Range, kv
Thoriated Tungsten	1	$1.3–2.0\times10^6$	11.1–17.1
Thoriated Tungsten	1	$1.2–2.6\times10^6$	10.3–24.2
Pure Tungsten	1	$2.0–2.8\times10^6$	16.7–23.4
Pure Tungsten	0.6	$1.5–2.67\times10^6$	8.4–14.9

the breakdown progressed with two thoriated tungsten filaments and also two pure tungsten filaments. In all four cases the upper limit of the range was set by the filament separating during the breakdown. One must not necessarily infer that, had the filament remained intact, the breakdown would not have progressed to higher values.

This is probably particularly true of the two thoriated tungsten filaments since there was no indication that the field, at which breakdown was successively occurring, was approaching a steady value. On the other hand, prior to the breaking of the one-mil pure tungsten filament, approximately the same value of the applied field, 2.8×10^6 v/cm, gave many successive breakdowns. There is, therefore, some considerable justification for thinking that with this filament the maximum breakdown field has been reached. There was similar although less extensive evidence with the 0.6-mil tungsten filament that the maximum breakdown field had been approximately reached.

Factors controlling breakdown

1. *Degree of thoriation of cathode.* Tests were made with one of the thoriated filaments in which, by the proper heat treatment, different degrees of thoriation were obtained along with the accompanying value of the breakdown field. Table III summarizes those tests.

One readily sees that there is no significant difference between the value of the breakdown fields for the widely different degrees of thoriation. This result is not surprising in view of the experiments already described in which it was found that the field current characteristic curve was independent of the degree of thoriation of the filament.

TABLE III. *Breakdown fields for various degrees of thoriation of filaments.*

Test No.	f in %	Breakdown Field in v/cm
1	4	1.43×10^6
2	0	1.43
3	100	1.47
4	80	1.49
5	25	1.43
6	40	1.47
7	3	1.47
8	3	1.39
9	0	1.51
10	0	1.41

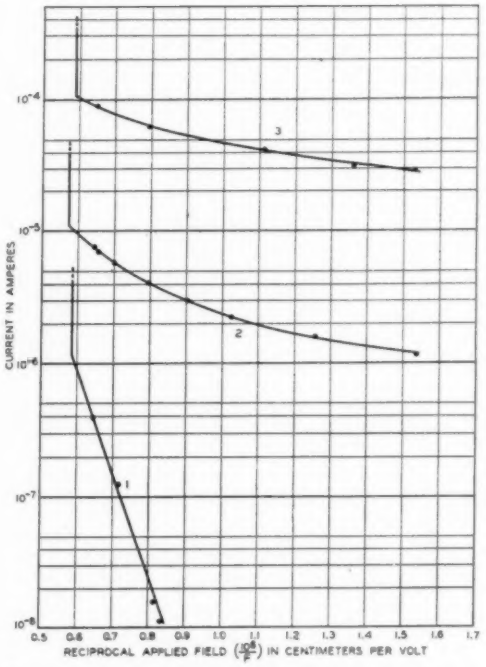

FIG. 9. Emission current *vs.* applied field data and the effect of filament temperature on breakdown. The vertical arrows indicate breakdown.

Curve 1 $T=$ 300°K
Curve 2 $T=$1340°K
Curve 3 $T=$1670°K.

2. *The temperature of the cathode.* If the onset of breakdown is determined at all by the energy dissipated in the tube or by the magnitude of the emission current then by raising the filament temperature, the resulting thermionic emission supplementing the field current by a large factor, one would expect the breakdown field to be decreased. Fig. 9 shows the results of such tests. With the filament successively at 300, 1340 and 1670°K, the breakdown fields were not different by a significant amount. Just before breakdown the current on curve 3 is about 300 times greater than the corresponding value on curve 1. Moreover at lower fields, the current is millions of times larger. Still the breakdown field is substantially unchanged.

This experiment shows that the energy dissipated in the anode or the emission current can be increased substantially without changing the breakdown field. This experiment however does not exclude the energy density dissipated on the

anode or the emission current density from the filament as a factor in breakdown. A simple calculation shows that, if all of the field current comes from 1 percent of the surface and the thermionic current is uniformly emitted over the filament surface, then just before breakdown the current densities for curves 1 and 3 are about the same. Later on in this paper experiments are described which show that the emission of current is necessary to induce breakdown and that the anode probably is not a factor in the phenomenon.

3. *Can breakdown be induced by field alone?* (*Filament as anode.*) If breakdown occurs independent of an emitted current when the applied electric field reaches a certain value, perhaps because the mechanical force ruptures the filament surface, then one ought to observe the typical increase in field current following the usual breakdown if the usual breakdown field is applied *with the filament as anode*. The results of such a test are given in Fig. 10. Curves 1, 1′; 2, 2′; 3, 3′ were obtained with the filament as cathode and show the usual breakdown and effects thereof. In each of the three cases, the original low current curve was restored approximately by heating the filament. Next, with the filament as anode, a field of 1.59×10^6 v/cm was applied as indicated by the dashed vertical line in Fig. 10. This field was slightly in excess of those for the above three breakdown cases. The filament was again made the cathode and the data of curve 4 was taken. It agreed very well with the pre-breakdown curves 1, 2, 3 rather than with those that followed breakdown. This shows that the electric field alone is not sufficient to produce breakdown but that an emission of current is necessary for the phenomenon.

4. *The suppression of breakdown by a high resistance in series with the anode.* Breakdown may be dependent upon the passage of the relatively large current of about 1.0×10^{-3} ampere at the breakdown field. This can be tested by using in the anode circuit a resistance of such magnitude that the voltage drop across it at 10^{-3} ampere greatly decreases the tube voltage. The results of such a test are shown in Fig. 11. With a resistance of 2.2×10^9 ohms, three excursions to $F=1.67\times10^6$ v/cm effected no increase whatever in the field current curve and there was of course no appearance of the characteristic large breakdown current. With a resistance of 1.0×10^8 ohms, the maximum field applied was $F=1.70\times10^6$ v/cm. Curve 4 resulted showing a relatively small but unmistakable increase over curves 1, 2 and 3. With a resistance of 1.0×10^5 ohms, which is the value used in the experiments already described, the field $F=1.70\times10^6$ v/cm resulted in the usual breakdown current and large increase in activity shown by curve 5. Subsequent measurements with this tube and a resistance of 1.0×10^5 ohms gave breakdown at $F=1.75, 1.64, 1.70, 1.56\times10^6$ v/cm. All of the above values of breakdown fields are corrected for the voltage drop across these resistances. Hence it is felt that in the tests of Fig. 11 the absence of breakdown was not because the maximum field was too small.

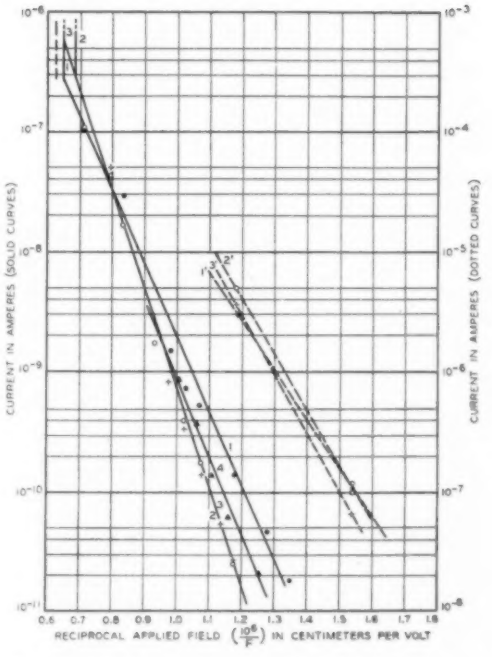
CURRENT IN AMPERES (SOLID CURVES)
CURRENT IN AMPERES (DOTTED CURVES)
RECIPROCAL APPLIED FIELD ($\frac{10^6}{F}$) IN CENTIMETERS PER VOLT

FIG. 10. Polarity of filament and breakdown. Curves 1, 1′, 2, 2′, 3, 3′ show usual breakdown. With filament as anode, $F=1.6\times10^6$ v/cm was applied after which curve 4 was obtained with filament as cathode.

Breakdown therefore can be suppressed by adding a sufficiently high resistance to the circuit, with this tube a resistance of about 2.2×10^9 ohms being sufficient. Other workers[11] investigating breakdown have observed much the same effect.

5. *Breakdown and the effect of the anode.* The tests so far described have been made with tubes in which the electrodes were in the form of concentric cylinders. The anode and exposed glass surfaces are possible factors influencing the breakdown. Tests on the effect of the anode on the breakdown are now described.

The experimental tube is shown in Fig. 12. The nickel anode is an accurately machined cylinder which is weighted on the inside so that it can be rotated by tipping the tube. One-third of the anode can thus be shielded from the discharge by the nickel shield shown. A definite curvature at the tip of the V-shaped 0.6-mil tungsten filament was obtained by shaping it around a 0.012-inch wire, applying tension, and flashing in hydrogen. The plan was to condition the tube with the portion *A* of the anode shielded until the tube would withstand breakdown at some voltage that was considerably higher than the first breakdown value. If a significant part of this conditioning process is a conditioning of the portion *B* of the anode, then by moving portion *A* to a position in front of the filament breakdown would occur at a value of the applied potential

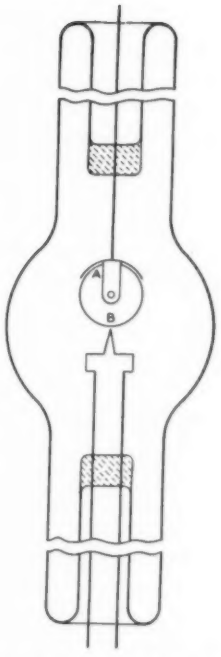

FIG. 12. Sketch of tube for investigating the effect of the anode on breakdown.

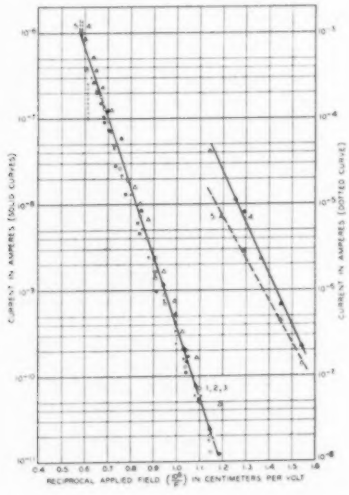

FIG. 11. Breakdown data and the effect of external resistance in anode circuit.

Curve	Resistance
1 (○), 2 (●), 3 (+)	2.2×10^{9} ohms
4 (▲)	1.0×10^{8} ohms
5 (Δ)	1.0×10^{6} ohms

Maximum field (dashed vertical line) is 1.64×10^{6} v/cm for curves 1, 2, 3.

that is significantly lower than the highest value observed with portion *B*.

In every case, with three different tubes, no effect on either the field current magnitude or the breakdown voltage was found when the portion *A* of the anode was placed in front of the filament. For example with one tube breakdowns were observed initially in the following order at 15.4, 22.0, 15.2, 16.0 kv. Then it was found that 19.2 kv could be applied without breakdown occurring. Then with the anode portion *A* next to the filament, breakdown did not occur until 21.8 kv was applied.

Therefore it appears to be quite definitely established that a tube which has been conditioned to withstand breakdown at a given voltage will not give breakdown at a significantly lower voltage when a portion of the anode, which has heretofore been shielded from the discharge, is exposed. Thus the anode would appear to be eliminated as a factor determining breakdown.

6. *Breakdown and the effect of exposed glass.* In the tests for an anode effect just described, the high degree of shielding of the filament and anode,

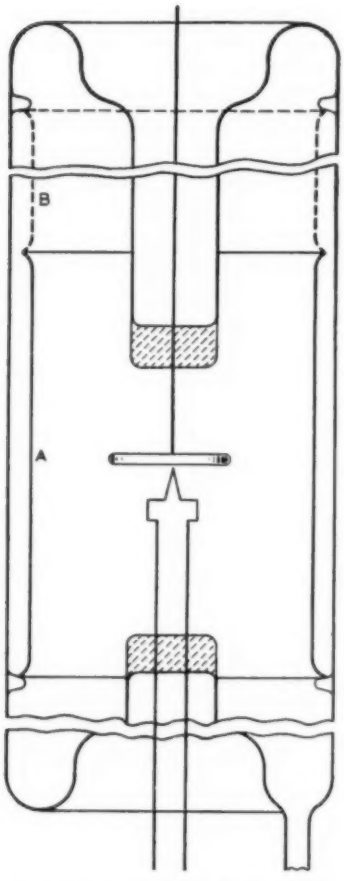

FIG. 13. Sketch of tube for investigating the effect of exposed glass on breakdown.

obtained with the concentric cylinder electrode arrangement, was dispensed with. In this case it is important to know how the exposed glass of the bulb may affect the breakdown phenomenon. This question is particularly pertinent with the tube of Fig. 12, since at breakdown much fluorescence appears on the glass.

This point was tested with a tube shown in Fig. 13. The anode consisted of a flat nickel disk. The tungsten filament assembly and electrode separation were the same as in Fig. 12. A glass sleeve was mounted inside the cylindrical glass envelope so that it could be at position *A* around the electrodes or at *B* away from them. The plan was to condition the tube with the glass sleeve at *A* until it would withstand breakdown at some voltage considerably higher than the initial breakdown value. If a significant part of this conditioning process is a conditioning of the glass sleeve then by moving it to *B*, thus exposing fresh glass, the voltage would be appreciably lowered.

The results of such an experiment are shown in Fig. 14. The first breakdown occurred at 16.2 kv and as shown after the sixteenth breakdown, the tube withstood 25 kv at which point the tube was removed from the pumps. Three more breakdowns then occurred as shown, after which the tube withstood 24 kv without breakdown. The glass sleeve was then moved to *B* and again several breakdowns occurred at potentials appreciably lower than 24 kv, the first one occurring at the same point as the initial breakdown with this tube.

Thus with this type of tube shown in Fig. 13 the condition of the exposed glass is a definite contributing factor in the breakdown. An examination of the concentric cylinder electrode tube used in the bulk of the experiments herein described will show that the filament and anode are very completely shielded from the glass of the tube. The data of Fig. 14 show that this shielding is necessary and important in breakdown studies of this sort.

7. *Unsuccessful attempts to produce breakdown.* An interesting case was encountered with one of the tubes of the type shown in Fig. 12. A number of breakdowns were observed which began at 15 kv and progressed up to 22.2 kv at which point the filament was separated by the breakdown discharge. After replacing the filament one break-

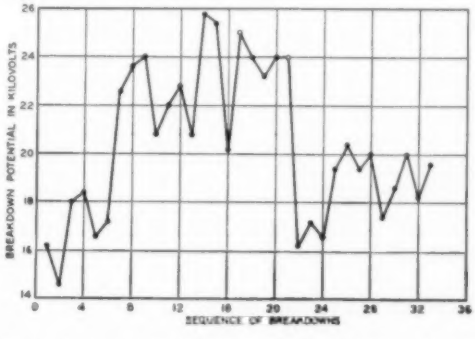

FIG. 14. Data on breakdown as affected by exposed glass. Fresh glass was exposed after breakdown No. 21.

down at 22.4 kv was observed after which the tube successfully withstood 25.4 kv.

The following attempts were then made to induce breakdown. *With the tube sealed off from the pumps*, the entire tube was heated to 500°C for about four minutes. Then with the tube at room temperature *breakdown did not occur* at 24.6 kv. Next the anode system was heated to a red heat for 40 minutes by high frequency induction. Again with the tube at room temperature the tube withstood 25.0 kv. The tube was opened up for three days, then pumped down, baked at 480°C, filament glowed, etc. *Again no breakdown occurred at 23.6 kv.* The diffusion pump was then stopped the pressure rising to 1×10^{-2} mm Hg for twenty-five minutes. Again, no breakdown occurred at 26.4 kv after the pressure had been reduced to about 1×10^{-6} mm Hg. The tube was then removed from the pumps and after standing at room temperature for several days, no breakdown occurred at 26.0 kv, but after standing for several days more a breakdown occurred at 26.4.

At one point in these tests the filament tip and anode were photographed with the voltage applied. From this the potential gradient form factor at the tip of the filament was calculated to be about 178. Thus with a potential of 26.4 kv, the average electric field of 4.7×10^{6} v/cm at the filament surface is *insufficient* to produce breakdown. This was the highest electric field ever observed to be insufficient to produce breakdown. Cases have been observed, with this type of tube, in which the tubes would withstand about 27 kv but because of a smaller form factor the average potential gradient at the filament was smaller than the above quoted value.

In the above tests no measure of the pressure was obtained when the tube was removed from the pumps. During the heat treatments the gas pressure undoubtedly increased considerably. Therefore there was much opportunity for gas contamination of the electrodes. These treatments do not appear to influence the occurrence of breakdown. They furnish no further information on the factors which do affect the phenomenon.

Breakdown with pure tungsten

In addition to the tests just described on the effect of the anode and exposed glass, breakdown experiments were made using pure tungsten filaments in tubes of the concentric cylinder electrode arrangement. In no way significantly different from the case of thoriated tungsten, breakdown occurred very abruptly after which it was found that the characteristic field current curve was raised to enormously higher currents. After breakdown, low temperature heating was not observed to increase the field current in contrast to the thoriated tungsten case already described. The characteristic curve can be reduced approximately to its original value simply by heating the filament to a high temperature in much the same way as with thoriated tungsten. In one respect, the breakdown phenomenon was unlike the thoriated tungsten case. The thermionic activity of the cathode remained unchanged by the breakdown. This proves that the increase in thermionic activity observed with thoriated tungsten is actually due to a thoriation of the filament by the breakdown and is not caused by contamination of the filament from some external source such as the anode.

Discussion

Experiments at the General Electric Laboratory[10] are briefly described in which electrical breakdown was observed. Abnormally large currents set in at a definite voltage and following this the characteristic curve at lower voltages was observed to be shifted to higher currents. These high currents were erased by cathode heating at or about 1600°K. With continued experimentation, the voltage required for breakdown gradually increased. Heating the anode, which was in the form of a filament, at 2500° while the bulb was in liquid air had no effect on the magnitude of the field currents.

Chambers[11] reported on breakdown studies with tungsten filaments which had received intense heat treatment. After 2800°K heat treatment a 0.5-mil tungsten filament gave breakdown at 11 kv whereas with a 1.6-mil filament it occurred at 23 kv. These voltages correspond to average fields of about 2.6×10^{6} v/cm and 2.0×10^{6} v/cm respectively. In addition, he found that with the 0.5-mil filament, immediately after heating the anode to a bright red heat for one

[10] Compton and Langmuir, Rev. Mod. Phys. **2**, April (1930).

[11] Chambers, J. Frank. Inst. **218**, No. 4, October (1934).

hour, breakdown did not occur at 25 kv but after several hours it again occurred at 11 kv. This and other tests were interpreted to mean that the breakdown is caused by positive ions which are emitted from the anode under electron bombardment and which in turn bombard the cathode surface.

Bennett[12] has reported breakdown studies in a series of papers. Many of his experiments were with electrodes of a form that could not be heated readily to high temperatures for outgassing purposes. Tests are reported with electrodes of different materials which were designed to show the effect of the anode and the effect of cathode bombardment on the breakdown. The experiments have been interpreted as showing that the anode has a large effect on breakdown. The results would appear to be confused by unknown effects introduced by exposed glass as described in his 1933 paper.

Probably the most important question regarding the electrical breakdown is the following: When breakdown occurs, is the determining factor the potential between anode and cathode or the applied field at the cathode? If breakdown occurs at a certain voltage it most likely is primarily an anode effect of some sort, but if it occurs at a certain value of the field it probably is primarily a cathode effect. Therefore probably the equivalent of the above question is as follows: Is breakdown caused by an effect originating at the anode such as the emission of positive ions from the anode and the cathode bombardment therewith; or is the breakdown caused by an effect originating at the cathode as, for example a rupture of the cathode surface by the electric field? The evidence from the present experiments although not conclusive indicates that the breakdown is determined primarily by conditions at the cathode. Some fairly direct evidence on this point is offered by the experiments summarized in Table II in which two different sizes of tungsten filaments were used. The maximum breakdown fields observed were about the same for the 0.6-mil filament and the 1.0-mil filament. However, the breakdown voltage for the larger filament was greater by about 60 percent. Of the four tubes listed in Table II, it should be noted that the initial breakdown voltage is lowest for the 0.6-mil filament although the corresponding value of the field is not thus distinguished. Although the evidence of Table II is not conclusive, it favors the thesis that breakdown is determined by the field at the cathode rather than by the applied voltage.

The experiment in which no effect on breakdown was observed when different parts of the anode were used is quite definite evidence that either the anode is not a factor in the breakdown or at least that the progression to higher fields is due to a conditioning of the cathode alone. Regardless of the mechanism by which exposed glass affects the breakdown as already described, this experiment indicates the importance of shielding the electrodes to eliminate the glass as a factor. In the concentric cylinder electrode tubes used in most of the experiments this shielding is very complete. It would be impossible for positive ions from the glass to reach the central portion of the filament. The electrostatic shielding of the electrodes against any "charging up" of the glass is very adequate. It seems very unlikely that neutral particles such as fine bits of glass would be deposited on a small central portion of the filament. It therefore seems reasonable that the effect of exposed glass as shown with the tube of Fig. 13 is adequately guarded against in the concentric cylinder electrode tubes. The experiments on the effect of the anode itself indicated no influence on the breakdown so that we have no direct evidence that the breakdown is not initiated at the cathode.

The test in which high fields were applied to the filament as anode show that breakdown cannot be produced by the electric field alone; an emission of electrons is necessary. The experiments in which the external circuit resistance was varied show that breakdown does not occur if the current that can pass is limited by such resistances.

When once it was experimentally observed that the field currents were independent of the degree of thoriation of a thoriated tungsten filament it was not surprising that the breakdown field was also independent of the degree of thoriation since an emission of field currents is necessary to obtain breakdown.

[12] Bennett, Phys. Rev. **37**, 582 (1931); **40**, 416 (1932); **44**, 859 (1933).

A proposed mechanism of the breakdown process

The electrical breakdown, which from the present experiments appears to be determined primarily by conditions at the cathode, might be tentatively pictured as follows: Before breakdown the field currents come from a few of the surface projections where the local applied field is greatest. Likewise the mechanical force associated with the electric field will be much greater at these projections. Depending on the size, geometry, etc., of these projections and their thermal contact with the body of the cathode, there will be a certain amount of local i^2r heating on the cathode. As the electric field is increased sufficiently, a rupture occurs on that projection where conditions of mechanical force, i^2r heating, and tensile strength are most favorable. When the rupture occurs, due to the greatly enhanced local field the large breakdown current passes and at lower fields much larger field currents are obtained. Heating the filament to a sufficiently high temperature after breakdown tends to smooth down and heal these ruptures thus reducing the local fields and currents as observed experimentally.

The next rupture and breakdown might occur again at the same projection. On the other hand succeeding breakdowns might occur at other projections at progressively higher fields in the order of their susceptibility to rupture.

Experimentally one observes that in general, repeated breakdowns occur at progressively higher fields. The experimental fact that a thoriated tungsten filament becomes partially activated by the breakdown is substantial evidence that at breakdown there is considerable local heating of the filament.

A similar picture of rupture and breakdown might be described wherein positive ions bombarding the cathode are the important factor. The breakdown experimentally observed might be a combination of both. An experiment, in which a transfer of anode material to the cathode could be detected, would give information on whether or not positive ions were bombarding the cathode. Such tests might be made with a tungsten filament cathode and a thorium filament anode.

If breakdown experiments with filaments, whose diameters were different by a factor of about 10, were made, the question of whether the field or the voltage is the determining factor could be quite convincingly settled.

Summary

1. Electron field currents from thoriated tungsten, with different degrees of thoriation, were found to be independent of temperature.

2. The characteristic field current curve was found to be independent of the degree of thoriation of a thoriated tungsten filament. It is not known whether this means that field currents are independent of the work function of the cathode or that the work function of the areas emitting field currents is unchanged during the thoriation cycles.

3. An electrical breakdown, a sudden discontinuity in characteristic field current curve, occurs with thoriated tungsten and pure tungsten cathodes.

4. This breakdown raises the field current curve to higher currents by an enormous factor. Current increases by factors from 10,000 to 10,000,000 were usually obtained.

5. With pure tungsten no change in the thermionic activity of the cathode results from the breakdown; with thoriated tungsten, the thermionic activity is increased showing that a partial thoriation of the filament has occurred.

6. Heat treatment at about 1300°K following breakdown generally further increases the field currents from thoriated tungsten but produces no such effect with pure tungsten.

7. The high field currents following breakdown can be erased by heating the cathode to about 2600°K for a couple of minutes.

8. The value of the applied field at which breakdown occurs is independent of the temperature and the degree of thoriation of a thoriated tungsten filament.

9. The emission of electron field currents is necessary for breakdown to occur. The application of an electric field of the usual magnitude with the filament as anode produces none of the usual effects of breakdown. Breakdown does not occur if a sufficiently high resistance is inserted in the circuit.

10. In general with successive breakdowns, the breakdown occurs at increasingly higher values of the applied field. None of this progressive

increase in the applied field at which successive breakdowns occur can be attributed to a conditioning of the anode. A definite part of this progressive increase in field can be attributed to conditioning of glass surfaces when they are exposed to the discharge.

11. A few tubes eventually would not give breakdown at about 26 kv which was the highest voltage available. Tests with one, in which there was opportunity for much gas contamination did not result in the subsequent occurrence of breakdown.

12. The highest electric field that could be applied to a cathode without breakdown occurring was about 4.7×10^6 v/cm.

13. The evidence favors the conclusion that the electric field applied to the cathode surface rather than the applied voltage is the more important factor in producing breakdown. The evidence likewise favors the conclusion that the anode has no effect on the breakdown and that when the shielding against glass surfaces is complete, the breakdown is determined primarily by conditions at the cathode.

14. The suggestion is made that breakdown involves a rupturing of the cathode surface under the action of local heating and mechanical strain associated with the electric field.

The author acknowledges with pleasure the continued interest of Dr. H. E. Mendenhall during the progress of the experiments and is indebted to Dr. J. A. Becker for many suggestions regarding the interpretation of the data and the form of the manuscript.

AUGUST 1, 1936 PHYSICAL REVIEW VOLUME 50

The Approximate Solution of Nuclear Three and Four Particle Eigenvalue Problems

EUGENE FEENBERG AND SIMON S. SHARE, *University of Wisconsin*

(Received May 23, 1936)

The problem of determining intranuclear forces from the mass defects of the hydrogen and helium isotopes is investigated under the assumption that the interaction potentials are proportional to a function $f(\alpha r^2)$ having the general form of a potential well and possessing the power series expansion

$$f(\alpha r^2)=1-\alpha r^2+c_1(\alpha r^2)^2/2!-c_2(\alpha r^2)^3/3!+\cdots$$

about the origin. With this assumption the Rayleigh-Schroedinger perturbation theory is applicable to the two, three and four particle eigenvalue problems. The perturbation calculation yields small corrections to the eigenvalues given by the "equivalent" two particle method. The corrections are checked very satisfactorily in a special case by means of a complicated variational calculation. Numerical results are given for two extreme forms of the neutron-proton model: Model I—Interaction between unlike particles only, Model II—Equal interactions between all pairs of particles. These results put close upper and lower bounds on the strength of the interaction between like particles in the model, intermediate between (I) and (II), which corresponds most closely to the experimental facts.

I. INTRODUCTION

THE mass defects of the hydrogen and helium isotopes appear to require a nuclear model with strong attractive forces between neutrons and protons and somewhat weaker attractive forces between like particles.[1, 2, 3] However in the study of the eigenvalue problems it is convenient to consider two extreme forms of the neutron-proton model with

(I) Interactions between neutrons and protons only;
(II) Identical interactions between all pairs of particles.

The model which corresponds most closely to the experimental facts is intermediate between (I) and (II). If the eigenvalue problems associated with (I) and (II) are solved, the corresponding solutions for intermediate models can be obtained by a simple process of interpolation. The Hamiltonian operators for models (I) and (II)

[1] Feenberg and Knipp, Phys. Rev. **48**, 906 (1935).
[2] R. D. Present, Phys. Rev. **49**, 640 (1936).
[3] Massey and Mohr, Proc. Roy. Soc. **A152**, 693 (1935).

are taken to have the form

$$H_I(H^3) = -\tfrac{1}{2}(\Delta_1+\Delta_2+\Delta_3) - A_I f(\alpha r_{12}^2) - A_I f(\alpha r_{13}^2) - A_I f(\alpha r_{23}^2), \quad (1)$$

$$H_I(He^4) = -\tfrac{1}{2}(\Delta_1+\Delta_2+\Delta_3+\Delta_4) - A_I f(\alpha r_{13}^2) - A_I f(\alpha r_{14}^2) - A_I f(\alpha r_{23}^2) - A_I f(\alpha r_{24}^2), \quad (2)$$

$$H_{II}(H^3) = -\tfrac{1}{2}(\Delta_1+\Delta_2+\Delta_3) - \tfrac{2}{3}A_{II} f(\alpha r_{12}^2) - \tfrac{2}{3}A_{II} f(\alpha r_{13}^2) - \tfrac{2}{3}A_{II} f(\alpha r_{23}^2), \quad (3)$$

$$H_{II}(He^4) = -\tfrac{1}{2}(\Delta_1+\Delta_2+\Delta_3+\Delta_4) - \tfrac{2}{3}A_{II} f(\alpha r_{12}^2) - \cdots - \tfrac{2}{3}A_{II} f(\alpha r_{34}^2), \quad (4)$$

in which $f(\alpha r^2)$ is a function possessing the power series expansion

$$f(\alpha r^2) = 1 - \alpha r^2 + c_1(\alpha r^2)^2/2! - c_2(\alpha r^2)^3/3! + \cdots \quad (5)$$

about the origin and vanishing rapidly for large values of r. The factor of two-thirds in Eqs. (3) and (4) is introduced in order to make A_I and A_{II} directly comparable. We wish to determine the normal state eigenvalues $E_I(H^3)$, $E_I(He^4)$, $E_{II}(H^3)$, $E_{II}(He^4)$ as functions of the parameters in the interaction potential.

II. The Perturbation Method

A detailed discussion of the symmetrical three particle problem is given to illustrate the general method. The starting point is the Schroedinger equation

$$\{-\tfrac{1}{2}(\Delta_1+\Delta_2+\Delta_3) - \tfrac{2}{3}A_{II} f(\alpha r_{12}^2) - \tfrac{2}{3}A_{II} f(\alpha r_{13}^2) - \tfrac{2}{3}A_{II} f(\alpha r_{23}^2)\}\psi = E_{II}(H^3)\psi. \quad (6)$$

For small values of α the potential function $f(\alpha r^2)$ may be replaced by the first two terms in the power series expansion (5). With this approximation Eq. (6) reduces to

$$\{-\tfrac{1}{2}(\Delta_1+\Delta_2+\Delta_3) - 2A_{II} + \tfrac{2}{3}\alpha A_{II}(r_{12}^2+r_{13}^2+r_{23}^2)\}\psi^0 = E_{II}^0\psi^0. \quad (7)$$

In terms of the internal coordinates

$$\xi_1 = (16\alpha A_{II}/9)^{\frac{1}{4}}(x_1 - \tfrac{1}{2}(x_2+x_3)), \quad \xi_2 = (\alpha A_{II})^{\frac{1}{4}}(x_2 - x_3), \quad (8)$$

Eq. (7) takes the simple form

$$\{\Delta_1+\Delta_2+\epsilon^0 - s_1^2 - s_2^2\}\psi^0 = 0, \quad (9)$$

which we recognize as the wave equation for a system of six independent linear harmonic oscillators.[4] The same coordinate transformation applied directly to Eq. (6) yields the equation

$$\{\Delta_1+\Delta_2+\epsilon_{II}(H^3) - s_1^2 - s_2^2 + (3/8)c_1(\alpha/A_{II})^{\frac{1}{2}} \times (s_1^4 + 4(s_1\cdot s_2)^2/3 + 2s_1^2 s_2^2/3 + s_2^4) - (1/96)c_2(\alpha/A_{II})(9s_1^6 + \cdots + 11s_2^6) + \cdots\}\psi = 0, \quad (10)$$

in which

$$\epsilon_{II}(H^3) = [E_{II}(H^3) + 2A_{II}]/(\alpha A_{II})^{\frac{1}{2}}. \quad (11)$$

The wave function ψ can be expanded in terms of the solutions of the oscillator Eq. (9) and the usual perturbation theory applied to obtain $\epsilon_{II}(H^3)$ as a power series in $(\alpha/A_{II})^{\frac{1}{2}}$, c_1, c_2:

$$\epsilon_{II}(H^3) = \epsilon^0 + (\alpha/A_{II})^{\frac{1}{2}}\epsilon^{(1)} + (\alpha/A_{II})\epsilon^{(2)} + \cdots. \quad (12)$$

The results of the perturbation calculation are

$$\epsilon^0 = 6, \quad \epsilon^{(1)} = -(15/4)c_1, \quad \epsilon^{(2)} = (5/128)\{112c_2 - 129c_1^2\}. \quad (13)$$

The same procedure when applied to the other three problems yields results similar to (13). The energy eigenvalues are given by the expressions

$$E_I(H^3) = -2A_I\{1 - 3(0.933\alpha/A_I)^{\frac{1}{2}} + (15/8)c_1(0.933\alpha/A_I) + (2.5664c_1^2 - (35/16)c_2)(0.933\alpha/A_I)^{\frac{3}{2}} + \cdots\}, \quad (14)$$

$$E_I(He^4) = -4A_I\{1 - 3(0.7286\alpha/A_I)^{\frac{1}{2}} + (15/8)c_1(0.7286\alpha/A_I) + (2.5089c_1^2 - (35/16)c_2)(0.7286\alpha/A_I)^{\frac{3}{2}} + \cdots\}, \quad (15)$$

$$E_{II}(H^3) = -2A_{II}\{1 - 3(\alpha/A_{II})^{\frac{1}{2}} + (15/8)c_1(\alpha/A_{II}) + (2.5195c_1^2 - (35/16)c_2)(\alpha/A_{II})^{\frac{3}{2}} + \cdots\}, \quad (16)$$

$$E_{II}(He^4) = -4A_{II}\{1 - 3(0.75\alpha/A_{II})^{\frac{1}{2}} + (15/8)c_1(0.75\alpha/A_{II}) + (2.4902c_1^2 - (35/16)c_2)(0.75\alpha/A_{II})^{\frac{3}{2}} + \cdots\}. \quad (17)$$

In the special case

$$f(\alpha r^2) = e^{-\alpha r^2}, \quad (c_1 = c_2 = 1), \quad (18)$$

the expansions in powers of $(\alpha/A)^{\frac{1}{2}}$ appear to converge quite rapidly. However the range in which Eqs. (14), (15), (16), (17) may be expected to be moderately accurate does not extend into the physically interesting region ($\alpha^{-\frac{1}{2}} < 2.8\times10^{-13}$ cm).

[4] See W. V. Houston, Phys. Rev. **47**, 942 (1935) for a discussion of the general "harmonic oscillator" model.

III. The "Equivalent" Two-Particle Equations

The procedure described in the preceding section can be applied to obtain the normal state eigenvalue of the two-particle Hamiltonian operator

$$H = -\Delta - Bf(\beta r^2). \tag{19}$$

The resulting expression for the eigenvalue is

$$\varepsilon = -B\{1 - 3(\beta/B)^{\frac{1}{2}} + (15/8)c_1(\beta/B) + (2.5781c_1^2 - (35/16)c_2)(\beta/B)^{\frac{3}{2}} + \cdots\}. \tag{20}$$

We get "equivalent" two particle problems by giving B and β the values

Model I

$$\left.\begin{aligned} B &= 2A_{\mathrm{I}} \\ \beta &= 1.8660\alpha \end{aligned}\right\} \mathrm{H}^3, \tag{21}$$

$$\left.\begin{aligned} B &= 4A_{\mathrm{I}} \\ \beta &= 2.9142\alpha \end{aligned}\right\} \mathrm{He}^4. \tag{22}$$

Model II

$$\left.\begin{aligned} B &= 2A_{\mathrm{II}} \\ \beta &= 2\alpha \end{aligned}\right\} \mathrm{H}^3, \tag{23}$$

$$\left.\begin{aligned} B &= 4A_{\mathrm{II}} \\ \beta &= 3\alpha \end{aligned}\right\} \mathrm{He}^4. \tag{24}$$

These results were originally found by a variational method[5] which does not require that any restrictions be placed on the potential function $f(\alpha r^2)$; in particular the power series expansions about the origin may contain odd powers of r. It is clear from the original variational derivation that the eigenvalues $\varepsilon_{\mathrm{I}}(\mathrm{H}^3)$, $\varepsilon_{\mathrm{I}}(\mathrm{He}^4)$, $\varepsilon_{\mathrm{II}}(\mathrm{H}^3)$, $\varepsilon_{\mathrm{II}}(\mathrm{He}^4)$ of the "equivalent" problems do not differ very much from the eigenvalues of the corresponding three and four particle problems. The differences can now be estimated since the two sets of eigenvalues are related by the equations

$$E_{\mathrm{I}}(\mathrm{H}^3) = \varepsilon_{\mathrm{I}}(\mathrm{H}^3) + 0.021\alpha(\alpha/A_{\mathrm{I}})^{\frac{1}{2}}c_1^2 + \cdots, \tag{25}$$

$$E_{\mathrm{I}}(\mathrm{He}^4) = \varepsilon_{\mathrm{I}}(\mathrm{He}^4) + 0.172\alpha(\alpha/A_{\mathrm{I}})^{\frac{1}{2}}c_1^2 + \cdots, \tag{26}$$

$$E_{\mathrm{II}}(\mathrm{H}^3) = \varepsilon_{\mathrm{II}}(\mathrm{H}^3) + 0.117\alpha(\alpha/A_{\mathrm{II}})^{\frac{1}{2}}c_1^2 + \cdots, \tag{27}$$

$$E_{\mathrm{II}}(\mathrm{He}^4) = \varepsilon_{\mathrm{II}}(\mathrm{He}^4) + 0.228\alpha(\alpha/A_{\mathrm{II}})^{\frac{1}{2}}c_1^2 + \cdots. \tag{28}$$

[5] Feenberg, Phys. Rev. **47**, 850 (1935), Eq. (26); reference 1, Eq. (13).

The Eqs. (25), (26), (27), (28) reduce the three and four particle eigenvalue problems to the much simpler problem of computing the lowest eigenvalue of the one dimensional equation[6]

$$\{d^2/dr^2 + \varepsilon + Bf(\beta r^2)\}\varphi = 0. \tag{29}$$

Calculations to test the accuracy of the Eqs. (25), (26), (27), (28) are described in the appendix. The results, as far as they go, indicate that these equations are quite accurate in the physically interesting range of α values.

IV. Numerical Results

A table from which any one of the quantities ε, B, β can be computed when the other two are known is available in the case of the Gaussian potential (Eq. 18).[7] The conditions

$$E_{\mathrm{I}}(\mathrm{He}^4) = E_{\mathrm{II}}(\mathrm{He}^4),$$

$$-E_{\mathrm{I}}(\mathrm{He}^4) + (\text{coulomb correction})^{8} = 54mc^2 \tag{30}$$

are sufficient to determine A_{I} and A_{II} as functions of α. These quantities in turn determine $E_{\mathrm{I}}(\mathrm{H}^3)$ and $E_{\mathrm{II}}(\mathrm{H}^3)$, which are given in Table I.

Table II gives the depth of the neutron-proton well, A_{pr}, as a function of α and the binding energy of the deuteron.

Attractive forces between like particles are necessary to account for the difference between A_{pr} and A_{I}, A_{II}. Let A_{pp} and A_{rr} represent the depths of the neutron-neutron and proton-proton wells. The inequality[9]

$$2(A_{\mathrm{I}} - A_{pr}) \leqq A_{pp} \leqq 2(A_{\mathrm{II}} - A_{pr}) \tag{31}$$

is an immediate consequence of the two assumptions

Table I.* A_{I}, A_{II}, $E_{\mathrm{I}}(\mathrm{H}^3)$, $E_{\mathrm{II}}(\mathrm{H}^3)$.

α^{-1}	α	A_{I}	A_{II}	$E_{\mathrm{I}}(\mathrm{H}^3)$	$E_{\mathrm{II}}(\mathrm{H}^3)$
2.8×10^{-13} cm	10	64	65	19.8	17.9
2.0×10^{-13} cm	20	97	98	17.1	14.3
1.6×10^{-13} cm	30	126	129	14.9	11.6

* Units—Energy—$mc^2 = 510{,}000$ e.v.
Length—$\hbar/c(Mm)^{\frac{1}{2}} = 8.97 \times 10^{-13}$ cm.

[6] An "equivalent" two particle equation was used by Wigner in his pioneer investigation of the three and four particle eigenvalue problems, Phys. Rev. **43**, 252 (1933).
[7] Reference 1, Table I; also reference 5, section II.
[8] Reference 1, Table II.
[9] Feenberg, Phys. Rev. **49**, 273 (1936).

TABLE II. $A_{\tau\tau}(\alpha, E(H^2))$.

α \ $E(H^2)$	$-3.5mc^2$	$-4.0mc^2$	$-4.5mc^2$
10	48	50	51
20	82	84	86
30	114	117	120

TABLE IV. $g(\alpha, E(H^2))$.

α \ $E(H^2)$	$-3.5mc^2$	$-4.0mc^2$	$-4.5mc^2$
10	0.22	0.23	0.24
20	0.17	0.18	0.19
30	0.14	0.15	0.16

TABLE III. *Upper and lower limits on A_{pp} (Eq. 31).*

α \ $E(H^2)$	$-3.5mc^2$		$-4.0mc^2$		$-4.5mc^2$	
	U	L	U	L	U	L
10	33	31	30	28	26	24
20	32	29	28	24	24	20
30	30	24	25	18	20	13

TABLE V. *Upper and lower limits on A_{pp} (Eq. 33).*

α \ $E(H^2)$	$-3.5mc^2$		$-4.0mc^2$		$-4.5mc^2$	
	U	L	U	L	U	L
10	44	42	41	39	38	36
20	46	43	43	40	40	37
30	46	40	42	36	39	32

(a) $A_{pp} \sim A_{\tau\tau}$,

(b) Neutron-proton interaction independent of spin orientation. The upper and lower limits on A_{pp}, computed from Eq. (31) are shown in Table III.

Assumption (b) is probably incorrect. It appears necessary to assume a dependence on spin orientation in the neutron-proton interaction as suggested by Wigner in order to account for the very large scattering cross section of slow neutrons in hydrogen.[10, 11] We replace (b) by the assumption:

(c) Depth of the neutron-proton well
$= A_{p\tau}$ (triplet interaction),
$= (1-2g)A_{p\tau}$ (singlet interaction).

The constant g is determined by the condition[12]

$$E(H^2, \text{singlet}) \sim 0. \tag{32}$$

Values of g computed from Eq. (32) are listed in Table IV.

The inequality (31) must be replaced by

$$2(A_{\mathrm{I}} - A_{p\tau}) + gA_{p\tau} \leqq A_{pp} \leqq 2(A_{\mathrm{II}} - A_{p\tau}) + gA_{p\tau} \tag{33}$$

and Table III by a similar table based on Eq. (33).

For $\alpha = 10$, the like particle depth A_{pp} is almost identical with the effective neutron-proton depth $(1-g/2)A_{p\tau}$. Consequently at this point

$$A_{pp} = 2(A_{\mathrm{II}} - A_{p\tau}) + gA_{p\tau}. \tag{34}$$

In the range $10 \leqq \alpha \leqq 20$ the upper limit on A_{pp} coincides with the accurate value. Also in this range the eigenvalue $E_{\mathrm{II}}(H^3)$ does not differ very much from the eigenvalue $E(H^3)$ of the physical model under assumption (c). No correction is needed at $\alpha = 10$. At $\alpha = 20$ the departure from complete symmetry lowers the eigenvalue by the amount $0.3mc^2$. This correction includes the effect of changing from ordinary to Majorana forces between unlike particles.[13] For intermediate points the linear interpolation formula

$$E(H^3) = -17.9 + 0.33(\alpha - 10), \quad 10 \leqq \alpha \leqq 20, \tag{35}$$

is sufficiently accurate.

Let $-E(He^4)$ represent the correct (unknown) binding energy of the alpha-particle. The quantity

$$\delta E(He^4) = E(He^4) + 54 \tag{36}$$

measures the deviation from the value $54mc^2$ used in Eq. (30). There are corresponding deviations δA_{pp} and $\delta E(H^3)$ from the tabulated values of A_{pp} and $E(H^3)$. The relations

$$\delta A_{pp} \sim -1.1\delta E(He^4), \quad \delta E(H^3) \sim 0.4\delta E(He^4), \quad 10 \leqq \alpha \leqq 20, \tag{37}$$

permit the calculation of corrections to the tabulated values when $\delta E(He^4)$ is known.

The nuclear masses and energies given recently by Aston,[14] Oliphant,[15] K. T. Bainbridge,[16] Bethe and Livingston[17] determine the energies

[10] Reference 1, section V.
[11] L. A. Young, Phys. Rev. **48**, 913 (1935).
[12] The numerical integration of Eq. (28) with $\mathcal{E} = 0$ yields the result $(1-2g)A_{p\tau} \sim 2.7\alpha$.
[13] Eqs. (8) and (9), reference 1, are used to compute the corrections.
[14] F. W. Aston, Nature **137**, 357 (1936).
[15] M. L. Oliphant, Nature **137**, 396 (1936).
[16] Cornell Symposium (July 1936).
[17] Bethe and Livingston, unpublished (we are indebted to Dr. Bethe for communicating to us the results tabulated in (38)).

$$\begin{aligned} E(H^2) &= -4.34 \pm 0.12 mc^2, \\ E(H^3) &= 2E(H^2) - 7.82 \pm 0.03 mc^2, \\ E(He^3) &= 2E(H^2) - 6.26 \pm 0.20 mc^2, \\ E(He^4) &= 2E(H^2) - 4.65 \pm 0.3 mc^2. \end{aligned} \tag{38}$$

Using Eqs. (35) and (37) the experimental binding energy of H^3 determines α to have the value $16(\alpha^{-1} \sim 2.25 \times 10^{-13}$ cm).[18] From Table V and Eq. (37), $A_{rr} \sim 41 mc^2$ at $\alpha = 16$.[19] These values fit moderately well with new results on the anomalous scattering of fast protons in hydrogen.[20, 21]

Appendix. Variational Calculations

The Gaussian wave function

$$\psi^0 = N \exp\left[-(\nu/2)(r_{12}^2 + r_{13}^2 + r_{23}^2)\right] \tag{39}$$

may be taken as an approximation to the normal state eigenfunction of the Hamiltonian operator $H_{II}(H^3)$. A better approximation which should give fairly accurate values for the energy is

$$\psi = (1 + cH_{II})\psi^0. \tag{40}$$

In the variation method of calculating the energy the following matrix elements are required

$$\begin{aligned} &(0|1|0) = 1, \quad (0|H_{II}|0) = 3\alpha\sigma - 2A_{II}(\sigma/(\sigma+1))^{\frac{1}{2}}, \\ &(0|H_{II}^2|0) = 12\alpha^2\sigma^2 - 6\alpha A_{II}\{-3\sigma(\sigma/(\sigma+1))^{\frac{1}{2}} + \sigma(\sigma/(\sigma+1))^{5/2}\} \\ &\qquad + (4/3)A_{II}^2\{(\sigma/(\sigma+2))^{\frac{1}{2}} + 16\sigma^3/(2\sigma+1)^{\frac{1}{2}}(2\sigma+3)^{\frac{1}{2}}\}, \\ &(0|H_{II}^3|0) = 60\alpha^3\sigma^3 - (3/2)A_{II}\alpha^2(\sigma/(\sigma+1))^{7/2}(48\sigma^2 + 136\sigma + 103) \\ &\qquad + 4A_{II}^2\alpha\{(\sigma/(\sigma+2))^{\frac{1}{2}}(3\sigma^2 + 9\sigma + 2)/(\sigma+2) + 64\sigma^3(3\sigma^3 + 9\sigma^2 + 5\sigma)/(2\sigma+1)^{5/2}(2\sigma+3)^{5/2}\} \\ &\qquad - (8/9)A_{II}^3\{48\sigma^3/(4\sigma^2 + 12\sigma + 6)^{\frac{1}{2}} + 16\sigma^3/(2\sigma+3)^3 + (\sigma/(\sigma+3))^{\frac{1}{2}}\} \end{aligned} \tag{41}$$

where ν has been replaced by $\frac{2}{3}\alpha\sigma$.

The corresponding treatment of the "equivalent" two particle Hamiltonian given by Eq. (19) is based on the approximate wave function

$$\psi^0 = N \exp\left[-(\mu/2)r_{12}^2\right]. \tag{42}$$

The matrix element $(0|1|0)$ is the same as in Eqs. (41). If we replace B by $2A_{II}$ and β by 2α, $(0|H|0)$ is also the same as in (41). The other matrix elements are

$$\begin{aligned} &(0|H^2|0) = 15\alpha^2\sigma^2 - 12A_{II}\alpha(\sigma/(\sigma+1))^{5/2}(\sigma+2) + 4A_{II}^2(\sigma/(\sigma+2))^{\frac{1}{2}}, \\ &(0|H^3|0) = 105\alpha^3\sigma^3 - 2A_{II}\alpha^2(\sigma/(\sigma+1))^{7/2}(45\sigma^2 + 156\sigma + 156) \\ &\qquad + 12A_{II}^2\alpha(\sigma/(\sigma+2))^{\frac{1}{2}}(3\sigma^2 + 12\sigma + 4)/(\sigma+2) - 8A_{II}^3(\sigma/(\sigma+3))^{\frac{1}{2}}, \end{aligned} \tag{43}$$

where μ has been replaced by $2\alpha\sigma$. In using (41) and (43) it is convenient to give A_{II} values which make the exact eigenvalue of the "equivalent" problem independent of α. This will occur if we set $A_{II} = A_{rr}(E(H^2) = -4.0)$. Then the exact eigenvalue of Eq. (29) is $-8mc^2$.

Table VI. *Comparison of the values of E and ℰ calculated from (43) with the term $0.117\alpha(\alpha/A_{II})^{\frac{1}{2}}$ in Eq. (27).*

α	$(0\|H\|0)$	ℰ	E	$E-$ℰ	$0.117\alpha(\alpha/A_{rr})^{\frac{1}{2}}$
10	−5.46	−7.34	−6.78	0.56	0.53
20	−2.77	−6.53	−5.40	1.13	1.14
30	−0.07	−5.60	−3.91	1.69	1.78

We now expect that the difference in the energies E calculated from (41) and ℰ calculated from (43) should agree with the term $0.117\alpha(\alpha/A_{II})^{\frac{1}{2}}$ in Eq. (27) if this equation is accurate. Table VI shows that Eq. (27) is quite accurate in the physically important range of α values.

[18] The coulomb interaction between the protons in He^3 accounts for about 80 percent of the experimental difference between $E(H^3)$ and $E(He^3)$. See reference 1, Table III.

[19] The condition $A_{rr} < (1-2g)A_{rr}$ which is satisfied for $\alpha > 15$ precludes the existence of a di-neutron or di-proton. At $\alpha = 16$, A_{rr} is about 5 percent smaller than the neutron-proton singlet interaction with $E(H^2, \text{singlet}) = 0$.

[20] Tuve, Heydenburg, Hafstad, Phys. Rev. **49**, 402 (1936).

[21] Breit, Condon and Present (to appear in the Physical Review).

LETTERS TO THE EDITOR

Prompt publication of brief reports of important discoveries in physics may be secured by addressing them to this department. Closing dates for this department are, for the first issue of the month, the eighteenth of the preceding month, for the second issue, the third of the month. The Board of Editors does not hold itself responsible for the opinions expressed by the correspondents.

Communications should not in general exceed 600 words in length.

The Ionosphere, Solar Eclipse and Magnetic Storm

The total solar eclipse of June 19, 1936 was visible chiefly in Siberia. The National Bureau of Standards made extensive ionosphere measurements at Washington from June 17 to 20 for comparison with similar measurements made in the eclipse area. These measurements indicated that the ionosphere at Washington was in an abnormal condition from about the time of the beginning of the eclipse, which was at night in Washington, through the entire following day and night. Widely separated magnetic observatories reported a severe magnetic storm beginning at 1245 EST June 18 and ending at 0200 EST June 20. Since the abnormal conditions found in the ionosphere on June 19 resembled those found by us during many other magnetic disturbances it is believed that they were caused mainly by conditions associated with the magnetic storm rather than with the eclipse.

Fig. 1 summarizes the principal results. Ionosphere conditions were normal on June 17 and until 2200 EST on June 18. The $f_{F_2}{}^x$ then decreased sharply to an abnormally low value at 0100 EST June 19, simultaneous with a severe disturbance of Z. Values of $f_{F_2}{}^x$ then oscillated abnormally, with high absorption of F_2 reflections until about 0600 EST. The $f_{F_2}{}^x$ was lower than $f_{F_1}{}^x$ from then until about 1400 EST. The $f_{F_2}{}^x$ then rose slowly until about sunset, decreased again to low values late at night and became normal after sunrise June 20. The $f_{F_2}{}^x$ did not fall at the beginning of the magnetic storm on June 18 but did remain abnormally low during all of June 19. The rise of $f_{F_2}{}^x$ during the late afternoon of June 19 is chiefly a diurnal variation and is found on magnetically disturbed days as well as normal summer days.

The $f_{F_1}{}^0$ was also depressed on June 19 but no abnormal f_E values were observed. The sporadic E was much less in evidence on June 19 than on other days. The latter effect was also noted on field intensity records of W1XK (9570 kc/s, 600 km distant). These emissions were usually propagated by sporadic E for several hours during the early

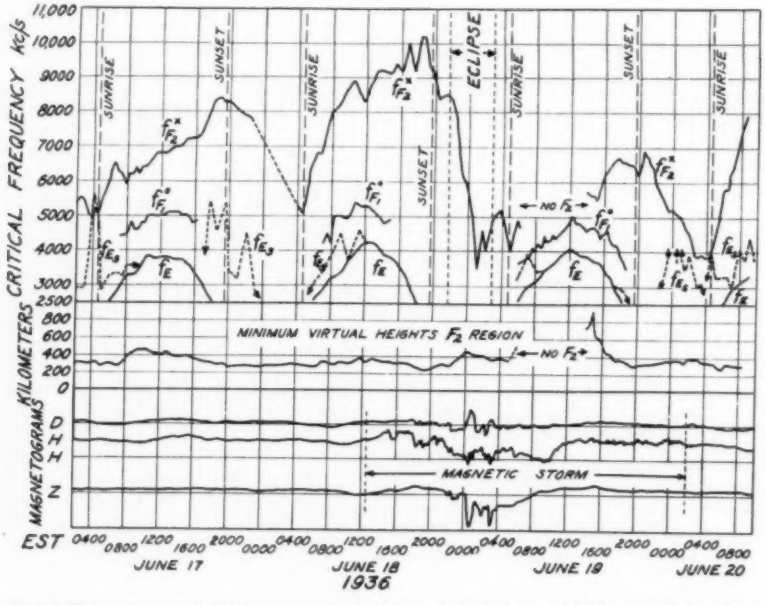

FIG. 1. The upper part of this figure shows the variation of critical frequencies with time. $f_{F_2}{}^x$ = critical frequency F_2 region extraordinary ray. $f_{F_1}{}^0$ = critical frequency F_1 region ordinary ray. f_E = critical frequency E region. f_{E_s} = upper frequency limit of sporadic E. The middle part of the figure shows variation of minimum F_2 virtual heights with time. The lower part of figure shows the Cheltenham magnetograms. D, H and Z represent variations of declination, horizontal component and vertical component of the earth's magnetic field.

forenoon but failed on June 19. Weak transmission by scattered reflections also failed. Absorption of E transmission from W8XAL (6060 kc/s, 650 km distant) was greater than normal on June 19. The F_2 virtual heights were very high when $f_{F_2}{}^x$ began to increase above $f_{F_1}{}^x$ from 1400 to 1600 EST June 19.

This example of correlation of the condition of the ionosphere with a magnetic storm corroborates previous evidence obtained by us: (1) Disturbed radio conditions correlate much better with disturbances of the Z than with disturbances of the H component. (2) A severe magnetic disturbance beginning during the daytime may show little correlation with radio data while a severe magnetic disturbance before sunrise is accompanied by disturbed radio conditions during the whole of the following day. (3) The disturbed radio conditions include lowered critical frequencies, increased absorption, and increased virtual heights, indicating a diffusion of the ionosphere. (4) During a magnetic disturbance the higher part of the ionosphere is the most disturbed.

S. S. KIRBY
T. R. GILLILAND
N. SMITH
S. E. REYMER

U. S. Department of Commerce,
National Bureau of Standards,
Washington, D. C.,
June 30, 1936.

On the Magnetic Scattering of Neutrons

The direct experimental evidence of the neutron, obtained so far, indicates its mass and the range of forces within which it interacts with other heavy particles. The angular moments of nuclei make it practically sure that it has an angular momentum $\frac{1}{2}h/2\pi$. Furthermore there are good theoretical reasons to believe that it should have a magnetic moment of the same order of magnitude as the measured moment of the proton but having the opposite direction with respect to the angular momentum; these conclusions are partly based on Fermi's theory of the β-decay, partly on the known magnetic moment of the deuteron. Since the Stern-Gerlach method may meet considerable difficulties when applied to neutron beams, we want to propose a different way of obtaining information about the magnetic moment of the neutron which seems considerably simpler and promising in several other respects.

Consider an atom (or molecule) which in its ground state has a total magnetic moment $\mathfrak{y}$ caused by the spin or the orbital motion of the atomic electrons. The magnetic field around and within the atom can in any case be described by an average dipole density distribution $\mathfrak{y}g(\mathfrak{r})$ with $\int g(\mathfrak{r})d\tau = 1$. It will scatter neutrons on account of two reasons:

(1) Because of the interaction of the neutron with the atomic nucleus (or nuclei);
(2) Because of the inhomogeneous magnetic field in its surrounding acting on the magnetic moment of the neutron.

Although the forces on the neutron due to the second cause have to be assumed to be extremely much weaker than those due to the first cause, they act on distances so much larger that the scattering effect of both on slow neutrons becomes of the same order of magnitude. Treating the interaction due to both causes as small disturbances of the plane waves, which represent the incoming and scattered neutron one readily obtains a formula for the magnetic influence on the scattering process.

Let Θ be the angle between the orientation of $\mathfrak{y}$ and the direction of incidence of a neutron with velocity v, $\gamma_n = \mu_n/[(e/Mc)\cdot(h/4\pi)]$ the magnetic moment of the neutron μ_n, measured in units of the Bohr magneton, divided by the ratio of masses M/m of the neutron and electron and $\mathfrak{q} = \mathfrak{k}_0 - \mathfrak{k}_1$ the difference between the vectors of propagation of incident and scattered wave, both having equal magnitude $k_0 = k_1 = 2\pi Mv/h$. The cross-section ϕ_ω per unit solid angle for scattering under an angle ϑ against the direction of incidence and an azimuth φ against the common plane of $\mathfrak{y}$ and $\mathfrak{k}_0$ is then given by

$$\phi_\omega = \sigma_\omega \left| 1 \pm \frac{\gamma_n \gamma_e}{2(\sigma_\omega)^{\frac{1}{2}}} \frac{e^2}{mc^2} \left(\sin\theta \cos\frac{\vartheta}{2} \cos\varphi - \cos\theta \sin\frac{\vartheta}{2} \right)^2 F(\mathfrak{q}) \right|^2, \quad (1)$$

where γ_e is the absolute magnitude of the atomic moment μ, measured in units of the Bohr magneton, and

$$F(\mathfrak{q}) = \int \exp\,(i(\mathfrak{q}\cdot\mathfrak{r}) g(\mathfrak{r}) d\tau \quad (2)$$

is an atomic form factor, determined by the distribution of magnetism in the atom, which approaches unity for $1/q$ being large compared with atomic dimensions. The plus or minus sign in formula (1) is valid for neutrons with a magnetic moment oriented parallel or antiparallel to $\mathfrak{y}$, respectively.

Formula (1) for the scattering cross section per atom remains practically valid also for the case of a ferromagnetic polycrystalline substance, the only difference being that for the determination of $\mathfrak{q}$ only such neutron velocities v are to be used for which the condition of interference at microcrystals with properly chosen orientation can be satisfied. Furthermore one has to consider that γ_e becomes temperature dependent:

$$\gamma_e(T) = \gamma_e(0) \frac{I(T)}{I(0)} \quad (3)$$

[$I(T)$ = Intensity of magnetization at saturation and at absolute temperature T] because of the decreasing average magnetization per atom as the temperature T approaches the Curie point; at saturation the angle θ in (1) is the angle between the magnetizing external field and the direction of incidence of the neutrons. While for fast neutrons the second term in (1) is negligible, it is quite considerable for neutrons with thermal energy, for which the wave-length is comparable with atomic dimensions, since $F(\mathfrak{q})$ has then the order of magnitude one. The importance of the magnetic effect is measured by the number $k = (\gamma_n \gamma_e / 2(\sigma_\omega)^{\frac{1}{2}}) \cdot (e^2/mc^2)$ which, for example for magnetized iron with $\gamma_e \leqq 2$, $(\sigma_\omega)^{\frac{1}{2}}$ = radius of the iron nucleus = 5.10^{-13} cm and assuming $\gamma_n = 1$ becomes $k \leqq 0.7$.

Since for $T>$Curie temperature γ_e vanishes, one can obtain for temperatures of the ferromagnetic scatterer above the Curie point independent information about σ_ω alone. For temperature below the Curie point the effect then depends solely on the product $\gamma_n F(\mathbf{q})$ since all other quantities in the second term of (1) are known.

We suggest the following applications.

(a) Measurement of γ_n and thus of the magnetic moment of the neutron by measuring the scattering cross section for very slow neutrons or under small angles, so that $q \leqq 0$ and $F(\mathbf{q})$ becomes practically one.

(b) Production of polarized neutron beams by letting neutrons pass through magnetized iron and observing that due to the cross product in the expansion of (1) the weakening of the beam due to scattering is different for neutrons with opposite orientation of their magnetic moment with respect to the magnetizing field. For example, the intensity of a neutron beam after having passed through two plates of iron should be different whether both are magnetized parallel to the beam or one is magnetized parallel and the other antiparallel.

(c) An experimental study of the distribution of the magnetizing electrons in ferromagnets, particularly whether they are conduction electrons or belong to inner shells, by investigating the scattering for different values of $\mathbf{q}$ and thus obtaining some information about the function $F(\mathbf{q})$ or the magnetic distribution function $g(\mathbf{q})$ related to it by Formula (2).

Experiments are under way here to test the predicted effect and its implications. Even if no magnetic scattering could be observed this should lead to the interesting conclusion that the magnetic moment of the neutron is considerably less than that theoretically to be expected.

F. BLOCH

Stanford University,
July 6, 1936.

On the Probability of γ-Ray Emission

The radiation of a system of charged particles can be described, according to its symmetry properties, as dipole, quadrupole, etc., radiation. For each higher order of symmetry, the probability of emission generally decreases by a factor (wave-length of radiation/dimension of radiating system)^2. In particular for γ-rays of about 1 MEV emitted by radioactive nuclei one should expect the ratio of dipole and quadrupole intensities to be about $(10^{-10}/10^{-12})^2 = 10^4$. The investigation of the internal conversion of γ-rays[1] has shown that both types of transitions actually occur; however, they are known to be of about equal intensity. Furthermore, the comparison of the probability of γ-ray emission with that of long range α-particles[2] seems to indicate that the probability of radiative nuclear transitions is that of quadrupole lines. These facts show that for atomic nuclei the probability of dipole transitions is for some reason reduced by a factor of several thousands.

We want to point out here that this may be understood by taking into account the exchange of charge between neutrons and protons which, according to the present views[3] is to a large extent responsible for the binding forces between nuclear constituents. In fact the frequency ν_0 of this exchange is very large compared to the frequency ν of radiative oscillations. Considering for simplicity a proton and a neutron oscillating against each other inside the nucleus, it can be easily seen that due to this mechanism the effective dipole moment will be reduced by a factor $A \leqq \nu_0/\nu$; in the limiting case of $A = \infty$ there will remain only a quadrupole moment corresponding to two positive half-charges oscillating relative to each other. This circumstance reduces the probability of dipole transition by a factor $(\nu_0/\nu)^2$, while it leaves that of quadrupole radiation practically unchanged. In order to estimate the magnitude of A one has to consider that $h\nu_0 = U_0$ is of the order of magnitude of the potential energy between neutron and proton which can be estimated[4] to be at least 30 MEV. Thus for γ-radiation of about 1 MEV the intensity of dipole radiation has to be reduced by approximately a factor 1000 and so becomes just about that of quadrupole radiation.

The reduction factor for the radiation of the nucleus as a whole depends on the adopted nuclear model and cannot easily be calculated. But it seems plausible that the total effect will be essentially the same as for two particles.

F. BLOCH

Stanford University,

G. GAMOW

George Washington University,
July 9, 1936

[1] X. Taylor and N. Mott, Proc. Roy. Soc. **A138**, 665 (1932).
[2] M. Delbruch and G. Gamow, Zeits. f. Physik **72**, 492 (1931).
[3] W. Heisenberg, Zeits. f. Physik **77**, 1 (1932).
[4] H. Bethe, Rev. Mod. Phys. **8**, 82 (1936).

Continuous Spectrum Observed in Raman Scattering

It has been found that, in addition to the Stokes and anti-Stokes lines, a continuous spectrum is observed in Raman scattering.[1] A satisfactory explanation of this has not yet been offered.

I believe it can be explained very simply as follows. A molecule in a solid or a liquid can be considered as confined to a small space due to the mutual repulsion of molecules at close approach. If we consider such a space to be force-free and regard its boundary to be an infinite field of force preventing the molecule from escaping from the space, we can look upon the molecule in the space as similar to the case of an "electron shut up in a box." In such a case, regarding the space to be a square, the molecule, according to wave mechanics, can have quantized energies given by

$$E = (h^2/8ma^2)(n_x^2 + n_y^2 + n_z^2).$$

This part of the energy of a molecule can increase or decrease in discrete units corresponding to changes of quantum numbers, n_x, n_y or n_z by one or more units. Since a large number of such changes are possible in the interaction of light quanta with the molecules, it is natural that we should expect what, in effect, appears to be a continuous spectrum.

Changes of energy postulated above may take place along with changes of rotational or vibrational energy of the molecules in which case, the principal lines will be broadened and appear as bands.

It is improbable that the picture postulated above corresponds to facts in the case of liquids of low viscosity or liquids heated to high temperatures. We should naturally expect in such cases the disappearance of the continuous spectrum or its becoming very faint.

The magnitude of a is probably of the order of the size of a molecule, i.e., 10^{-8} cm. It may be three or four times the size of a molecule. In other words, a may be approximately equal to the size of the diameter of the average spherical volume associated with a molecule by Wheeler[2] in his papers on the theory of liquids.

S. V. Chandrashekhar Aiya

Khar, Bombay,
May 27, 1936.

[1] Bhagavantam, Indian J. Physics **5**, 237 (1930).
[2] Wheeler, Proc. Ind. Acad. Sciences **2**, 466 (1935).

Ionization of Mercury Vapor by Positive Sodium Ions

In 1930, Kirschstein[1] reported observing the excitation of mercury vapor by sodium ions having as little energy as 35 volts. The observations were made photographically on the 2537 line by means of a quartz spectroscope. If this excitation really occurred, then ionization of mercury by sodium ions could also be anticipated and probably at sodium ion energies of less than 100 volts.

A balanced space-charge method of detecting positive ions has been used recently by one of the writers to study ionization of gases by positive alkali ions.[2] With minor modifications, this apparatus was suitable for examination of the effects of sodium ions on mercury. Preliminary results indicate that ionization of the mercury sets in when the sodium ions reach an energy of 88 volts. This value of 88 volts is probably accurate to about ± 4 volts. It confirms qualitatively the observation of Kirschstein. It is also in agreement with the conclusions on relative ionization potentials drawn in reference 2 and by others.[3] The conclusion in reference 2 was that when the ionization energy of the positive sodium ions was corrected for conservation of momentum, the potential for ionization of Ne by Na^+ should be less than that for any other substance ionized by Na^+. The corrected ionization energy for Ne was 61 volts; for Hg it turns out to be 79 volts.

The efficiency of ionization of Hg by Na^+ is qualitatively of the same order of magnitude as that of Ne by Na^+. The ionization of other gases (A, Kr, Xe, He, H_2, N_2, CO_2) by Na^+ if it occurred at all was so weak as to be undetectable by the balanced space-charge method. The fact that ionization by alkali ions was only observed in the noble gases led to the belief that only these gases with their completed outer electron shells could be ionized at all by alkali ions. The new results on mercury indicate that the outer electron shell may not be as important in determining the efficiency of ionization as the atomic or molecular nature of the gas. No molecular gas has been observed to be ionized by the writers. Mercury is the first atomic gas beside the noble gases to have been tried.

Caesium ions have been tried in this tube on the mercury vapor. The results seem to indicate an ionization inset at 59 volts. Further experiments with this apparatus are in progress.

The writers are much indebted to Professor L. B. Loeb who called their attention to the work of Kirschstein and suggested this investigation.

R. N. Varney
W. C. Cole

Physics Department,
University of California,
Berkeley, California,
July 1, 1936.

[1] B. Kirschstein, Zeits. f. Physik **184**, 60 (1930).
[2] R. N. Varney, Phys. Rev. **47**, 483 (1935).
[3] W. Weizel and O. Beeck, Zeits. f. Physik **76**, 250 (1932).